Contributions to the Chemistry of Metal Nitrides and Inorganic Nanomaterials

A Thesis
Submitted for the degree of
Doctor of Philosophy
by

A. Gomathi

Chemistry and Physics of Materials Unit
Jawaharlal Nehru Centre for Advanced Scientific Research
(A Deemed University)
Bangalore – 560 064

March 2010

DECLARATION

I hereby declare that the matter embodied in this thesis entitled “Contributions to the Chemistry of Metal Nitrides and Inorganic Nanomaterials” is the result of investigations carried out by me under the supervision of Prof. C. N. R. Rao, FRS, at the Chemistry and Physics of Materials Unit, Jawaharlal Nehru Centre for Advanced Scientific Research, Bangalore, India, and that it has not been submitted elsewhere for the award of any degree or diploma.

In keeping with the general practice in reporting scientific observations, due acknowledgement has been made whenever the work described is based on the findings of other investigators.

A. Gomathi

CERTIFICATE

I hereby certify that the matter embodied in this thesis entitled “Contributions to the Chemistry of Metal Nitrides and Inorganic Nanomaterials” has been carried out by Ms. A. Gomathi at the Chemistry and Physics of Materials Unit, Jawaharlal Nehru Centre for Advanced Scientific Research, Bangalore, India under my supervision and that it has not been submitted elsewhere for the award of any degree or diploma.

_____

C. N. R. Rao

(Research Supervisor)

Acknowledgements

I am indebted to my advisor Prof. C. N. R. Rao, FRS. He suggested all my research problems and guided me throughout my long days. He has been a constant source of inspiration for me and certainly I acquired most, if not all, my scientific knowledge from him. Everybody who knows our professor would greatly admire his enthusiasm towards science and I am not an exception to it. Sir constantly reminds me that one could be happy by just doing science. I now realize that he has shaped a role model of a researcher and teacher in my mind. I express my hearty gratitude to him for giving me an opportunity to work under his esteemed guidance.

I am thankful to the past and present chairmen of CPMU for allowing me to use the facilities of the center.

I would like to express my sincere thanks to Dr. A. Govindaraj who has helped me a great deal in carrying out the various experiments. It has been a good learning experience working with him in the lab.

My sincere thanks to my seniors, Dr. G. Gundiah, Dr. F.L. Deepak, Dr. U.K. Gautam, S.R.C. Vivekchand and Dr. K. Sardar for helping me out in the various research problems.

I am thankful to Basavaraj, Usha Madam, Anil, Vasu, Selvi and Dr. Basavaraj for their help with the SEM, TEM, XRD, UV/IR FESEM and AFM studies. I thank Neena, Bhuvana and Angappane for their help with the XPS measurements. I thank Vengadesh, Pranab and Madhu for their help with the magnetic measurements. I am thankful to Nivas for FESEM studies. I thank Krishna for the AFM studies. I thank Dr. Ranjan Datta for the HRTEM images from TITAN.

I am thankful to all the faculty members of JNC. In particular, I would like to thank Prof. G. U. Kulkarni, Prof. Swapan Pati, Prof. Umesh V Waghmare, Prof. Chandrabhas Narayana, Prof. K. S. Narayan, Prof. A. Sundaresan and Dr. M. Eswaramoorthy for their courses.

I would like to thank my lab members Dr. Sardar, Kanishka, Sandeep and Urmi for their help and co-operation. My special thanks to Urmi with whom I have spent my significant amount of time in the Nitride Lab.

My heartfelt thanks to my next door neighbors and friends in AMRL who have put up with me for five long years, DJ, Saiki, Dutta and Piyush from catalysis lab, Rakesh, Reji and Kalyani from synthesis lab, Claudy, Chappar, Krishna, Kalyan, Dr. Angshuman, and Jyoti from ceramics/frameworks lab and pain Guru, strong Sameer, Prakash and Sudip Boss from molecular materials lab. Not really next door but my thanks are due Nivas, Neenu, Bhat, Subbu, Anupama, Barun, Pearl, Dr. Late, Dr. Prasanth and Manjunath from NanoLab. I really appreciate the discussions I had with Krishna, Rakesh and Nivas from which I benefitted a lot. I thank my scholar's roommates for their support and arguments, both scientific and non-scientific. My special thanks to Krishna and Claudy for our valuable tea times.

I thank Avinash, Joey, Gopalakrishnan, Reshma, Ramya, Sundar and Jafar for their help in carrying out some of my projects.

I would like to thank Mrs. Indumati Rao for her encouraging words and hospitality. I think I would never be able to forget madam, for she always had a warm smile and kind words for me. And more importantly her dinners were always par excellence. I also thank Mr. Sanjay for his hospitality.

I thank Mrs. Shashi, Mrs. Sudha, Mr. Gowda Mr. Victor and Mr. Xavier for their help. I thank Mr. Srinath and Mr. Srinivas for technical help. I thank Mr. Arokiyanathan, Mr. Narsimamoorthy and Mr. Sunil for their help.

I am thankful to Shithal, Satish, Vikas, Dharma, Ravi and Nishaj of computer lab for their help.

Special thanks to Claudy, Dhava, Ganpathi, Selvi, Siva and Venky for- though many would come into one's life, only a few could make such a difference that it changes your way of living.

My parents, Venkat anna, and Subati, they were always there on my side when I needed them. They not only allowed me to pursue what I wanted, but were really supportive. Hema Aunty and Nagaraj Uncle helped me lot in their own ways. And from Harish, I have learnt a lot like how to love doing science, hard work, music, trekking etc. He has made my life much easier which could have been otherwise without him. I cannot express my thanks and love for them in words. Maybe I will just have to spend the rest of my life showing them how grateful I truly am.

Preface

This thesis consists of three parts. In Part 1 of the thesis, a simple and novel method for the synthesis of metal nitrides and oxynitrides in which urea is used as the nitrogen source is described. The various binary nitrides prepared by the reaction of urea with metal halides and metal oxides are BN, TiN, NbN, γ-Mo_2N and δ-MoN. The ternary nitrides prepared by heating metal molybdates with urea are Fe_3Mo_3N, Co_3Mo_3N and Ni_2Mo_3N. The oxynitrides prepared by the heat treatment of alkaline earth carbonates and metal oxides with urea are $CaTaO_2N$, $SrTaO_2N$, $BaTaO_2N$, $SrNbO_2N$, $BaNbO_2N$, $LaTaON_2$, $LaTiO_2N$ and $SrMoO_{3-x}N_x$. All these materials have been characterized appropriately. The urea route has been used to coat carbon fibers and other one-dimensional inorganic nanostructures with ceramic BN.

Part 2 of the thesis deals with the functionalization and solubilization of inorganic nanomaterials such as nanoparticles of CeO_2, Fe_3O_4 TiO_2, ZnO, Fe_2O_3, BN and GaN, nanowires of TiO_2, ZnO and Al_2O_3 and carbon nanotubes. The strategies employed for the functionalization includes use of the surfactants and interaction with organosilane or organotin reagents. The functionalized-materials were suitably characterized. Using polyoctasilsesquioxane (POSS)-functionalized inorganic nanoparticles, composites of polymers have been prepared and characterized.

Part 3 describes the investigation of two-dimensional graphene-like WS_2. The methods used to synthesize inorganic graphene analogues of WS_2 are to intercalate bulk WS_2 with lithium followed by exfoliation in water and by heating tungstic acid with thiourea in a nitrogen atmosphere. Few-layer WS_2 was characterized by using atomic force microscopy, Raman spectroscopy and other techniques.

Contents

Part 3 Graphene Analogues of WS_2

List of Abbreviations

XRD – X-ray Diffraction

SEM – Scanning Electron Microscope

FESEM – Field Emission Scanning Electron Microscope

EDAX – Energy Dispersive X-ray

TEM – Transmission Electron Microscope

HRTEM – High Resolution Transmission Electron Microscopy

SAED – Selected Area Electron Diffraction

FTIR – Fourier Transform Infrared Spectroscopy

TGA – Thermogravimetric Analysis

XPS – X-ray photoelectron spectrum

FC – Field Cooled

ZFC – Zero Field Cooled

UV-vis – Ultraviolet and visible

PL – Photoluminescence

FWHM – Full Width at Half Maximum

0-D – zero-dimensional

1-D – one-dimensional

2-D – two-dimensional

CNT – Carbon nanotubes

MWNT – Multi-Wall Carbon nanotubes

SWNT – Single-Wall Carbon nanotubes

EG – Exfoliated Graphene

CTAB – cetyltrimethylammonium bromide

SDS – sodium dodecyl sulphate

PEG – polyethylene glycol

PEO – polyethylene oxide

TX-100 – Triton X-100

PVA – polyvinyl alcohol

AOT – sodium bis(2-ethylhexyl) sulphosuccinate

APTES – γ-aminopropyltriethoxysilane

HDTMS – hexadecyltrimethoxysilane

TEOS - Tetraethylorthosilicate

POSS – Polyoctasilsesquioxane

DMF – Dimethyl formamide

CCl_4 – Carbon tetrachloride

PART 1

Novel Urea-based Synthetic Route to Metal Nitrides and Oxynitrides

Summary[*]

This chapter of the thesis deals with the synthesis and characterization of metal nitrides and oxynitrides and coating of BN on inorganic nanostructures by urea route. Urea route is a method of synthesis of nitrides in which urea is used as nitrogen source. In a typical synthesis, compounds of metal whose nitride we desire, is ground with urea in different ratios followed by a heat treatment in a nitrogen atmosphere. By heating mixtures of H_3BO_3, $TiCl_4$, and $NbCl_5$ with urea in 1:6 molar ratios in the 1173-1273 K range, nanoparticles of BN, TiN and NbN have been obtained respectively. By carrying out the urea reaction over Au islands deposited on Si substrates, nanowires of TiN could be obtained. Nanoparticles (~ 4 nm diameter) of cubic γ-Mo_2N were prepared by the reaction of $MoCl_5$ with urea at 873 K. The nanoparticles show a superconducting transition around 6.5 K. The γ-Mo_2N nanoparticles are readily transformed to nanoparticles of δ-MoN with a slightly larger diameter on heating in a NH_3 atmosphere at 573 K. Phase-pure δ-MoN obtained by this means shows a superconducting transition around 5 K. The nanoparticles of γ-Mo_2N and δ-MoN exhibit magnetic hysteresis at 300 K as a surface property, just as nanoparticles of various oxides.

For the synthesis of the ternary nitrides, the respective molybdates were used as precursors. The nitrides were obtained by heating the molybdate precursors, $FeMoO_4$, $CoMoO_4$ and $NiMoO_4$ with urea in the 1:12 molar ratio and heating the mixture in the 1173–1273 K range in a N_2 atmosphere. Fe_3Mo_3N and Co_3Mo_3N are obtained in pure form. The nickel nitride has the composition Ni_2Mo_3N and therefore is in admixture with nickel.

Ternary metal oxynitrides of the formulae $MTaO_2N$ (M = Ca, Sr or Ba), $MNbO_2N$ (M = Sr or Ba), $LaTiO_2N$ and $SrMoO_{3-x}N_x$ are obtained by heating the corresponding metal

carbonates and transition metal oxides with excess urea. The materials have been characterized by x-ray diffraction and other physical techniques.

The process of coating BN on carbon fibers, carbon nanotubes and inorganic nanowires involved heating them with a mixture of H_3BO_3 and urea, followed by heat treatment at 1273 K in a N_2 atmosphere. We have been able to characterize the BN coating by transmission electron microscopy as well as x-ray photoelectron spectroscopy. The urea decomposition route affords a simple method to coat boron nitride on one-dimensional nanostructures.

* Papers based on above studies have been published in *Mater. Res. Bull.* ***(2006)****, J. Solid State Chem.* ***(2007)****, Mater. Res. Bull.* ***(2007)****, Mater. Sci. Eng. A* ***(2008)*** *and J. Solid State Chem.* ***(2009)****.*

1.1 Introduction

Search for new materials remains one of the major driving forces in contemporary solid state chemistry. Metal nitrides constitute an important class of materials which display structures and properties which differ from those of the better-known and more widely studied metal oxides and their properties can complement metal oxides in a variety of applications. For most elements of the periodic table, significantly fewer nitrogen compounds as compared to oxygen compounds are known. This is because, in the synthesis of nitrides, the dominant factor in nitride thermodynamics is the strong N_2 triple bond (941 kJ mol^{-1} versus 500 $kJmol^{-1}$ for O_2, for example). The enthalpy of dissociation of N_2, which is about two times larger than that of the O_2 molecule, makes direct reaction with nitrogen sometimes difficult. This also implies that nitriding reactions are generally high-temperature reactions and that they often involve nitrogen containing species, such as ammonia, which are more reactive than molecular nitrogen [1].

Compared with the corresponding metal oxides, the thermal dissociation of many nitrides with evolution of N_2 occurs at much lower temperatures. Thus, the elimination of N_2 from Si_3N_4 occurs at atmospheric pressure at about 2173 K, while SiO_2 can heated above 2273 K [2]. The affinity of most elements for oxygen is larger than that for nitrogen, thus the bond energies for element-oxygen bonds are generally higher than those of the corresponding element-nitrogen bonds. The formation of oxides is thus an important side reaction in the synthesis of nitrides. Thus, the preparation of nitrides in a pure state requires the complete exclusion of oxygen and this has certainly played an important role in hindering a detailed investigation of nitrides.

The above factors often make the solid state chemistry of the nitrides unusual and sometimes unique.

✓ *Binary nitrides*

Binary nitrides have considerable utility, yet the search for new nitrides has, until recently, been almost completely neglected. Juza and Laurent in Europe and Ward in the USA were among the few who published studies of ternary nitrides in the 6Os, 70s and early 80s. In the past half dozen years or so, the systematic study of ternary and more complex nitrides has really accelerated. These studies, initiated principally in the groups of Kniep and Jacobs in Germany and DiSalvo in the USA, and now continued by these and many other groups, show that synthesis and structural features of nitrides are often quite different from those of oxides, sulphides or phosphides. Indeed, unique features are often encountered in metal nitrides.

Nitrogen, the main component of the atmosphere, is omnipresent. The lightest element in the fifth mail group plays an important role in chemical compounds, in particular in the nitrides in which the oxidation state of nitrogen is –III. As shown in Figure 1.1, non-molecular binary nitrides are not as extensive as binary compounds of oxygen, sulphur or phosphorous, all of which combine with a wider variety of metals, such as the alkali metals, most of the late transition metals, and heavy main-group metals. Although there are reports of amorphous nitrides of the heavy main group metals, they all decompose at a few hundred degrees Celsius before crystallizing [3-6]. The structures of binary nitrides are often simple and familiar. For example, rare earth and many transition metal nitrides of composition MN have the rock salt structure. These compounds are hard, metallic (or semimetals in the case of the rare earths) and refractory; therein often lies the utility of some of the binary nitrides. Among the theoretically possible binary nitrides, many are either nonexistent or have until now not been applied in a pure and well-defined form because of their low stability.

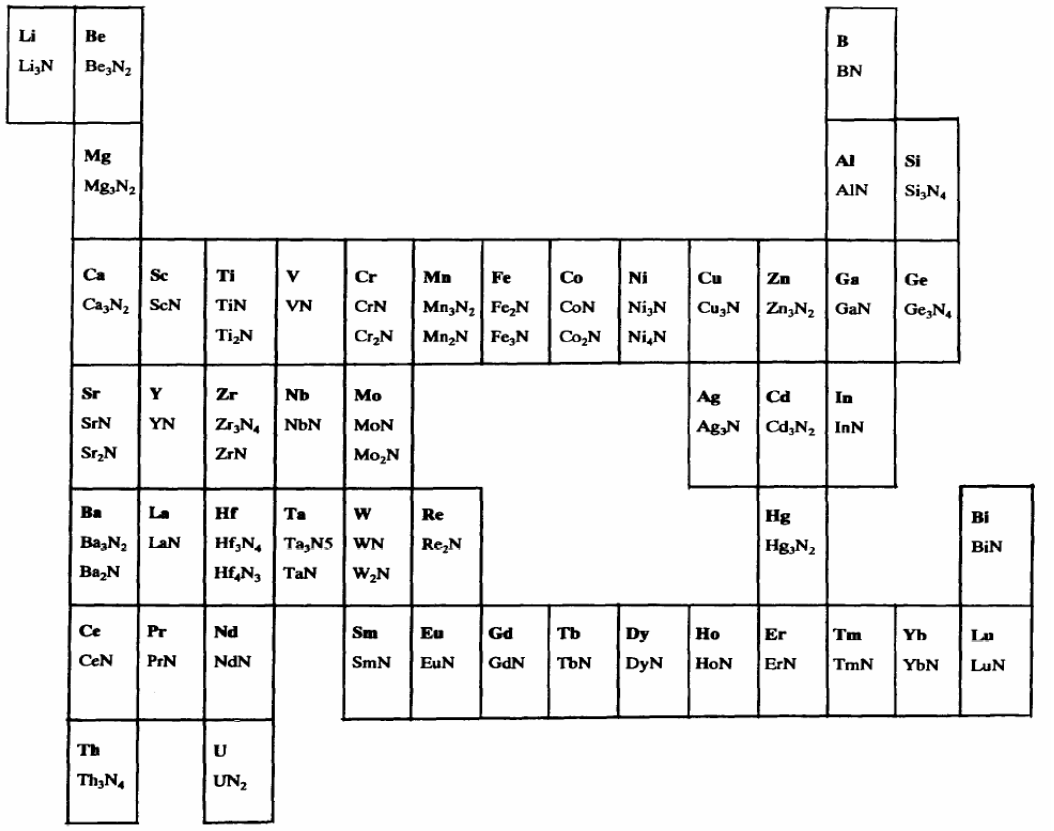

Figure 1.1: Periodic table showing the occurrence of the common binary nitrides.

Li_3N exhibits an unusually high tendency for formation, the reaction between lithium metal and molecular nitrogen starts at room temperature and atmospheric pressure. In contrast, there is no reliable evidence for the existence and the stability of analogous compounds of the heavier alkali metals. Apparently in the nitrides M_3N (M = Na, K, Rb, Cs) the high formal charge of the nitride ion make it impossible to form a stable ionic compound. For the alkaline earth metals, binary nitrides with the composition M_3N_2 are known for all elements.

In contrast to the ionic structures of the nitrides of lithium and alkaline earth metals, the elements from the third group onwards form nitrides with more covalent character. As the

group number increases, the heavier homologues in their highest oxidation state show a clearly decreasing tendency towards the stable binary nitride formation.

Inspite of this relatively small number, the nitride family includes some extremely useful compounds, for example boron nitride (BN). Hexagonal BN has a crystal structure similar to graphite; hence it is called 'white graphite'. However, it is an electrical insulator and intensively used as a carbon substitute for its much higher chemical inertness, especially at high temperature. BN does not interact with molten metals and have higher oxidation resistance than carbon [7, 8] and hence is used as a high-temperature crucible material, as a lubricant and in abrasives sector. Such excellent properties promote the broad applications of BN, which include high-temperature insulators, self-lubricating and heat dissipating coatings, passivation layers, diffusion masks and wear-resistant coatings [9, 10]. BN does not occur in nature and was first prepared in 1842 by reacting molten boric acid with potassium cyanide. However, it was not produced commercially until 1950s. Many methods have been used for the production of BN such as reacting boron oxide or boric acid with ammonia or urea at 1173-1773 K.

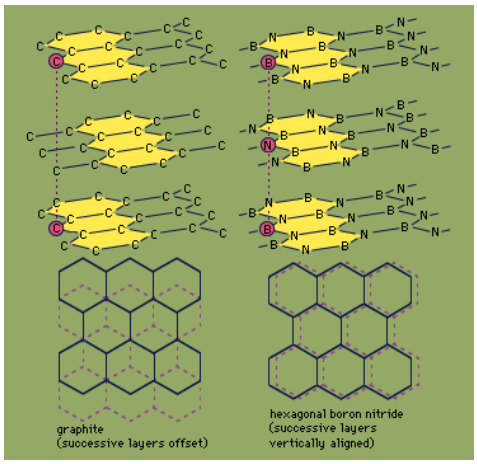

Figure 1.2: Comparison of structure of graphite and BN

Titanium nitride (TiN) which crystallizes in a B1 structure, space group *Fm3m*, may occur in a wide range of compositions. TiN exhibits a very broad range of interesting and

potentially valuable physical and chemical properties. TiN has been utilized to provide wear-resistant coatings for cutting tools and diffusion barriers in silicon semiconductor devices [11, 12]. Because of its gold-like color, TiN is used for scratch-resistent decorative coating [13, 14]. Among the transition metal nitrides, niobium nitride (NbN) has received a great deal of attention, owing to its high hardness, high wear resistance, high melting point, good temperature stability, good chemical stability at high temperature and superconducting properties [15].

Molybdenum nitrides, as materials with significant catalytic properties, have gained growing interest. There has been an increasing number of reports on molybdenum nitrides as heterogeneous catalysts for several hydrotreating reactions in petrochemical process [16], ammonia synthesis [17], ethane hydrogenolysis [18], carbon monoxide hydrogenation [19] and catalytic decomposition of hydrazine in satellite microthrusters [20]. At the same time, nitrides of molybdenum are well known as superconductors with superconducting properties retained over a wide range of nitrogen composition. Molybdenum nitride phases known to-date include the stoichiometric, hexagonal compound δ-MoN, and two nonstoichiometric compounds, cubic γ-Mo_2N and tetragonal β-Mo_2N. δ-MoN is a hard material with a low compressibility, showing a superconducting transition in the 4-12 K range [21, 22]. γ-Mo_2N is also known to be a superconductor with a T_c of 5.2 K [23]. A theoretical study has predicted that γ-MoN with a cubic NaCl type structure would have a superconducting T_c as high as 29 K [24].

✓ *Ternary nitrides*

Interstitial ternary nitride materials of the general formula MxM′yN; M and M′ being metals are generally much less studied than ternary metal oxides or sulfides since they are usually obtained under special reaction conditions. Many of these nitrides are closely allied to

the chemistry of their carbides i.e. they have the physical properties of ceramics and electronic properties of metals [5, 18, 25]. It is known that they exhibit a number of important properties such as superconductivity [26], catalytic activity [27-29], thermal emissivity [30], unusual magnetic behavior [31-35] and high hardness and strength [36-38] combined with good thermal and electrical conductivity. Ternary molybdenum nitrides constitute examples of promising catalytic materials. They have proved to be active and selective in processes involving hydrogen transfer reactions, such as hydrodenitogenation and hydrodesulphurizarion [39]. Recently it has been shown that the catalytic activity of molybdenum nitrides is enhanced by addition of another transition metal like vanadium [40].

✓ *Oxynitrides*

Oxynitride perovskites and related phases have received considerable attention owing to their potential applicability as nontoxic inorganic pigments and photocatalysts [41-43]. Oxynitrides can often be described as derivatives of oxides, formed by simultaneous substitutions of cation and anion components. For example, simultaneous substitution on the Ti^{+4} and O^{-2} sites converts the oxide $SrTiO_3$ to the oxynitride $SrTaO_2N$. The partial replacement of O^{-2} by N^{-3} narrows the band gap of the parent oxide by shifting its valence band edge upward. An immediate consequence of the band gap change occurs in the optical color of the compound. The d^0 perovskite oxides of Ta^{+5}, Nb^{+5}, or Ti^{+4} are white whereas the corresponding oxynitrides with the decreased band gaps from UV to visible light region can exhibit various colors ranging from white to yellow to brick-red to dark brown, which has an implication to the pigment applications. Most of the currently used pigment materials contain hazardous components to be replaced in the long run, for which the oxynitrides are considered a promising candidate [44].

✓ *BN coating on nanostructures*

Discovery of carbon nanotubes [45] has attracted significant interest to nanoscale one-dimensional structures. Prospective miniaturization of electronic devices relies primarily on well-structured inorganic nanowires or nanotubes. Significant efforts have been made with respect to the synthesis of assembling multiple nanotubes and/or nanowires [46-49]. Hexagonal BN is a covalently-bonded system with exceptionally strong sp^2 planar bonds. The desirable mechanical, electronic, thermal, and chemical properties of these materials suggest that BN may form a useful component in many nanosystems, especially as a coating material. Thus BN coating should be valuable for using the nanowires as a separate layer between semiconductor nanowire and electronic substrate due to the insulating nature of the BN [50], and as a promoting component for large field-emitting enhancement factor due to its negative electron affinity [51]. Indeed, it has been shown that surface addition of BN can greatly enhance the electron field-emission characteristics of carbon nanotubes, Si tips, and GaN films [52-54].

✓ *Synthetic strategies for nitrides*

In this session the basic methods generally employed for the preparation of the nitrides are described. The two most common methods for the commercial synthesis of nitrides which resort to a gas + solid reaction are discussed below followed by other synthetic procedures those are mainly developed for the preparation of various nitrides in nano-regime or some specially desired high surface area nitride materials for catalytic applications.

➢ *Elemental combination*

The first method consists of synthesizing a nitride through the direct combination of elements. This method is commonly used with electropositive metals such as rare earth metals. The nitriding temperature is generally between 1073 K and 1473 K and depends on

the mutual reactivity of both elements. The difficulty in preparing these nitrides lies mainly in the precautions which need to be taken, since traces of both moisture and oxygen must be avoided. At a given temperature, the reactivity of an element for oxygen is always greater than that for nitrogen. Thus, under nitriding conditions, a very low oxygen partial pressure is enough to irreversibly cause the displacement of nitrogen and the formation of an oxygenated product.

- ***Ammonolysis***

The second method concerns the reaction of ammonia with an oxide called ammonolysis. Volpe and Boudart [55] developed temperature programmed ammonolysis, which involves heating the metal oxide in flowing NH_3 while slowly raising the temperature. In this process often a topotactic relationship between the reactants and the products exists and the product can be pseudomorphic with the reactant, i.e. crystallographic orientations and particle size and geometry are retained from the reactant solid. The replacement of oxide by nitride ions can also generate porous, lower density nitride materials. This process can be used to prepare both nitrides and oxynitrides. Ammonia acts both as a reducing and as a nitriding agent. The reaction is carried out in flowing gas, and not under a static atmosphere as in the first method. The rate of ammonia flow depends on the temperature of the reaction: the higher the temperature, the higher the rate, because the dissociation of NH_3 into nitrogen and hydrogen must be minimized before there is any contact with the product. It has been shown that an equivalent mixture of nitrogen + hydrogen has no effect on oxides under the same conditions. The general equation is:

$$MO_x + NH_3 \longrightarrow MN_y + H_2O$$

It is clear that the reaction is not total: part of the ammonia is dissociated, and nitrogen and hydrogen coming from this dissociation help drive away the water produced by the reaction. This method, which uses, from a thermodynamic point of view, an out-of equilibrium reaction, is especially well-suited for the nitriding of refractory oxides.

In both the above mentioned synthetic pathways, the success of the reaction mainly depends upon the reactivities of the metal or metal oxides employed. So many a times either the reaction is incomplete or the elemental combination often leaves metal impurities in the product. To overcome this difficulty, highly reactive high surface area metal nanoparticles were synthesized and then were heated in N_2 or NH_3 to give the desired nitrides. This essentially reduced the reaction time and ensured the completion of the reaction. Metal chlorides are also commonly used as precursors to nitrides via CVD, often with ammonia present as the nitrogen source. Marchand et. al. [56] have shown that not only metals and oxides but high surface area sulfides and alkaline ternary oxides can also be used as precursors in ammonolysis reaction to obtain nitrides.

- ***Mechanochemical milling***

Nanocrystalline nitrides have also been obtained by combining elements under mechanochemical milling conditions [57]. This involves ball milling the metal powder under N_2 or NH_3, which continuously exposes new metal surfaces, increasing adsorption of the nitrogen species. Reactive surfaces are produced by the shearing action of the steel balls and friction between the balls increases the local temperature of the metal. Adsorbed nitrogen is pumped by successive collisions into the particles and their size is gradually reduced from the mm to the nm level. Reaction times tend to be long (several days) and large pressures of N_2/NH_3 can be required. Sometimes post-reaction annealing is applied.

- ***Metathesis***

Solid state metathesis has been effective in generating transition metal, main group and lanthanide nitrides. It involves reactions between metal halides and alkali or alkaline earth nitrides such as Li_3N, Mg_3N_2, Ca_3N_2 and NaN_3, yielding the metal nitride and alkali/alkaline earth salt. Reactions may be initiated by grinding reagents together at room temperature, heating in a furnace or igniting with a filament. Reactions are often highly exothermic due to the lattice energy of the alkali/alkaline earth halide, and are self propagating if the heat generated is sufficient to keep the halide in the molten state to act as a flux. Despite the very high temperature, small crystallites and occasionally some metastable phases can be obtained.

- ***Solvothermal method***

The word solvothermal is used simply to describe reactions carried out in a solvent above its boiling point, thus in an autoclave with autogenous pressure. For nitride synthesis typically a metathetical process like those described in the previous section is carried out in a solvent. The solvent dissipates the enthalpy of the exothermic metathetical reaction and reduces the diffusion barrier between reactants. Hence the reaction occurs at lower temperature providing better control over the size and morphology of the particles. Synthesis of TiN and NbN nanocrystals by the benzene-thermal route (using $TiCl_4$ in the case if TiN and $NbCl_5$ for NbN and NaN_3) is an example for the solvothermal route [58, 59]. One possible method to control particle size and reduce aggregation is to add a capping agent to solvothermal reactions. For example the solvothermal reaction between gallium cupferron and hexamethyldisilazane has been carried out in toluene with N-cetyl-N,N,N-trimethylammonium bromide [60].

- ***Decomposition of molecular precursors***

Molecular precursors can contain nitrogen for incorporation into the nitride (single source) or the nitrogen can be added from a second reagent (dual source). Often precursor decompositions or reactions are carried out at relatively low temperature followed by heat treatment of the amorphous product, so crystallite size can be controlled by the heating time and temperature. Molecular precursors have two major advantages in producing nanocrystalline nitrides. They can give access to different phases to those obtained by other routes, due to the possibility of performing structural motifs before crystallisation. They also are the most likely possibility for coming up with general synthetic strategies to capped nanocrystals. The literature on nitrides is this form is limited at present to GaN and InN. For example, Sardar et. al. [61] have employed single source urea precursor to synthesize group 13 metal nitride semiconductor nanostructures.

1.2 Scope of the present investigations

Exploring synthetic methods for **binary metal nitrides** such as BN, TiN, NbN and MoN_x is of interest because of the useful properties of these materials. These nitrides have been prepared by various means in bulk form and in some instances in the form of nanostructures. Chopra et al. [62] reported the synthesis of BN nanotubes by arc discharge between a BN-packed tungsten rod and a cooled copper electrode. Synthesis of BN nanotubes starting from boron powder, iron oxide and ammonium chloride has been reported [63]. Deepak et al. [64] have reported MWNT/activated carbon assisted synthesis of BN nanotubes and nanowires from boric acid. The synthesis of single-crystalline TiN nanorods by the metathesis reaction between $TiCl_4$ and NaN_3 was reported recently by Joshi et al. [65], while the preparation of TiN nanocrystals by the reaction of $TiCl_4$ and $NaNH_2$ was reported by two

groups [66, 67]. The metathesis reaction involving $TiCl_3$ and Ca_3N_2 also produces TiN nanorods [68]. Niobium nitride (NbN) nanocrystals were prepared by the reaction of $NbCl_5$ with NaN_3 by Shi et al. [69]. The benzene-thermal route has also been employed to synthesize NbN [58]. Identification of γ-Mo_2N as a catalytic material has led to considerable research efforts directed towards its synthesis. Most of the work reported has involved synthesizing the material by reacting the oxide with NH_3 at elevated temperatures. A process that has received much attention is the temperature programmed reaction of MoO_3 with NH_3 [27]. Other than this following are some of the methods by which molybdenum nitrides are synthesized. Lengauer [70] has investigated the formation of γ-Mo_2N and δ-MoN by the reaction between $MoCl_5$ and ammonia while Bull et al. [21] obtained phase-pure δ-MoN by this reaction carried out at 933 K. Marchand et al. [56] obtained powders of δ-MoN and Mo_5N_6 by the ammonolysis of MoS_2. Nanocrystalline γ-Mo_2N and δ-MoN with T_c values of 3.8 K and 7.5 K respectively, have been prepared by heating hydroxylamine complexes of molybdenum in NH_3 [71].

Transition metal-molybdenum **ternary nitrides** are technologically important class of materials owing to their potential catalytic activity [72]. The ternary interstitial nitrides, M_3Mo_3N (M = Fe, Co) were first synthesized by Bem et al [73] by ammonolysis of oxides and reported to be isostructural to η-Fe_3W_3C. Another approach to synthesize ternary nitrides of the type MWN_2 (M = Fe, Ni, Co) has been to heat the respective ternary oxide precursor in NH_3 [74-76]. Weil et al. [77] reported the synthesis of Fe_3Mo_3N, $FeWN_2$, Ni_3Mo_3N and Ti_3AlN using complex precursors. Synthesis of Fe_3Mo_3N by the ammonolysis of the oxide precursor has been reported [78]. The ternary nitride, Ni_2Mo_3N, has been prepared by heating a metalloraganic precursor in NH_3 [79]. Alconchel et al. [80] have reported a study on the influence of preparative variables on the ammonolysis of the molybdate precursors. Both the ammonolysis as well as plasma nitridation of $FeMoO_4$ and $CoMoO_4$ result in the respective

intermetallic nitrides [81]. Synthesis of Fe_3Mo_3N and Co_3Mo_3N by mechanochemical alloying and by the nitridation of the corresponding ternary carbide has also been reported [82].

Stoichiometric **perovskite oxynitrides** can be synthesized with $A^{+2}M^{+5}O_2N$, $A^{+3}M^{+4}O_2N$, or $A^{+3}M^{+5}ON_2$ type formulae. Other hypothetic compositions of $A^{+1}M^{+6}O_2N$, $A^{+2}M^{+6}ON_2$, or $A^{+4}M^{+4}ON_2$ families might be also designed but have not been realized yet. Oxynitrides of tantalum and niobium were synthesized by the ammonolysis of the corresponding metal oxides and alkaline earth carbonates [44, 83]. Clarke et al [84] synthesized tantalum oxynitrides by the reaction between alkaline earth oxides and tantalum oxynitride at 1723 K. Oxynitrides of different structures, $RTaO_2N$ and $R_2Ta_2O_5N$, have been prepared by heating metal tantalates of the formula $RTaO_4$ in NH_3 at elevated temperatures [85]. Nitridation of alkaline niobiates in flowing ammonia results in ternary niobium oxynitrides depending upon the reaction temperature [86]. Oxynitrides of tantalum and niobium of the Ruddlesden-Popper family are obtained by heating stoichiometric mixtures of the alkaline earth carbonates with tantalum/niobium oxide in an ammonia atmosphere at elevated temperatures [87, 88]. $LaZrO_2N$ has been synthesized by the ammonolysis of amorphous $La_2Zr_2O_7$ while $LnTiO_2N$ (Ln = rare earth, La, Nd) has been prepared by heating the corresponding oxide precursors in ammonia [43, 89]. $ZrTiO_{1.92}N_{1.23}$ and $ZrTiO_{1.06}N_{1.90}$, which are black in color can be prepared by the ammonolysis of $ZrTiO_4$ [90].Tantalum zirconium oxynitrides of various compositions in the Ta–Zr–O–N system have been synthesized by the ammonolysis of the amorphous tantalum zirconium oxides prepared by the sol-gel technique [91]. Antoine et al [92] have synthesized $LaVO_{3-x}N_x$ by the ammonolysis of $LaVO_4$ while Ba_2VO_3N was prepared by heating $Ba_3V_2O_8$ in ammonia [93]. Thermal nitridation of rare-earth tungstates in ammonia results in oxynitrides of type $LnWO_3N$ [94, 95] and bimetallic oxynitrides of tungsten, $Ba_3W_2O_6N_2$ and Na_3WO_3N, are obtained by the ammonolysis of the respective oxide

precursors [96, 97]. $SrWO_2N$ and $SrMoO_{2.5}N_{0.5}$ have been prepared by the ammonolysis of the corresponding $SrMO_4$ (M = W, Mo) precursor [98]. Logvinovich et al [99] have recently reported the synthesis of $SrMoO_{3-x}N_x$ by the ammonolysis of $SrMoO_4$. For the synthesis of members of the V-Mo-O-N system, amorphous bimetallic oxide precursors are heated in flowing ammonia [100].

Uuniform coatings on nanostructures are of crucial importance for attaining important properties and BN is clearly one of the most suitable candidates for ceramic coatings owing to its excellent chemical and thermal stability. Chen et al. [101] have coated BN on carbon nanotubes (CNTs) by means of boric acid (H_3BO_3) infiltration followed by treatment with NH_3 at 1473 K while Yoo et al. [102] coated BN films on CNTs using a radio frequency sputtering. BN-coated SiC nanowires have been prepared by heating a mixture of Si and In_2O_3 powders in a BN crucible [103]. Gao et al. [104] obtained the BN/Si_3N_4 nanocomposite by nitriding a $Si_3N_4/NH_4HB_4O_7$ mixture in ammonia gas. Al_2O_3/BN nanocomposites have been fabricated by hot-pressing α–Al_2O_3 powders covered partly with turbostratic BN (t-BN) [105]. GaN–BN core–shell nanocables were synthesized by thermal chemical vapor deposition using $GaN/B_2O_3/NH_3$ reaction [106]. Zhang et al. [107] have reported the synthesis of semiconductor GaN nanowires sheathed with BN layers by chemical vapor deposition.

We have sought to develop a simple synthetic method for synthesis of nitrides, with specific interest in their nanostructures. For this purpose, we have chosen the urea route which involves heating a mixture of urea with an appropriate compound of boron, titanium and niobium at an appropriate temperature. In the past few years, there has been some effort to prepare metal nitrides using urea (NH_2CONH_2), which is readily available and is environmentally benign. The idea behind using urea is motivated by the fact that heating urea

at 423 K is known to yield NH_3 and thereby can replace hazardous precursors used as traditional nitrogen sources. Pure urea decomposes endothermically in several stages [108-110].

$$NH_2CONH_2 \longrightarrow HCNO + NH_3 \text{ (413 K)}$$

$$NH_2CONH_2 \longrightarrow H_2CN_2 + H_2O \text{ (413 K)}$$

$$NH_2CONH_2 + HCNO \longrightarrow H_2NCONHCONH_2 \text{ (453 K, biuret)}$$

In oxygen free atmosphere, non-oxygen containing products, H_2CN_2, $H_4C_2N_4$ and $H_6C_3N_6$ are also formed. On heating to higher temperatures however, all the nitrogen compounds decompose. In 1995 Podsiadlo et al. [109, 110] demonstrated that when urea reacts with Ga or In metal in a N_2 atmosphere it forms a mixture of metal nitrides and oxides. They could obtain pure GaN only by reacting Ga metal with urea in an ammonia atmosphere at 1123 K. In another experiment they obtained a mixture of InN, In_2O_3 and In metal at 973 K by the reaction of In metal with urea. The formation of pure InN took place only when the reaction was performed in an ammonia atmosphere. We thought it would be worthwhile to develop a relatively simple method to synthesize nitrides by using urea the nitrogen source.

1.3 Experimental and related aspects

(a) Synthesis:

1.3.1 Metal Nitrides

Binary metal nitrides

The basic synthetic procedure employed for the synthesis three binary nitrides was to heat a compound of boron, titanium or niobium with urea at an appropriate temperature. The compounds used for this purpose were H_3BO_3, $TiCl_4$, and $NbCl_5$.

In the synthesis BN, 100 mg of H_3BO_3 and 600 mg of urea, taken in the molar ratio 1:6 was ground to give an intimate mixture. The mixture was then taken in an alumina boat and heated in a tube furnace at 1273 K for 3 h in a N_2 atmosphere.

In the case of TiN, a $TiCl_4$-urea complex ($TiCl_4$:urea::1:6) was prepared by mixing $TiCl_4$ with urea in acetonitrile medium. In order to synthesize the $TiCl_4$-urea complex, about 0.2 ml of $TiCl_4$ was dissolved in acetonitrile to give a yellow solution and to this was added 700 mg of urea dissolved in acetonitrile. The solution was stirred for 2 h to ensure the completion of the reaction. Then the complex was heated at 1173 K for 3 h in a N_2 atmosphere. The golden yellow product obtained at the end of the reaction was collected for further analysis.

TiN nanowires were prepared by thermal decomposition of the $TiCl_4$-urea complex in the presence of gold nanoclusters as catalyst. First 10-20 nm thick films of Au nanoclusters were deposited using DC sputtering technique on selected area of Si (100) substrates by the help of a mask. In each reaction approximately 30-50 mg of the $TiCl_4$-urea complex was placed on the top of the Au coated Si (100) substrates on an alumina boat. Figure 1.3.1.1 shows the schematic of the experimental set up.

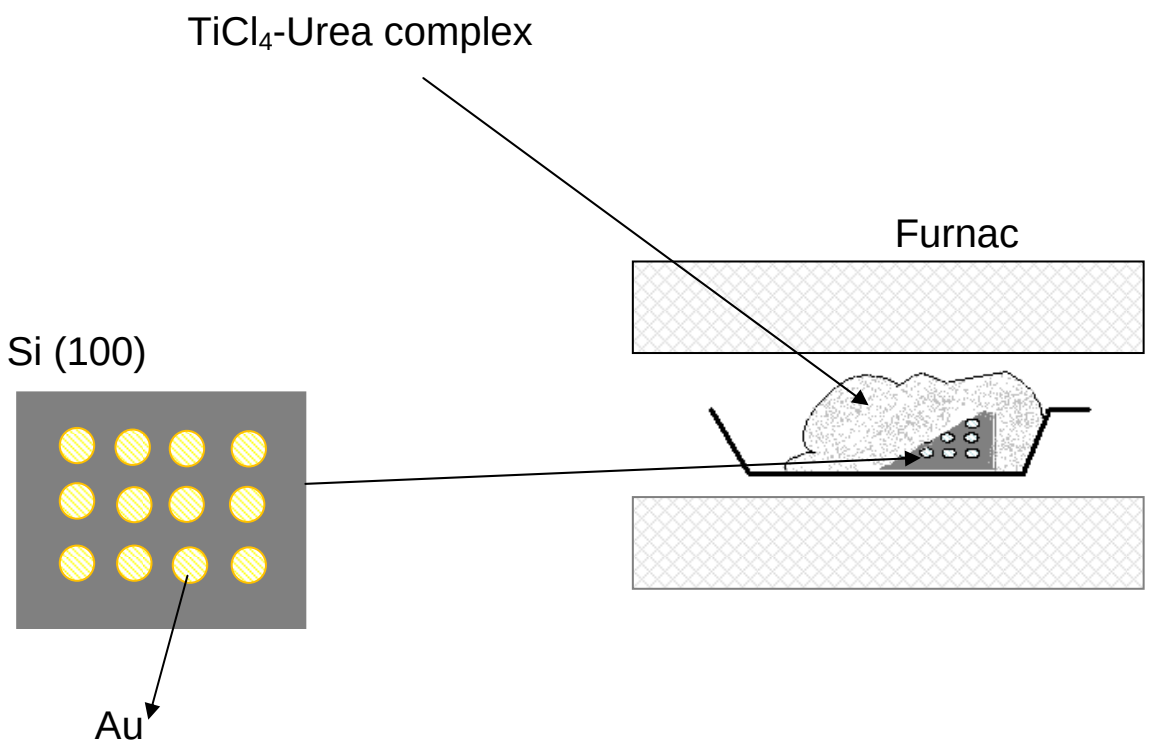

Figure 1.3.1.1: Schematic of the strategy used for the growth of TiN nanowires.

To synthesize NbN nanoparticles, a mixture of 100 mg $NbCl_5$ and 150 mg urea taken in the molar ratio 1:6 was ground well and the resulting mixture was heated at 1173 K for 3 h in a N_2 atmosphere. The resulting product was silver-grey in color.

For the synthesis of γ-Mo_2N a mixture of $MoCl_5$ and urea taken in the molar ratio 1:12 was heated at 873 K in an inert atmosphere. In a typical reaction 0.273 g of $MoCl_5$ was mixed with 0.720 g of urea. The mixture was then placed in an alumina boat and heated at 873 K in a quartz tube furnace for 3h in a N_2 atmosphere. The product obtained was black powder. Alternatively a molybdenum-urea complex can be used to synthesize γ-Mo_2N. For 0.273 g of $MoCl_5$ dissolved in acetonitrile about 0.720 g of urea in acetonitrile was added and the solution was stirred for 2h to ensure the completion of the reaction. At the end of 2h a brown precipitate was formed. The precipitate was taken in an alumina boat and heated at

873 K for 3h in a nitrogen atmosphere which resulted in a black powder. δ-MoN was synthesized by heating γ-Mo_2N obtained by the above reaction in NH_3 atmosphere for 72h.

Ternary nitrides

***(i) Synthesis of oxide precursors*:**

The metal molybdates were prepared by the dropwise addition of 400 mL (0.25 M) of an aqueous solution of the metal chloride ($FeC1_2$, $CoCl_2$ or $NiC1_2$) to a 150-mL (0.55 M) $Na_2MoO_4.(H_2O)_2$ solution, and the solution stirred for 2 h to ensure completion of the reaction. The solid product was isolated by vacuum filtration and rinsed with two washings of distilled water followed by a washing with ethanol. The solid was air-dried overnight followed by a drying at 423 K for 24 h. The products were amorphous and had brown, violet and green colors in the case of $FeMoO_4$, $CoMoO_4$ and $NiMoO_4$ respectively.

***(ii) Synthesis of the ternary nitrides*:**

To prepare the nitrides, an intimate mixture of the molybdate precursor and urea taken in a molar ratio 1:12 was taken in an alumina boat. The boat was then placed in a quartz tube furnace. Prior to the heat treatment, the furnace was purged with nitrogen for 15 minutes to ensure an inert atmosphere. The molybdate-urea mixture was then heated at 1173 K for 3 h in a N_2 atmosphere. In the case of all nitrides the product obtained was black in color.

1.3.2 Metal Oxynitrides

Metal oxynitrides were prepared by the nitridation of alkaline earth carbonates and transition metal oxides with urea. To obtain crystalline metal oxynitrides, a stoichiometric (with respect to the cations) mixture of an alkaline earth carbonate and a transition metal

oxide ground with excess urea was taken in an alumina boat, placed in quartz tube and then heated at 1223 K for 3 h in a N_2 atmosphere.

Metal oxynitrides of type $MTaO_2N$ (M = Ca, Sr or Ba) were prepared as follows. A stoichiometric mixture of the corresponding $CaCO_3$, $SrCO_3$ or $BaCO_3$, and Ta_2O_5 was ground with excess urea. The mixture was placed in an alumina tube kept inside a quartz tube located in a tubular furnace. The furnace was purged with nitrogen to remove any oxygen present and the temperature raised to 1223 K at a heating rate of 12 K/min and held at that temperature for 2 h. The furnace was cooled to room temperature in a nitrogen atmosphere. The colored products obtained were collected for further analysis.

Metal oxynitrides of type $MNbO_2N$ (M = Sr or Ba) were prepared employing a procedure similar to that of $MTaO_2N$ with a slight modification. Here, $SrCO_3$ or $BaCO_3$ was ground with Nb_2O_5 (Sr, Ba : Nb :: 1 : 1) and excess urea and the mixture was placed in an alumina boat kept inside the quartz tube. The furnace was heated at a rate of 10 K/min upto 1123 K and held at that temperature for 1 h. After that the temperature was raised to 1123 K in 10 min and held at that temperature for 1 h. After the reaction, the temperature was lowered to room temperature in a nitrogen atmosphere and the samples were collected for analysis.

We attempted to synthesize $LaTaON_2$ and $LaTiO_2N$ by heating a stoichiometric mixture of La_2O_3 with Ta_2O_5 or TiO_2 along with excess urea at 1223 K. The La_2O_3 used was pre-heated at 1173 K for 12 h prior to the reaction. In the case of $LaTiO_2N$, an amorphous oxide precursor containing required proportions of La and Ti ions, obtained by the sol-gel technique, was also heated with excess urea. The oxide precursor was prepared by the polymerized complex (PC) method [89] wherein 5.7 g of titanium tetraisopropoxide and 8.7 g

of $La(NO_3)_36H_2O$ were dissolved in 98.8 g of ethylene glycol at room temperature. 76.4 g of anhydrous citric acid, and 102.0 g of methanol was added to the solution, and the mixture was stirred at 403 K until a transparent gel was formed. The polymer was carbonized at 623K and calcined in air at 923 K for 2 h to remove carbon. The amorphous oxide precursor was heated with excess urea.

1.3.3 Coating of BN on one dimensional nanostructures

Multi-walled carbon nanotubes (MWNTs) were prepared by the arc-discharge method and functionalized by nitric acid treatment as reported in the literature [111]. MWNTs so obtained had an outer diameter of 25 nm. Carbon fibers prepared by the pyrolysis of PANI were obtained from National Physical Laboratory, New Delhi. The fibers had a diameter of 7 μm. Al_2O_3, SiC and GaN nanowires were synthesized by the carbothermal reduction method [112-114]. Treating the nanowires and carbon fibers with dilute HNO_3 functionalized their surfaces. The acid-treated MWNTs and inorganic nanowires were dried under dynamic vacuum at 353 K. The basic procedure employed for producing BN coating was to treat the carbon fibers or the inorganic nanowires with a mixture of H_3BO_3 and urea in the molar ratio of 1:6, followed by heat treatment at 1273 K for 3 h in a N_2 atmosphere. The 1:6 H_3BO_3-urea mixture was prepared by concentrating an aqueous solution containing 100 mg of H_3BO_3 and 600 mg of urea by heating. The acid-treated carbon fibers were kept in the H_3BO_3-urea mixture for an appropriate time period depending on the desired coating thickness. In order to get a heavy coating, the fibers were kept in the mixture for about 3 h at 343 K. In order to reduce the thickness of the coating, the fibers were taken out after dipping them in the H_3BO_3-urea mixture for 1h. The carbon fibers so treated were placed in an alumina boat and heated in a tube furnace at 1273 K for 3h under flowing N_2. For coating MWNTs and

nanowires with BN, the acid-treated nanotubes and nanowires were treated with the H_3BO_3-urea mixture for 1h, followed by heat treatment at 1273 K for 3 h in a N_2 atmosphere.

(b) Characterization Techniques

X-ray Diffraction: X-ray diffraction (XRD) patterns of the nitrides were recorded using Cu Kα radiation on a Rich-Siefert XRD-3000-TT diffractometer.

Scanning electron microscopy: Scanning electron microscope (SEM) images were obtained using a LEICA S440i SEM.

Field emission scanning electron microscopy: Field emission scanning electron microscopy (FESEM) images were obtained using a FEI NOVA NANOSEM 600.

Transmission electron microscopy: For transmission electron microscopy, the nitrides were dispersed in CCl_4 and dropped on to the holey carbon-coated copper grids. The grids were allowed to dry in the air. Transmission electron microscope (TEM) images were obtained with a JEOL JEM 3010, operating with an accelerating voltage of 300 kV.

Thermogravimetric analysis: Thermogravimetric analysis (TGA) was carried out on a Mettler-Toledo-TG-850 instrument

X-ray photoelectron spectroscopy: X-ray photoelectron spectra (XPS) were recorded with an ESCALAB MKIV spectrometer employing AlKα radiation (1486.6 eV).

Raman spectroscopy: Raman spectra were recorded with a LabRAM HR with the 633 nm line from HeNe laser. The excitation wavelength is 632.8 nm.

Magnetic properties: Magnetic measurements of the as-prepared powder samples were carried out with a vibrating sample magnetometer in Physical Property Measurements System (PPMS, Quantum Design).

1.4 Results and Discussion

1.4.1 Metal Nitrides

Binary Metal Nitrides

(a) BN nanostructures

The TGA curve shown in Figure 1.4.1.1 is of the mixture of H_3BO_3 and urea in 1: 12 molar ratio recorded under N_2. It showed the end product to be BN.

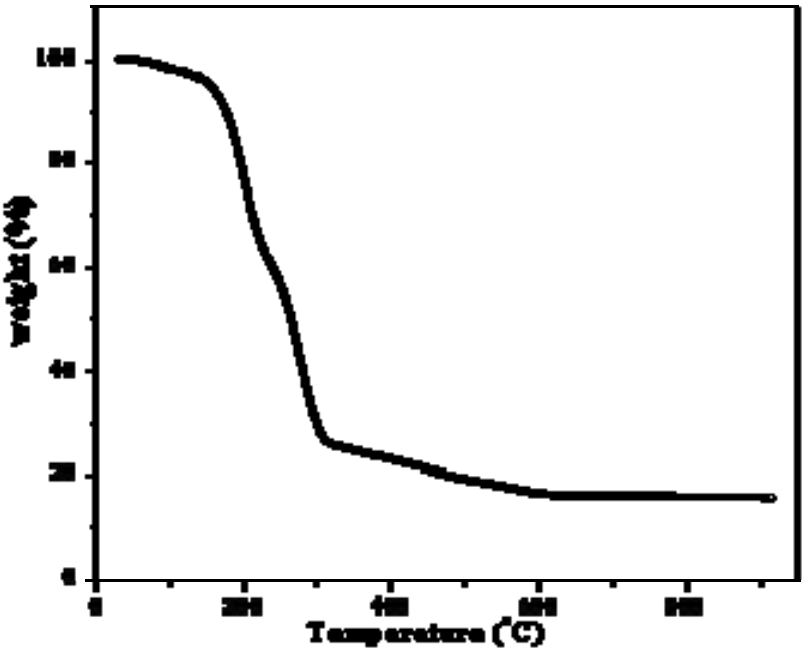

Figure 1.4.1.1: TGA curve of H_3BO_3:urea::1:12 in a N_2 atmosphere giving BN as the final product.

The formation of h-BN by heating H_3BO_3 and urea mixture is ascertained by the XRD pattern given in Figure 1.4.1.2. The pattern could be indexed with the space group $P6_3/mmc$ (JCPDS card no: 34-0421). From the pattern it is seen that the lines are rather broad and it

may be due to small particle size. By making use of the line widths, the average particle size of the h-BN is calculated from Scherrer formula and it is estimated to be 10 nm. The lattice parameters of the 10 nm particle of h-BN are a = 2.57 Å and c = 6.70 Å.

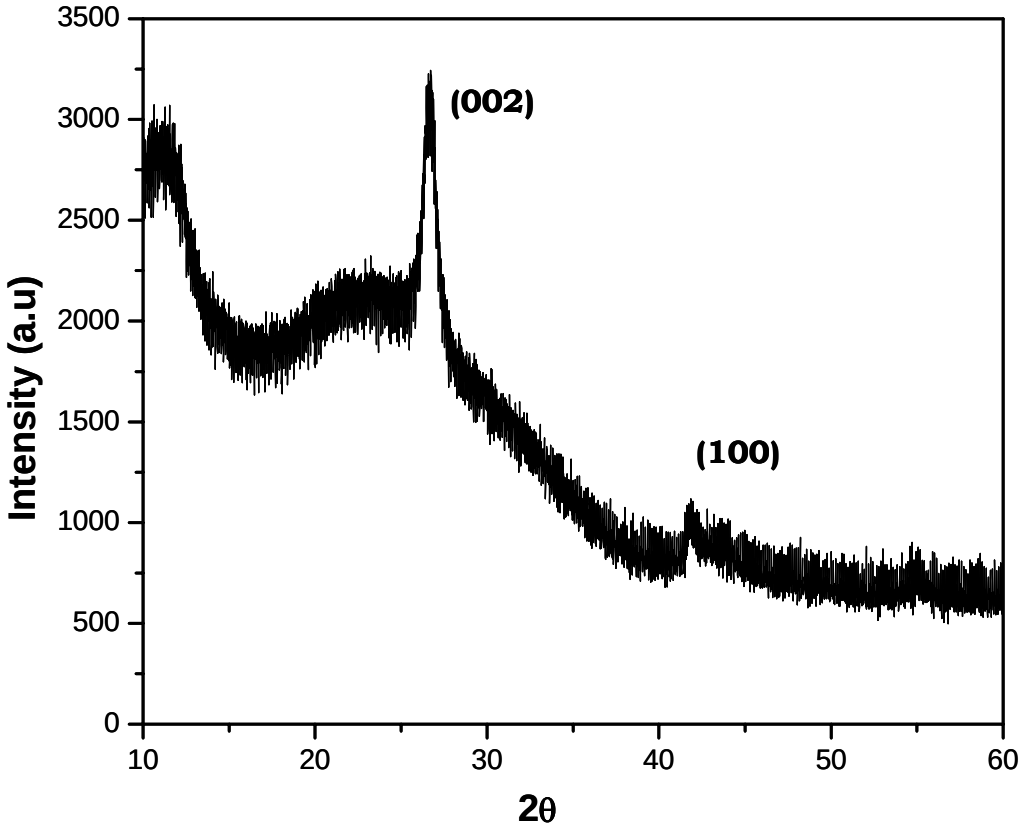

Figure 1.4.1.2: XRD pattern of BN nanoparticles.

In Figure 1.4.1.3 is given the electron microscope images of the BN nanoparticles. Figure 1.4.1.3 (a) is the SEM image of the BN nanoparticles. In Figures 1.4.1.3 (b) and (c), we have given the TEM images of the BN nanoparticles the particles appear to be elongated or rod-like and ~10 nm long in agreement with that estimated from XRD data. Figure 1.4.1.3 (d) is the high resolution electron microscope (HREM) image of the BN nanoparticles and it shows a lattice spacing of 0.33 nm corresponding to the spacing between the (002) planes of h-BN.

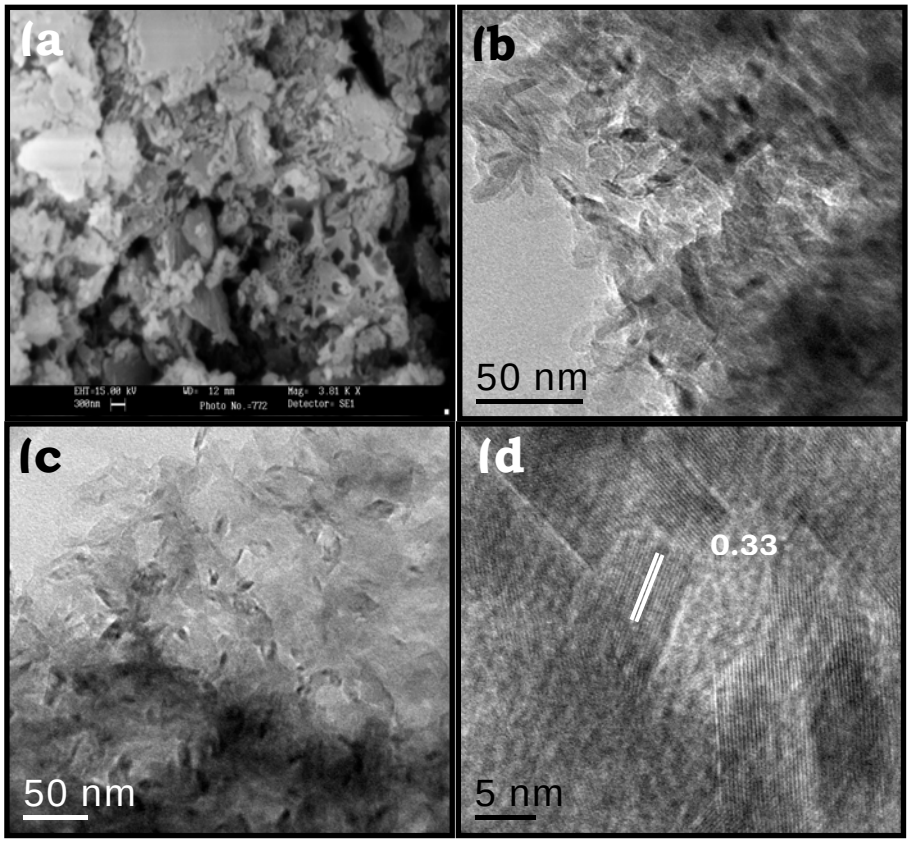

Figure 1.4.1.3: (a) SEM image of the BN particles. (b) and (c) TEM images of the BN nanoparticles. (d) HREM image of the BN nanoparticles.

We have characterized the nanoparticles of BN by XP spectrum. Figure 1.4.1.4 gives the XP spectrum of the nanoparticles which gives the characteristic binding energy (B.E) of 190 eV for B (1s) and 397.8 eV for N (1s).

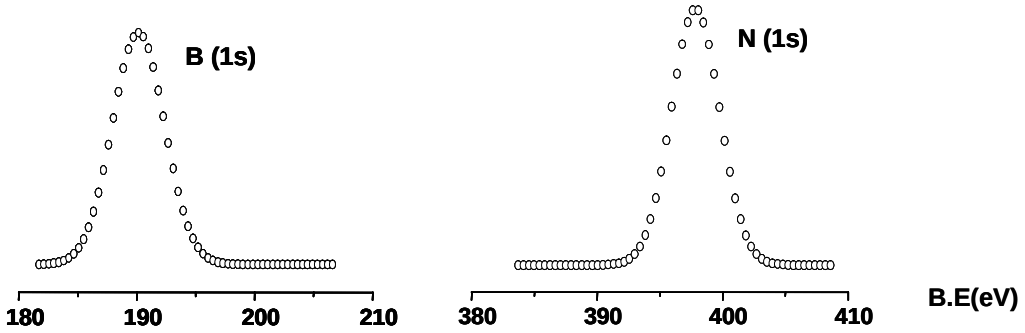

Figure 1.4.1.4: X-ray photoelectron spectrum of BN.

Figure 1.4.1.5 gives the Raman spectrum of the BN nanoparticles. The spectrum shows a dominant peak centred at 1372 cm^{-1}, corresponding to the E_{2g} vibrational mode of h-BN.

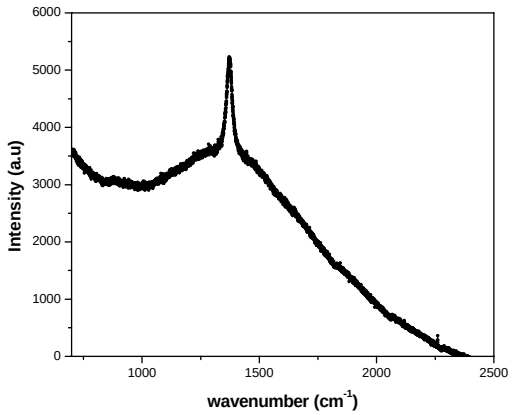

Figure 1.4.1.5: Raman spectrum of BN nanoparticles.

Heating the 1:6 H_3BO_3-urea mixture for a longer duration of 12 h at 1273 K produced BN nanotubes. Figure 1.4.1.6 (a) and (b) give the TEM images of the BN nanotubes so obtained. The inset in the Figure 1.4.1.6 (b) shows the selected area electron diffraction (SAED) pattern of the BN nanotubes with an interlayer spacing 0.33 nm characteristic of the (002) planes.

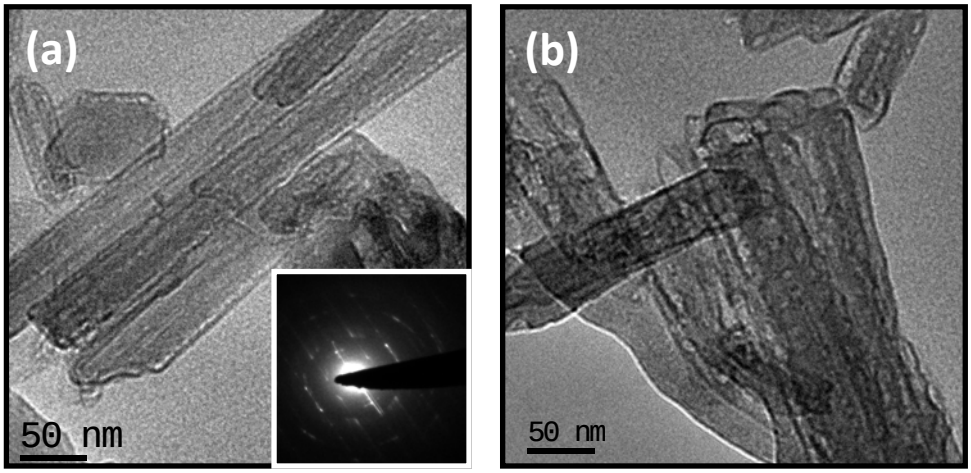

Figure 1.4.1.6: (a) and (b) TEM images of the BN nanotubes with the inset in (a) showing the SAED pattern of a tube.

(b) TiN nanostructures

The golden yellow product obtained by heating a 1:6 mixture of $TiCl_4$ and urea gave a XRD pattern shown in Figure 1.4.1.7, characteristic of cubic TiN. The pattern could be indexed with the *Fm3m* space group (38-1420) with the lattice parameter a = 4.17 Å. From the Scherrer equation based on XRD line-widths the particle size is estimated to be 35 nm.

In Figure 1.4.1.8 (a) we show a TEM image of TiN nanoparticles. The average particle size is around 35 nm and is comparable to that estimated from the XRD pattern. The SAED pattern shown in Figure 1.4.1.8 (b) shows the rings corresponding to (111), (200) and (220) planes.

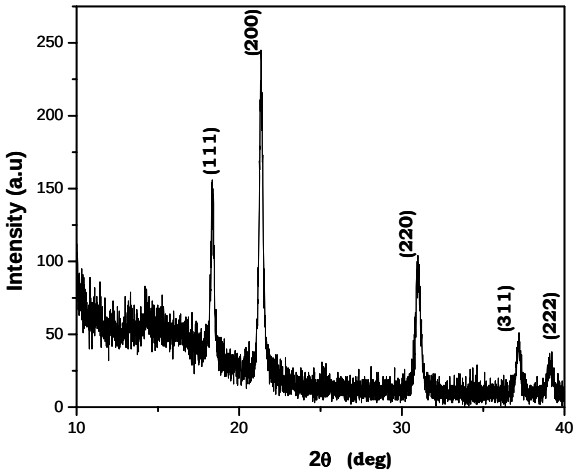

Figure 1.4.1.7: XRD pattern of TiN nanoparticles.

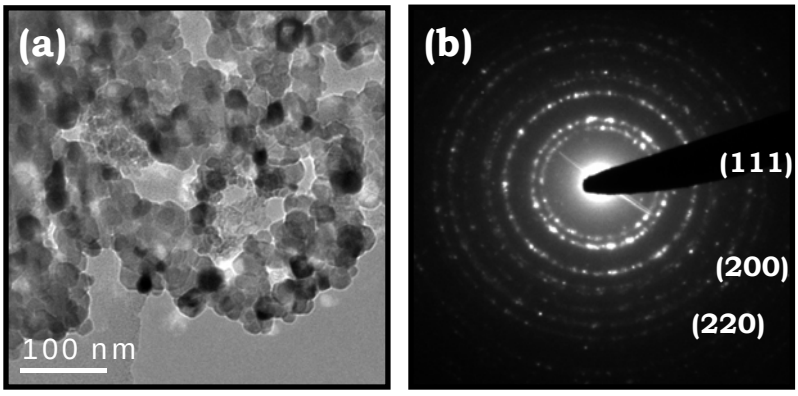

Figure 1.4.1.8: (a) TEM image of TiN nanoparticles. (b) SAED pattern of the TiN nanoparticles.

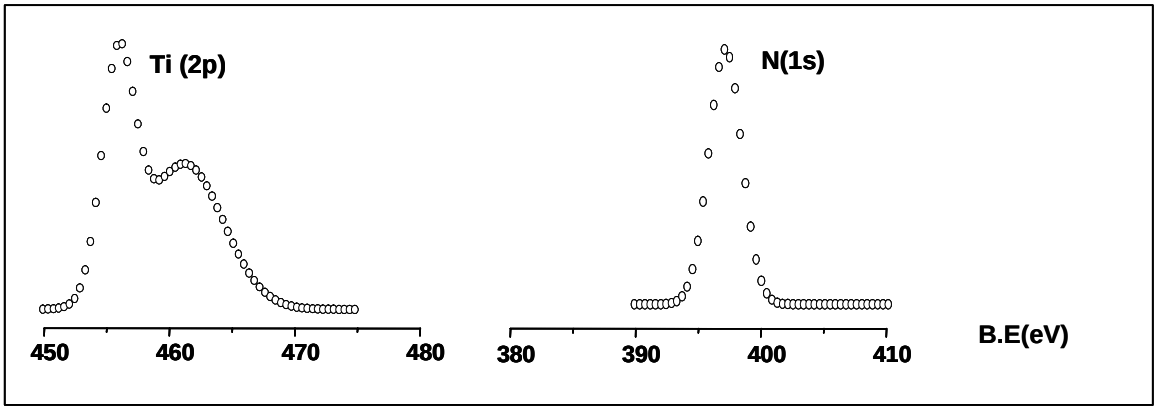

Figure 1.4.1.9: X-ray photoelectron spectrum of TiN

We have characterized the TiN nanoparticles by XPS. The XP spectrum given in Figure 1.4.1.9 gives characteristic BE values of 455 and 461 eV for Ti ($2p_{3/2}$) and Ti ($2p_{1/2}$) respectively and 397 eV for N (1s).

Figure 1.4.1.10 is the Raman spectrum of the TiN nanoparticles which shows four broad bands between 200 and 600 cm^{-1} in agreement with the literature.

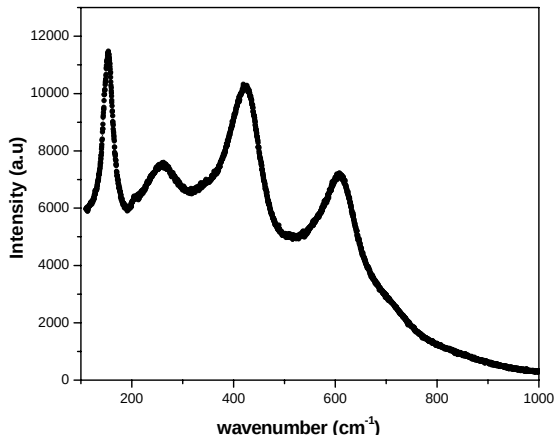

Figure 1.4.1.10: Raman spectrum of TiN nanoparticles.

In order to prepare TiN nanowires, we used Au coated Si substrates. The TiN nanowires formed on the Au islands are shown in the SEM image in Figure 1.4.1.11 (a). In Figure 1.4.1.11 (b) and as its inset are shown the TEM image and the SAED pattern of a TiN nanowire showing the (111) and (200) planes.

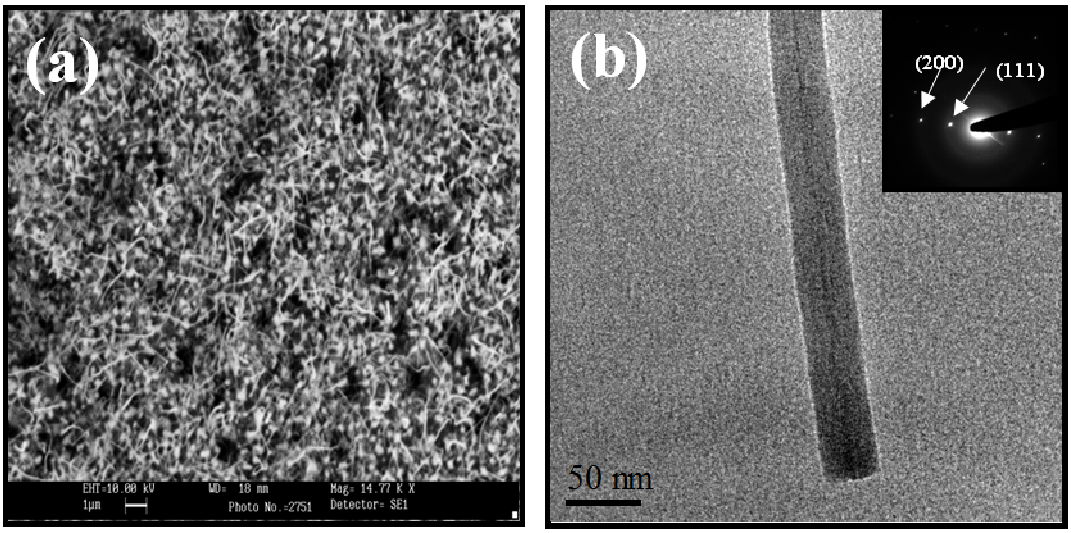

Figure 1.4.1.11: (a) SEM image of TiN nanowires. (b) and (c) TEM images of TiN nanowires. (d) SAED pattern of a TiN nanowire.

(c) NbN nanoparticles

The reaction of $NbCl_5$ with urea resulted in a silver grey product which gave a XRD pattern shown in Figure 1.4.1.12. The pattern is characteristic of cubic NbN (JCPDS = 74-1218) with lattice parameter a = 4.44 Å.

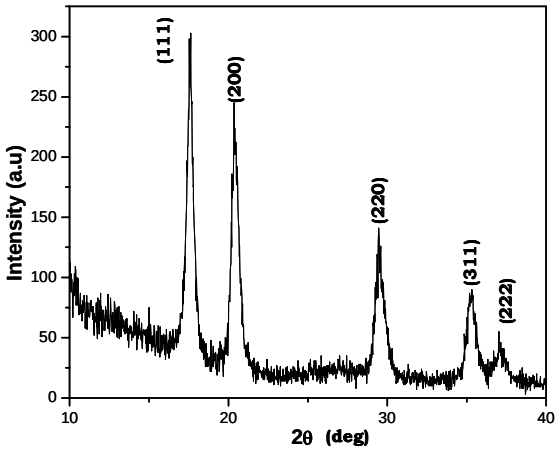

Figure 1.4.1.12: XRD pattern of NbN nanoparticles.

In Figure 1.4.1.13 (a) is shown a SEM image of NbN nanoparticles while the Figure 1.4.1.13 (b) gives a TEM image of NbN nanoparticles. The average particle size is around 20 nm which is comparable to that of estimated from the XRD line widths. The SAED pattern shown in Figure 1.4.1.13 (c) is of NbN nanoparticles and it clearly shows the rings corresponding to the (111), (200) and (220) planes. The HREM image of a NbN nanoparticle shown in Figure 1.4.1.13 (d) gives a lattice spacing of 0.22 nm corresponding to the (200) planes of NbN.

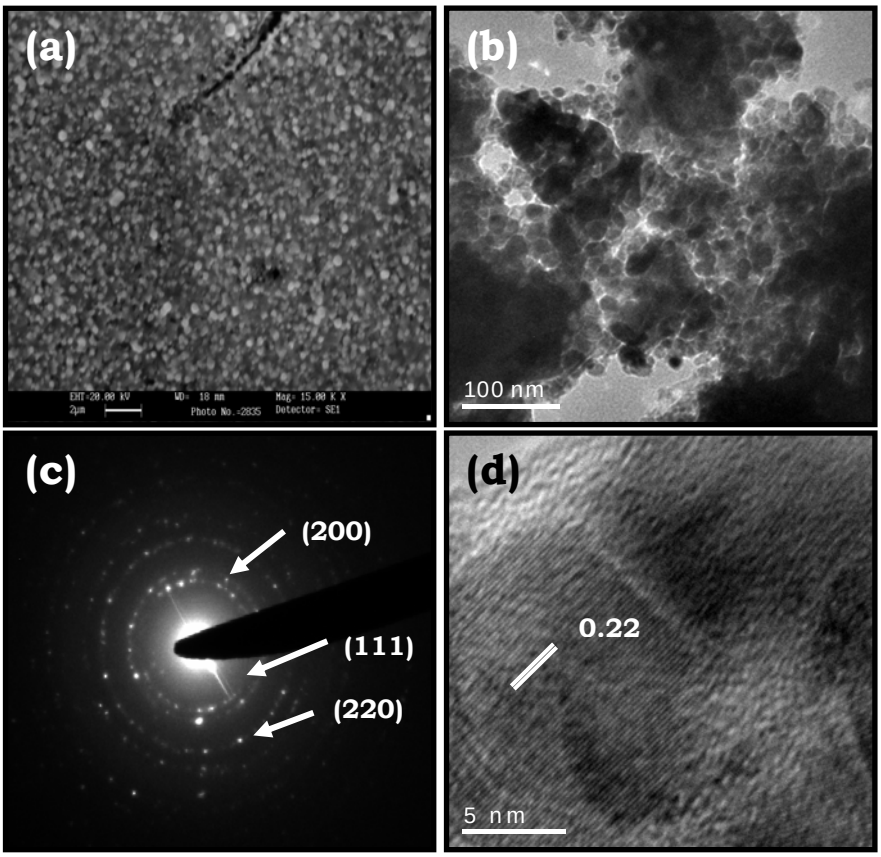

Figure 1.4.1.13: (a) SEM image of NbN nanoparticles. (b) TEM image of NbN nanoparticles. (c) SAED pattern of NbN nanoparticles. (d) HREM image of a NbN nanoparticle.

We have characterized the NbN nanoparticles by X-ray photoelectron spectroscopy. The XP spectrum of NbN particles in Figure 1.4.1.14 gives the BE values of Nb (3d) at 206.7 eV and that of N (1s) at 397 eV.

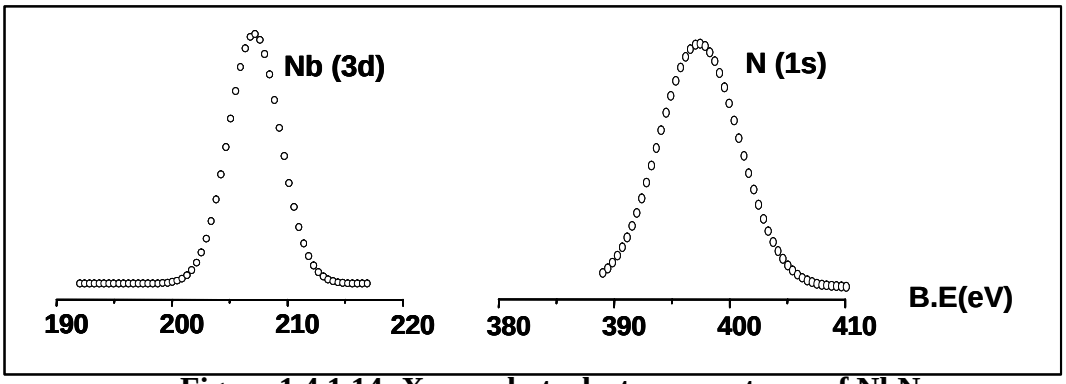

Figure 1.4.1.14: X-ray photoelectron spectrum of NbN.

(d) γ-Mo_2N nanoparticles

The product of heating the 1:12 mixture of $MoCl_5$ and urea at 873 K for 3 h gave the XRD pattern shown in Figure 1.4.1.15. The pattern is characteristic of cubic γ- Mo_2N.

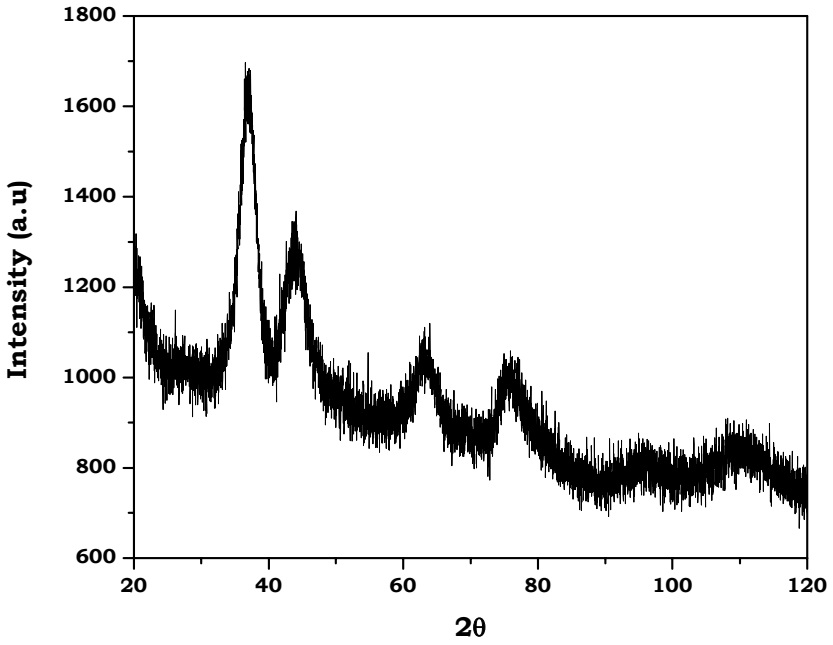

Figure 1.4.1.15: XRD pattern of γ-Mo_2N

The pattern could be indexed with the space group Pm3m (JCPDS card no: 25-1366) with a lattice parameter a = 4.1497 Å. Based on the line widths by making use of Scherrer formula we estimated the particle size to be ~6 nm.

The TEM image shown in Figure 1.4.1.16 (a) is that of as-prepared γ-Mo_2N nanoparticles. From the TEM image it is evident that the particles are agglomerated. The SAED pattern shown as inset of Figure 1.4.1.16 (a) shows rings corresponding to (111) and (200) planes. When the as-prepared γ-Mo_2N nanoparticles were sonicated in CCl_4 for 15 minutes they dispersed as evidenced by the TEM image shown in Figure 1.4.1.16 (b). From the TEM image, we calculated the average particle size to be ~4.5 nm as seen by the histogram given as an inset. The SAED pattern shown as an inset in Figure 1.4.1.16 (b) gives spots corresponding to the (111) and (200) planes of γ-Mo_2N.

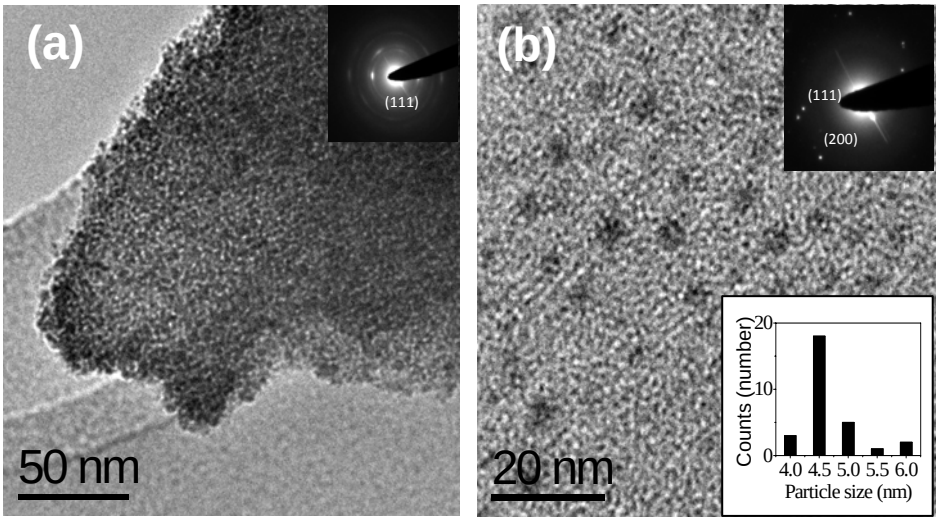

Figure 1.4.1.16: (a) TEM image of the as-synthesized γ-Mo_2N particles. The inset shows the SAED pattern of the particles (b) TEM image of γ-Mo_2N particles sonicated for 15 minutes with the inset showing the SAED pattern of a particle.

In order to calculate the stoichiometry of the γ-Mo_2N we carried out the TGA of the same in an oxygen atmosphere. In Figure 1.4.1.17 is given the TGA curve of the γ-Mo_2N carried out in oxygen atmosphere. The initial increase in mass is due to oxidation reaction. As per the mass loss, the final product corresponds to MoO_2. The XRD pattern of the product, shown as an inset in Figure 1.4.1.17, confirms the product to be MoO_2. The stoichiometry of the nitride calculated from TGA is $MoN_{0.56}$.

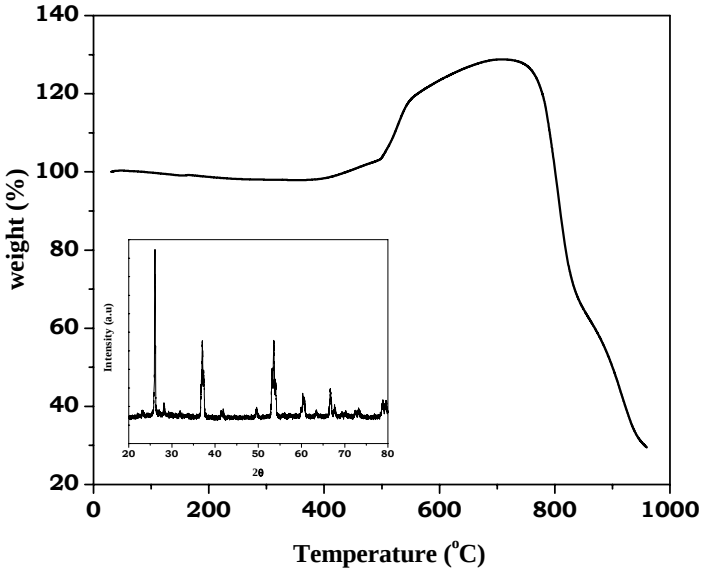

Figure 1.4.1.17: TGA of γ-Mo2N in oxygen atmosphere with inset showing the XRD pattern of the final product recorded using Cu Kα radiation.

From the literature it is known that γ-Mo_2N is known to be a superconductor with a T_c of 5.2 K [115]. In Figure 1.4.1.18, we show the results of magnetic measurements on the nanoparticles of γ-Mo_2N under zero-field-cooled (ZFC) conditions (at 19.6 Oe).

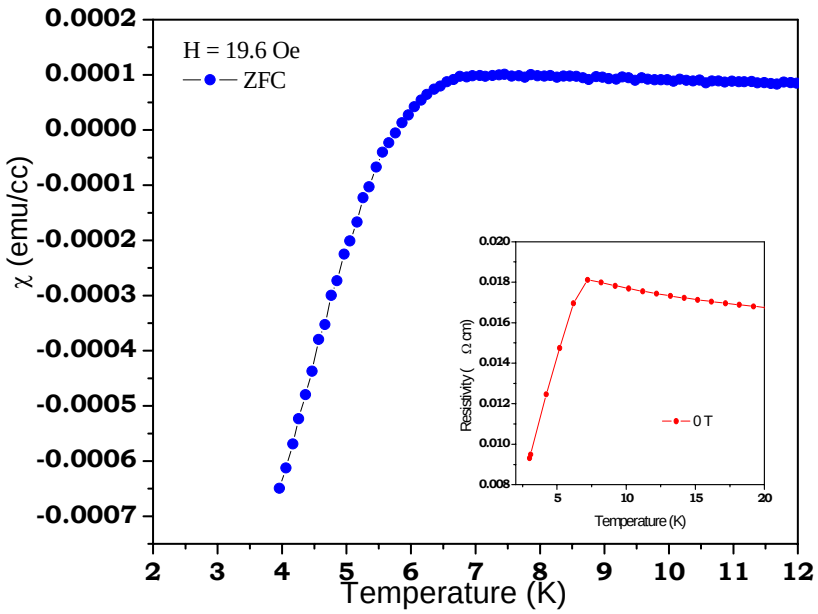

Figure 1.4.1.18: Temperature dependence of magnetic susceptibility of γ- Mo_2N nanoparticles with the inset showing resistivity of the sample as a function of temperature.

The data show a superconducting transition with an onset T_c around 6.5 K. Electrical resistivity measurements on the γ-Mo_2N nanoparticles (shown as an inset in Fig. 1.4.1.18) shows the superconducting transition with a T_c of around 7 K. The superconducting volume fraction is around 0.8 %. It is noteworthy that the nanoparticles of γ-Mo_2N with an average size of 4.5 nm exhibit superconductivity.

(e) Characterization of the δ-MoN *nanoparticles*

In order to prepare δ-MoN, we heated the 4.5 nm nanoparticles of γ-Mo_2N in a NH_3 atmosphere for 72 h at 573 K. The product gave the XRD pattern characteristic of δ-MoN as shown in Figure 1.4.1.19. It has a hexagonal structure of space group $P6_3/mmc$ with a = 5.68 Å, c = 5.56 Å (JCPDS card no: 25-1367). Based on the XRD line-widths, the particle size is estimated to be ~40 nm.

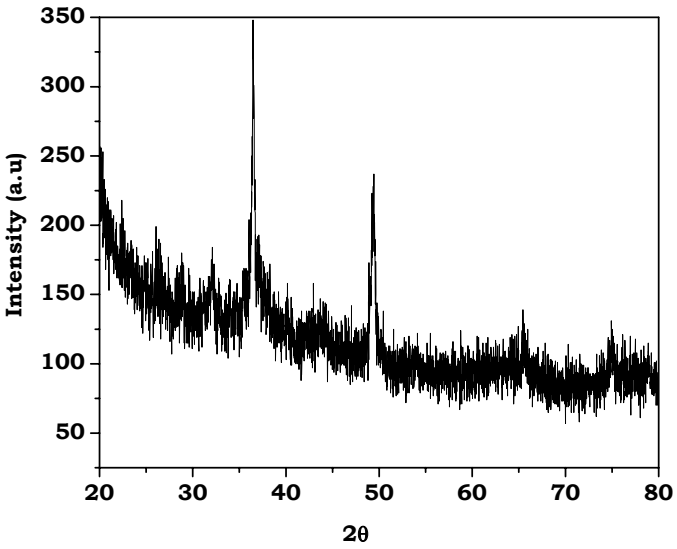

Figure 1.4.1.19: XRD pattern of δ-MoN

Figure 1.4.1.20 (a) shows the TEM image of the δ-MoN nanoparticles. From the TEM image, we estimate the particle size to be in the 30-35 nm range. It appears that the γ-Mo_2N to δ-MoN transformation in an NH_3 atmosphere is accompanied by an increase in particle size. The high resolution electron microscope (HREM) image in Figure 1.4.1.20 (b) reveals the nanoparticles to be single crystalline. It is interesting that single crystalline γ-Mo_2N transforms to single crystalline δ-MoN.

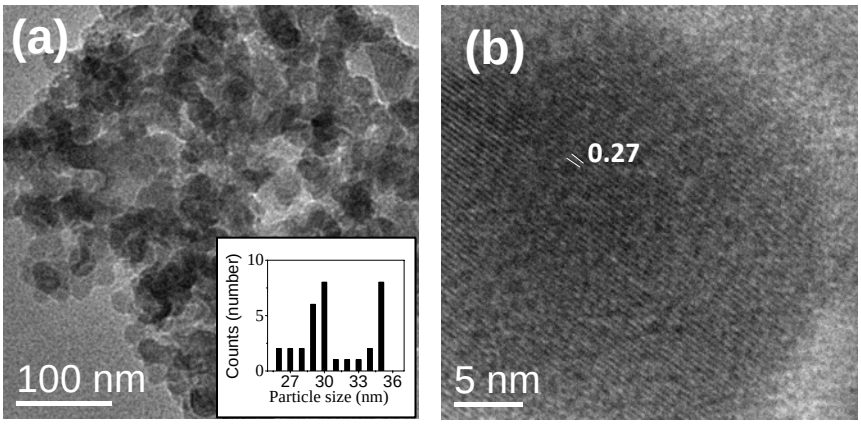

Figure 1.4.1.20: (a) TEM image of the δ-MoN nanoparticles (b) HREM image of a δ-MoN particle.

The TGA curve of δ-MoN carried out in an oxygen atmosphere is shown in Fig. 1.4.1.21. The TGA curve gave a mass loss corresponding to the formation of MoO_2 as confirmed by the XRD pattern of the product. Here again, the initial increase in mass is due to the oxidation reaction and the calculated stoichiometry of the nitride from TGA is $MoN_{0.95}$.

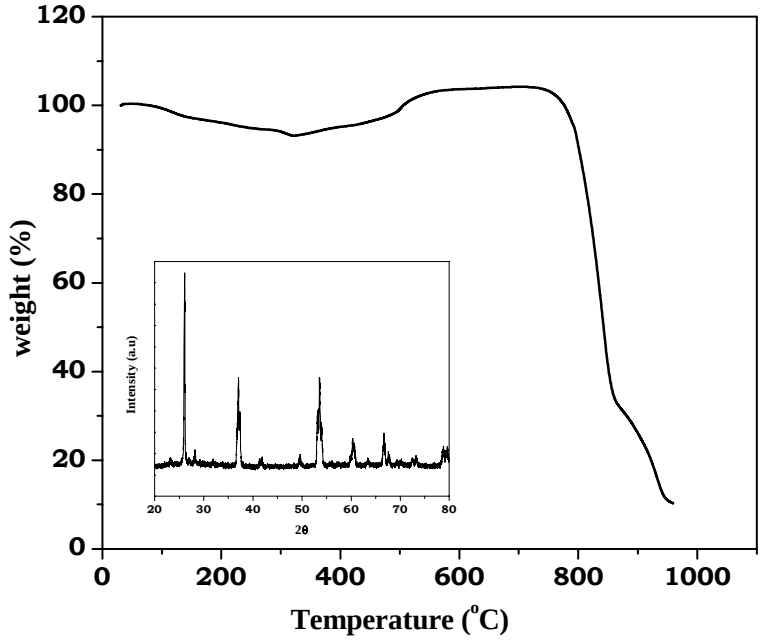

Figure 1.4.1.21: TGA of δ-MoN in oxygen atmosphere with inset showing the XRD pattern of the final product recorded using Cu Kα radiation.

We tried to prepare δ-MoN by the reaction of γ-Mo_2N with urea, but always ended with a slightly impure product. This is because when urea is decomposed at relatively low temperatures, there will be other side-products in addition to one mole of NH_3 for one mole of urea. The side products can be eliminated at high temperatures but under those conditions δ-MoN is not stable. It is known that δ-MoN is a hard material with a low compressibility, showing a superconducting transition in the 4-12 K range [21, 116]. In Figure 1.4.1.22, we show the results of magnetic measurements on the nanoparticles of δ-MoN under zero-field-cooled (ZFC) conditions (at 5 Oe). We see a superconducting transition around 5.6 K. The superconducting volume fraction is around 6.3 %. It is known that the superconducting

transition temperature of δ-MoN varies with the extent of disorder in the structure, the T_c of 4 K in highly disordered δ-MoN increasing to a value of 12.1 K in the ordered phase [116]. The T_c observed by us is in between these values.

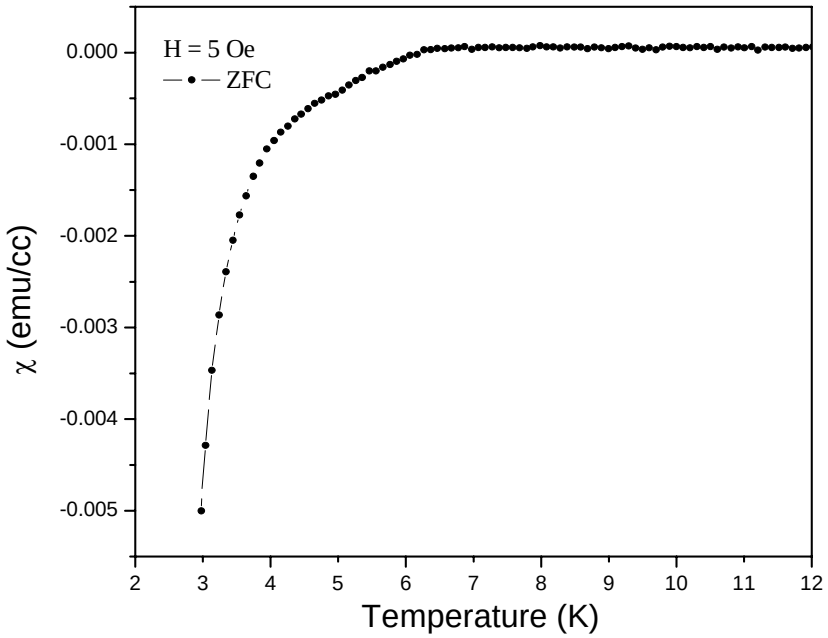

Figure 1.4.1.22: Temperature dependence of magnetic susceptibility of δ-MoN nanoparticles.

Ferromagnetism in binary metal nitride nanoparticles:

While the existence of ferromagnetism in transition metal-doped semiconducting oxides remains controversial [117], thin films of the band insulator HfO_2 have been reported to exhibit ferromagnetism at room temperature in the absence of any doping [118]. This is puzzling, since pure HfO_2 does not have any magnetic moment and the bulk sample is diamagnetic. Similar ferromagnetism has been reported in other nonmagnetic materials such as CaB_6, CaO, and SiC where the origin of ferromagnetism is believed to be due to intrinsic defects [119-121]. It has been suggested that ferromagnetism in thin films of HfO_2 may be related to anion vacancies [122]. It has been reported very recently that thin films as well as

nanoparticles of several metal oxides show ferromagnetism at room temperature, the corresponding bulk forms of these materials being diamagnetic [123, 124]. Thin films of these oxides might have defects or oxygen vacancies that could be responsible for the observed ferromagnetism. Herein we have investigated the ferromagnetism exhibited by the nanoparticles of superconducting γ-Mo_2N, δ-MoN and NbN prepared by the urea route.

Nanoparticles of γ-Mo_2N of ~4.5 nm in size were prepared by heating a mixture of $MoCl_5$ and urea taken in the molar ratio 1:12 at 873 K in an inert atmosphere. The γ-Mo_2N nanoparticles so obtained were heated in NH_3 atmosphere for 72 h to give δ-MoN. The average particle size of δ-MoN nanoparticles was 30-35 nm. NbN nanoparticles of ~20 nm were prepared by heating a 1:12 mixture of $NbCl_5$ and urea at 1173 K for 3 h in a N_2 atmosphere.

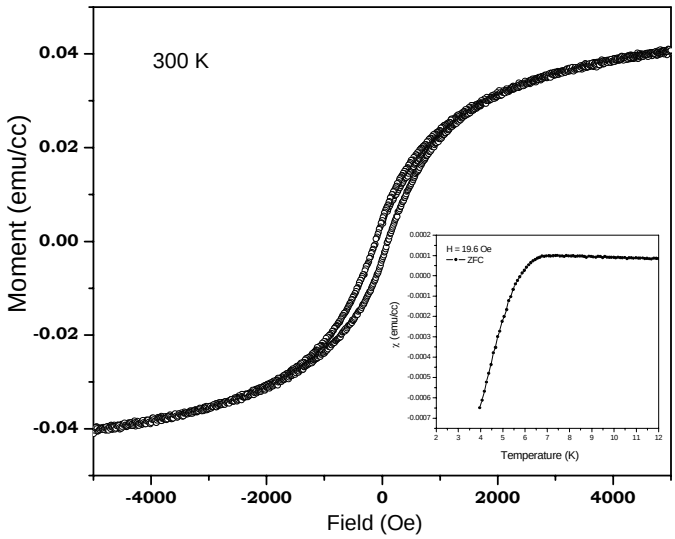

Figure 1.4.1.23: Magnetization curve of γ-Mo_2N nanoparticles at 300 K with the inset showing the superconducting transition of the same at ~6.5 K

In Figure 1.4.1.23 we show the magnetization-field curve of γ-Mo_2N nanoparticles. It is seen from the M(H) curve that the nanoparticles show ferromagnetic behavior. The γ-Mo_2N

nanoparticles show a superconducting transition with a T_c around 6.5 K. This is shown as inset in the Figure 1.4.1.23. In Figure 1.4.1.24 is shown the magnetization-field curve of δ-MoN nanoparticles with the inset showing the superconducting transition with a T_c around 5.6 K

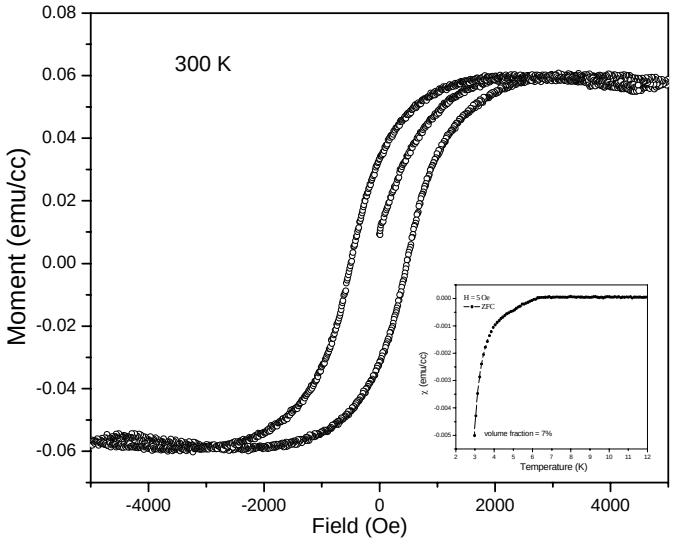

Figure 1.4.1.24: Magnetization curve of δ-MoN nanoparticles at 300 K with the inset showing the superconducting transition of the same at ~6 K

Having found magnetic hysteresis in nanoparticles of MoN_x, we attempted to see if this behavior is found in nanoparticles of other nitride superconductors. On examination, we found that the NbN nanoparticles of particle size ~20 nm in diameter with a superconducting transition around 8 K also exhibit ferromagnetic behavior at 300 K as shown in the Figure 1.4.1.25. In inset is given the variation of the volume susceptibility of the nanoparticles with temperature which gives a superconducting transition around 8 K.

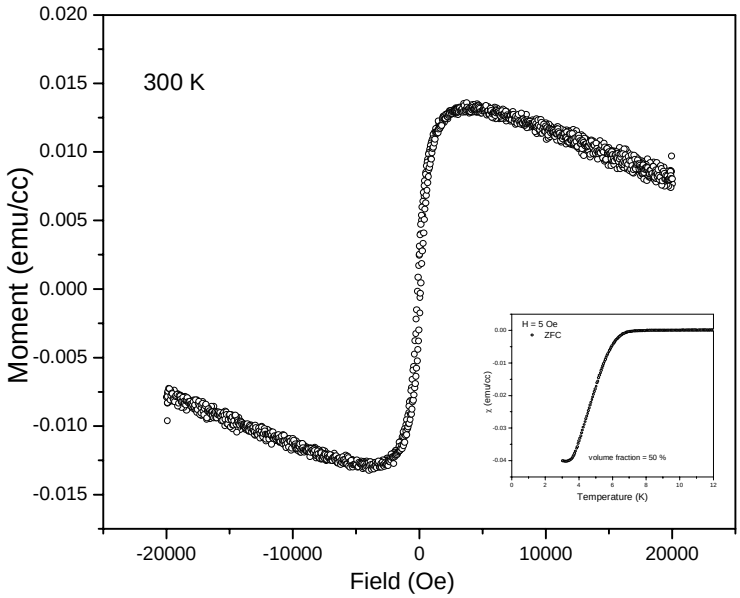

Figure 1.4.1.25: Magnetization curve of NbN nanoparticles at 300 K with the inset showing the superconducting transition of the same at ~8 K

The magnetic hysteresis found in nanoparticles of MoN_x and NbN are entirely the property of surface. We can therefore only say that the surface ferromagnetism occurs in superconducting nitrides, although below the superconducting transition temperature the magnetism could not be present. The presence of surface ferromagnetism as general characteristics of nanoparticles of metal nitrides and oxides is a significant observation.

Ternary Metal Nitrides

(a) Fe_3Mo_3N:

The product obtained by heating a mixture of $FeMoO_4$ with urea in a 1:12 molar ratio gave a XRD pattern given in Figure 1.4.1.26. The XRD pattern confirms the formation of Fe_3Mo_3N. The pattern could be indexed with the space group *Fd3m* (JCPDS card no: 48-1408) with a lattice parameter of a = 11.0620 Å. Fe_3Mo_3N adopts a pattern similar to that of the cubic *eta* carbide η-Fe_3W_3C. The structure consists of NMo_6 octahedra

that are corner shared, with the iron atoms occupying the sites between the octahedra. The iron atoms are located in 12-fold, pseudo-icosahedral coordination, surrounded by six molybdenum and six iron atoms, or four molybdenum, two nitrogen, and six iron atoms to give Fe-[Mo_6Fe_6] and Fe[$Mo_6Fe_4N_2$].

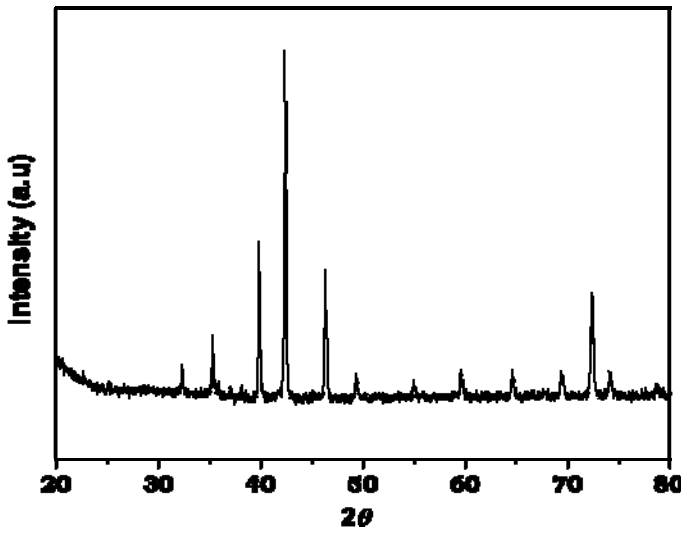

Figure 1.4.1.26: XRD pattern of Fe_3Mo_3N

We show the Mössbauer spectrum of Fe_3Mo_3N recorded at room temperature in Figure 1.4.1.27.

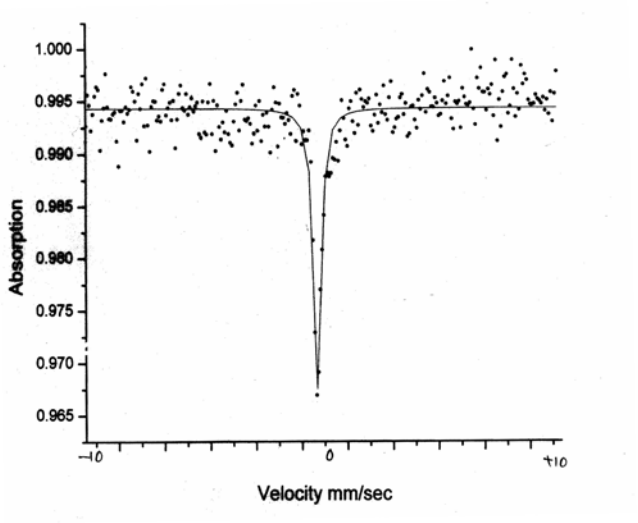

Figure 1.4.1.27: Mössbauer spectrum of Fe_3Mo_3N.

The spectrum shows a symmetric single line with an isomer shift of 0.213 mm s^{-1} characteristic of Fe_3Mo_3N as reported in the literature [78]. Mössbauer results give the distribution of iron sites. The isomer shift value, 0.213 mm s^{-1}, is very close to that of the alloys of Al-($Mn_{0.7}Fe_{0.3}$) whose isomer shift value is 0.22 mm s^{-1}. This suggests that, as in the case of icosahedral alloys, in Fe_3Mo_3N the Fe atoms are located in 12 fold, pseudo-icosahedral coordination surrounded by six Mo and six Fe atoms or six Mo, two N and four Fe atoms. That is the structure of Fe_3Mo_3N has iron atoms occupying the sites between the (NMo_6) octahedra which are corner-shared. The product consisted of sub-micrometer sized particles as revealed by the SEM image shown in Figure 1.4.1.28 (a).

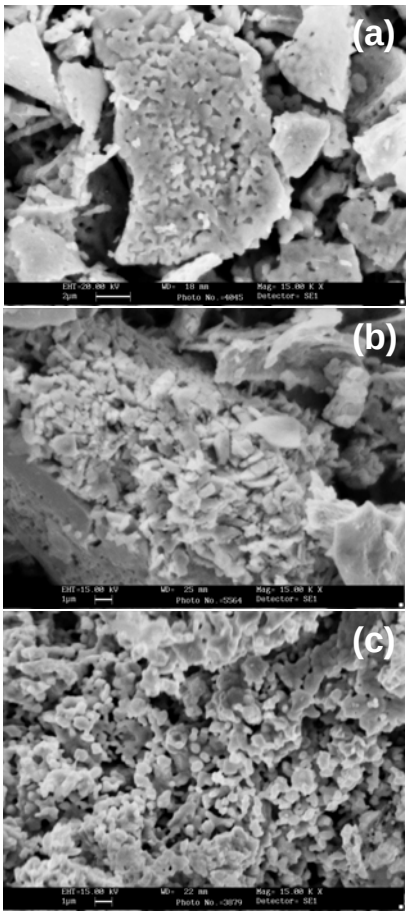

Figure 1.4.1.28: SEM images of (a) Fe_3Mo_3N (b) Co_3Mo_3N (c) Ni_2Mo_3N.

(b) Co_3Mo_3N:

By heating a 1:12 mixture of $CoMoO_4$ and urea, we obtained Co_3Mo_3N showing a XRD pattern characteristic of cubic eta carbide structure as shown in the Figure 1.4.1.29. The pattern could be indexed with the space group *Fd3m* with a cell parameter of 11.0134 Å.

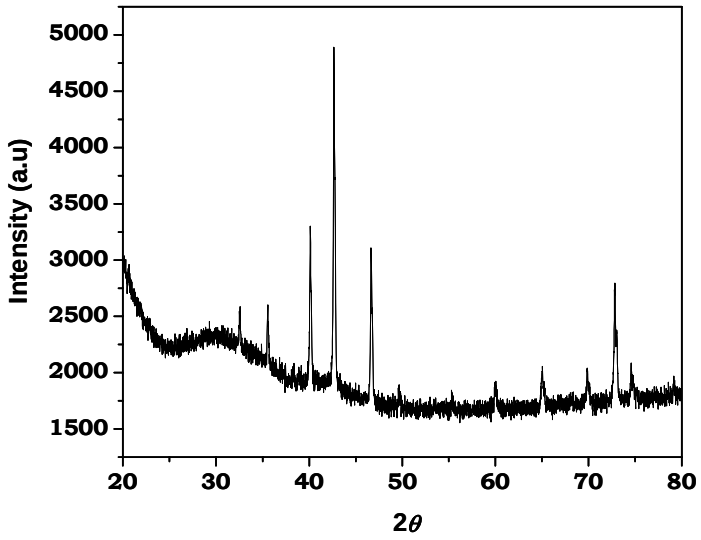

Figure 1.4.1.29: XRD pattern of Co_3Mo_3N

The product consisted of sub-micrometer sized particles as revealed by the SEM image in Figure 1.4.1.28 (b). The nitride was metallic as shown by the measurement of the temperature variation of resistivity in Figure 1.4.1.30.

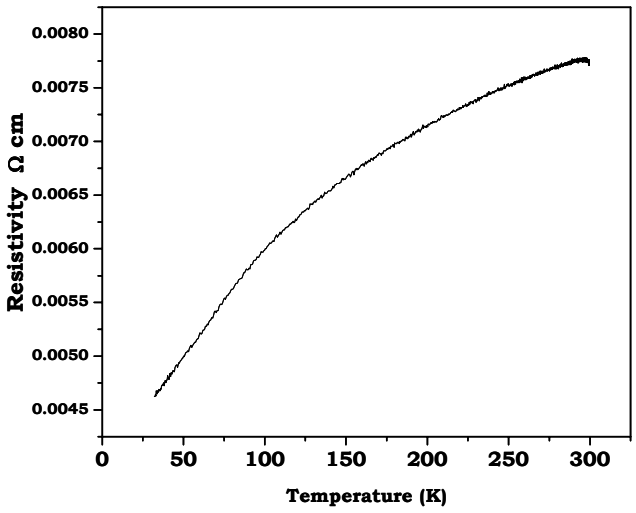

Figure 1.4.1.30: Variation of resistivity, ρ, of Co_3Mo_3N with temperature

The reactions involved in the formation of Fe_3Mo_3N and Co_3Mo_3N is likely to be **(1):**

$$3\ CoMoO_4 + 8\ NH_3 \longrightarrow Co_3Mo_3N + 12\ H_2O + 7/2\ N_2 \qquad \textbf{(1)}$$

(c) Ni_2Mo_3N:

The product of heating a mixture of $NiMoO_4$ and urea in the molar ratio 1:12 resulted in a mixture of Ni_2Mo_3N and Ni which is ascertained by the XRD pattern given in Figure 1.4.1.31. Unlike the ternary nitrides of iron and cobalt which forms the nitrides of type M_3Mo_3N which adopts a structure similar to that of eta carbide, the nickel molybdenum ternary nitride forms Ni_2Mo_3N which has a structure similar to that of Al_2Mo_3C which adopts filled β-Mn structure. The pattern could be indexed with the space group $P4_132$ with a lattice parameter a = 6.9001 Å and reveals the presence of nickel impurity as required by the reaction **(2)**.

$$3\ NiMoO_4 + 8\ NH_3 \longrightarrow Ni_2Mo_3N + Ni + 12\ H_2O + 7/2\ N_2 \qquad \textbf{(2)}$$

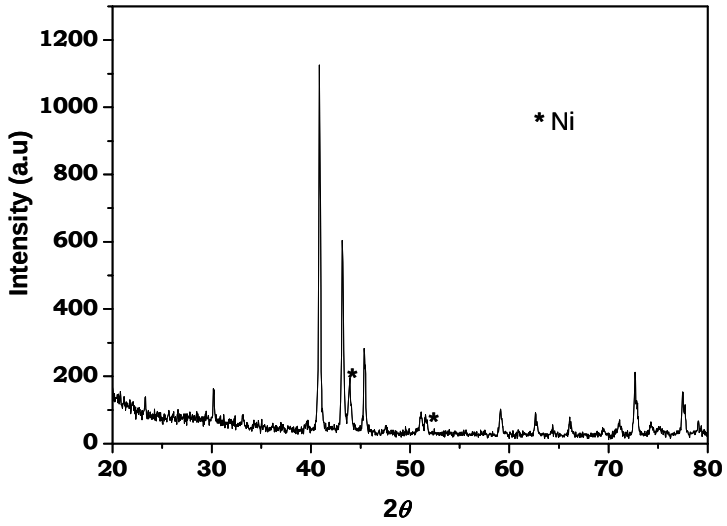

Figure 1.4.1.31: XRD pattern of Ni_2Mo_3N

In Figure 1.4.1.28 (c) we show the SEM image of the product obtained by heating the nickel molybdate-urea mixture, which reveals the morphology of product to be sub-micrometer sized particles. The presence of nickel was ascertained by magnetic measurements which showed ferromagnetism.

1.4.2 Metal Oxynitrides

When Ta_2O_5 was heated with $CaCO_3$, $SrCO_3$ and $BaCO_3$ in admixture with excess urea at 1223 K, the products obtained were $CaTaO_2N$, $SrTaO_2N$ and $BaTaO_2N$ respectively. Figure 1.4.2.1 (a) shows the XRD pattern of $CaTaO_2N$. It crystallizes in the space group *R*, with a = 5.592 Å, c = 13.66 Å (JCPDS card no: 39-0674). The XRD reflections are broad due to the small particle size. By employing the Scherrer formula we estimate the particle size to be around 75 nm. In Figure 1.4.2.1 (b) is shown the XRD pattern of $SrTaO_2N$.

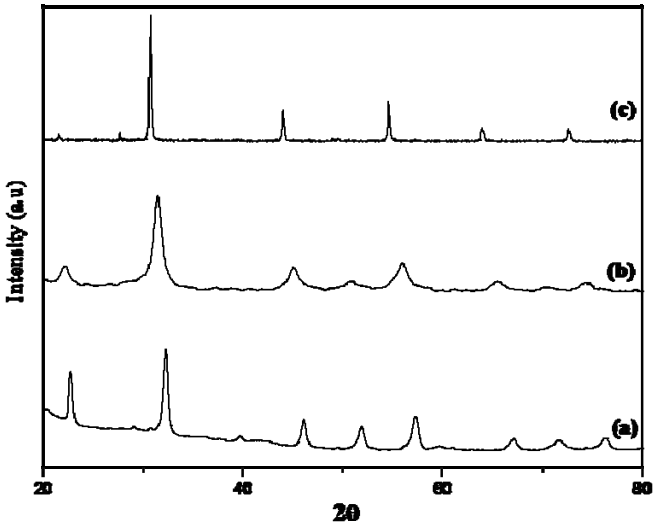

Figure 1.4.2.1: XRD patterns of (a) $CaTaO_2N$, (b) $SrTaO_2N$ and (c) $BaTaO_2N$

The pattern is characteristic of cubic $SrTaO_2N$ (space group = *Pm3m*, a = 4.033 Å, JCPDS card no: 78-1457). The XRD reflections are broad due to small particle size. We estimate the particle size from the Scherrer formula to be around ~50 nm. The XRD pattern of $BaTaO_2N$ shown in Figure 1.4.2.1 (c) confirms its identity. It has the space group *Pm3m* with a = 4.112

Å (JCPDS card no: 84-1748). From the Scherrer formula, the particle size was estimated to be ~100 nm.

TEM image of the oxynitride is shown in Figure 1.4.2.2 (a). From the TEM image the estimated average particle size is around 50 nm. In Figure 1.4.2.2 (b), we show a TEM image of the $SrTaO_2N$ particles which reveal the average particle size to be around 30 nm. From the TEM image shown in Figure 1.4.2.2 (c) we estimate the average particle size of as-synthesized $BaTaO_2N$ to be 60 nm.

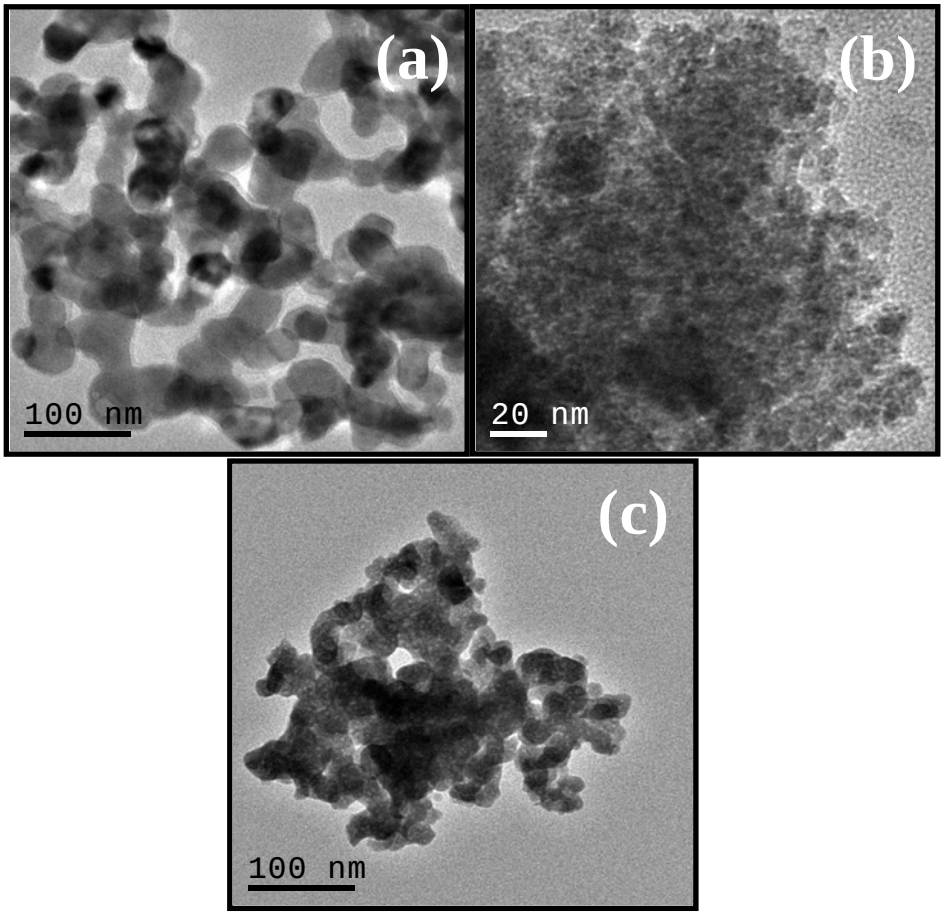

Figure 1.4.2.2: TEM images of (a) $CaTaO_2N$, (b) $SrTaO_2N$ and (c) $BaTaO_2N$

The oxynitrides prepared by the urea route were colored just as those prepared by ammonolysis although there was a slight variation from the literature. $SrTaO_2N$ was orange-

red in color while $BaTaO_2N$ and $CaTaO_2N$ were red-brown and green respectively. In Figure 1.4.2.3 we show the diffuse reflectance spectra of $CaTaO_2N$, $SrTaO_2N$ and $BaTaO_2N$.

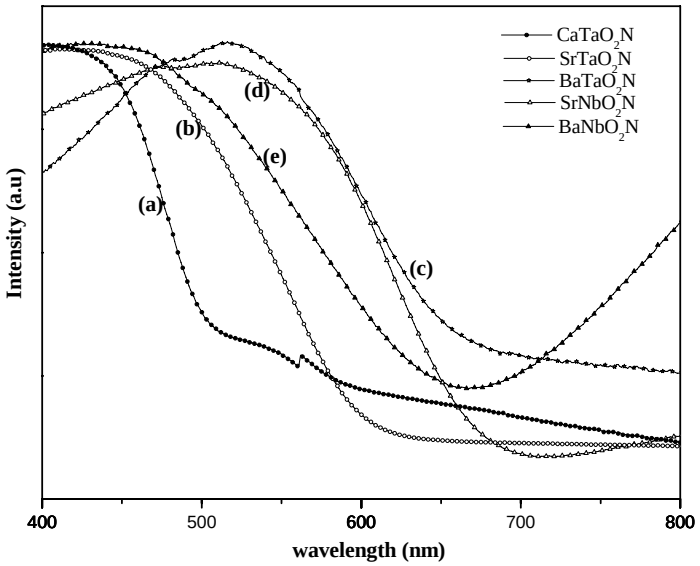

Figure 1.4.2.3: Diffuse reflectance spectra of (a) $CaTaO_2N$, (b) $SrTaO_2N$, (c) $BaTaO_2N$, (d) $SrNbO_2N$ and (e) $BaNbO_2N$.

The spectra agree with those reported in the literature [83]. The slight discrepancy in the color of the oxynitrides can be explained on the following basis. When there is enrichment in the nitrogen content of the oxynitride, it will lead to a decrease in the band gap which in turn will tune the color exhibited by the oxynitride. Thus there might be a slight variation in the nitrogen content of the oxynitrides prepared by us which has resulted in a difference in color of the product.

Reaction of a mixture of excess urea and Nb_2O_5 with $SrCO_3$ and $BaCO_3$ gave $SrNbO_2N$ and $BaNbO_2N$ as products. The XRD patterns of by $SrNbO_2N$ and $BaNbO_2N$ are given in Figures 1.4.2.4. Both crystallize in the space group *Pm3m*. The cubic lattice parameter of $SrNbO_2N$ is 4.044 Å (JCPDS card no: 78-1458) and of $BaNbO_2N$ is 4.128 Å (JCPDS card no: 84-1749). $SrNbO_2N$ was brown in color while $BaNbO_2N$ was brown-black

in color. From the XRD patterns we estimate the particles sizes of $SrNbO_2N$ and $BaNbO_2N$ to be around 270 nm and 300nm respectively. The diffuse reflectance spectra of $SrNbO_2N$ and $BaNbO_2N$ are shown in Figures 1.4.2.3 (d) and (e) respectively.

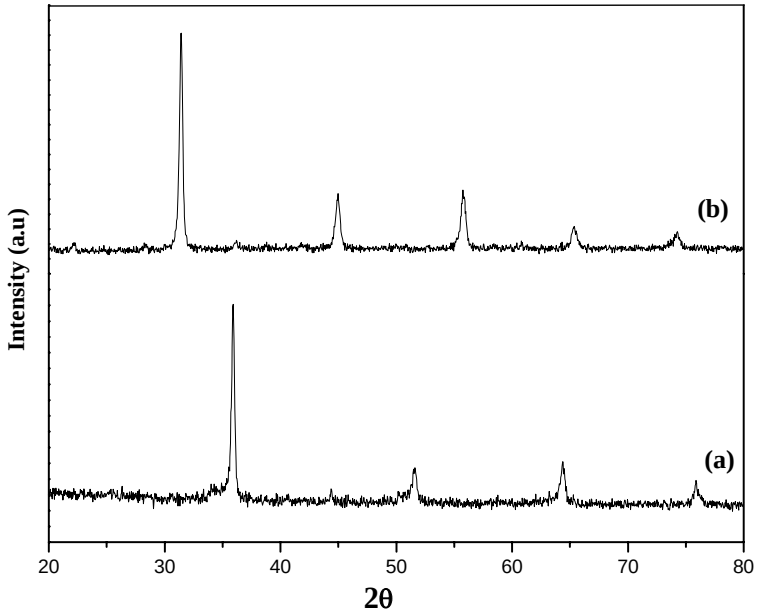

Figure 1.4.2.4: XRD patterns of (a) $SrNbO_2N$ and (b) $BaNbO_2N$

On heating excess urea with Ta_2O_5 and La_2O_3, the product obtained was a mixture consisting of $LaTaON_2$ along with Ta_2O_5 and TaON. The product was red in color. When the reaction time was increased, the percentage of impurities decreased. We could not, however, obtain pure phase of $LaTaON_2$. In Figure 1.4.2.5 (a) we show the XRD pattern of the product obtained by heating Ta_2O_5 and La_2O_3 with excess urea. The $LaTaON_2$ which was the major phase crystallizes in the space group *I-1* with the lattice parameters a = 5.721 Å, a = 5.721 Å and a = 8.093 Å (JCPDS card no: 47-1366). The particle size was estimated to be around 300 nm.

We obtained $LaTiO_2N$ as the major phase along with a small amount of TiO_2 on heating TiO_2 and La_2O_3 with urea. To obtain pure $LaTiO_2N$, we heated the amorphous oxide

precursor containing stoichiometric amounts of La and Ti ions with urea. When we carried out the ammonolysis of the amorphous oxide precursor without urea at 1123 K, the product obtained was $LaTiO_2N$. The product obtained was, however, not as crystalline as that obtained by the urea route. $LaTiO_2N$ obtained by the urea route was yellow in color. In Figure 1.4.2.5 (b) we show the XRD pattern of $LaTiO_2N$. It crystallizes in space group *I-1* with the lattice parameters a = 5.579 Å, a = 5.579 Å and a = 7.878 Å (JCPDS card no: 48-1230). The particle size estimated from the Scherrer formula is 40 nm.

When a stoichiometric mixture of $SrCO_3$ and MoO_3 was reacted with excess urea at 1173 K, $SrMoO_{3-x}N_x$ was obtained as the product. The XRD pattern of the oxynitride thus formed is given in Figure 1.4.2.5 (c). $SrMoO_{3-x}N_x$ crystallizes in the space group *Pm3m* with a = 3.969 Å (JCPDS card no: 81-0641). From the Scherrer formula, the particle size was estimated to be around 175 nm. $SrMoO_{3-x}N_x$ obtained by us was black in color, but the literature reports it to be blue-black [97].

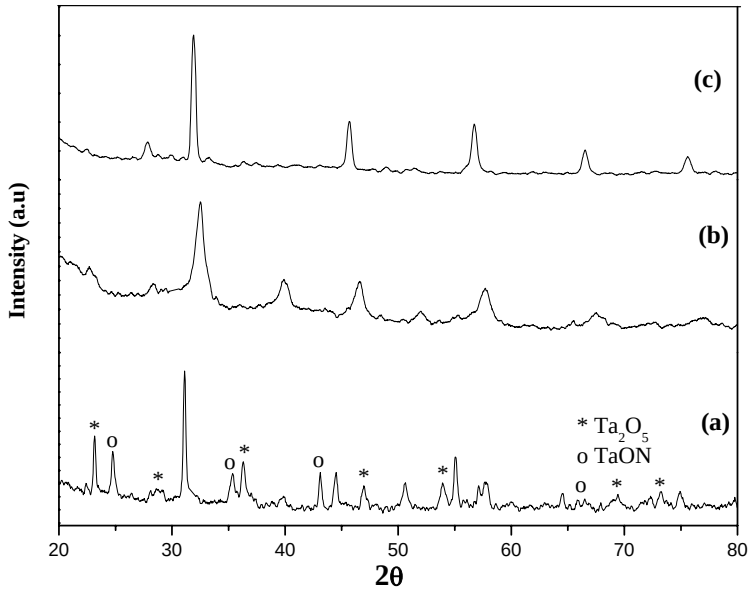

Figure 1.4.2.5: XRD patterns of (a) $LaTaON_2$, (b) $LaTiO_2N$ and (c) $SrMoO_{3-x}N_x$

1.4.3 Coating of BN on one-dimensional nanostructures

BN has many desirable properties owing to which it is commercially important and there are papers reporting successful filling of BN nanotubes by various methods including chemical and physical insertions and arc encapsulation. Herein, BN coatings have been obtained on the surface of carbon fibers, multi-walled carbon nanotubes and inorganic nanowires by means of simple route involving urea as the nitrogen source. This essentially happens in three stages. The first step is to generate reactive groups on the surface of the inorganic nanostructures. In the second step the surface-activated nanostructures are treated with the reaction mixture followed by the heat treatment at higher temperature which results in BN coating. Carbon fibers and MWNTs on acid treatment get functionalized with surface hydroxyl and carboxyl groups while the metal oxide nanowires necessarily possess hydroxyl groups on their surfaces [125-127]. We have made use of the surface functional groups on the carbon fibers, MWNTs and inorganic nanowires for reaction with the 1:6 H_3BO_3-urea mixture. On heating, H_3BO_3 gives B_2O_3 which reacts with NH_3 produced by the decomposition of urea to give BN as shown below:

$$2\ H_3BO_3 \xrightarrow{\Delta} B_2O_3 + 3\ H_2O$$

$$CO(NH_2)_2 \xrightarrow{\Delta} NH_3 + HCNO$$

$$B_2O_3 + 2\ NH_3 \xrightarrow{\Delta} 2\ BN + 3\ H_2O$$

This process is depicted schematically in Figure 1.4.3.1.

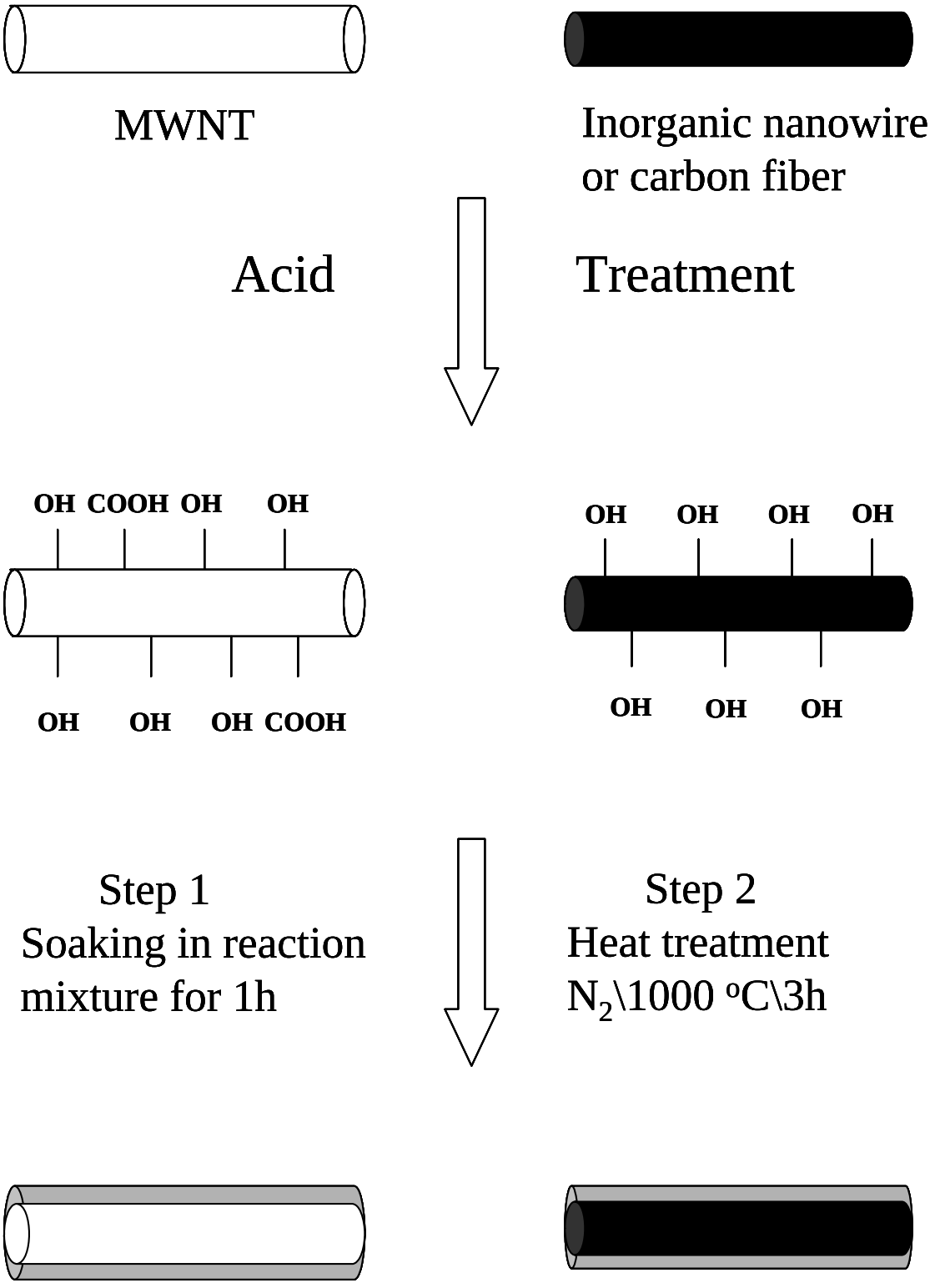

Figure 1.4.3.1: Schematic representation of the entire coating process.

In Figure 1.4.3.2 (a) is shown the FESEM images of the acid treated carbon fibers and average outer diameter is ~7μm. Figures 1.4.3.2 (b) and (c) show the FESEM image of heavily coated carbon fibers. The heavy coating was obtained by the reaction of the carbon fibers with the 1:6 H_3BO_3-urea mixture for 3 h followed by the heat treatment at 1273 K for 3 h in flowing N_2. In Figure 1.4.3.2 (d) is given the FESEM image of a single strand of a heavily coated carbon fiber. The thickness of the coating is ~2 μm.

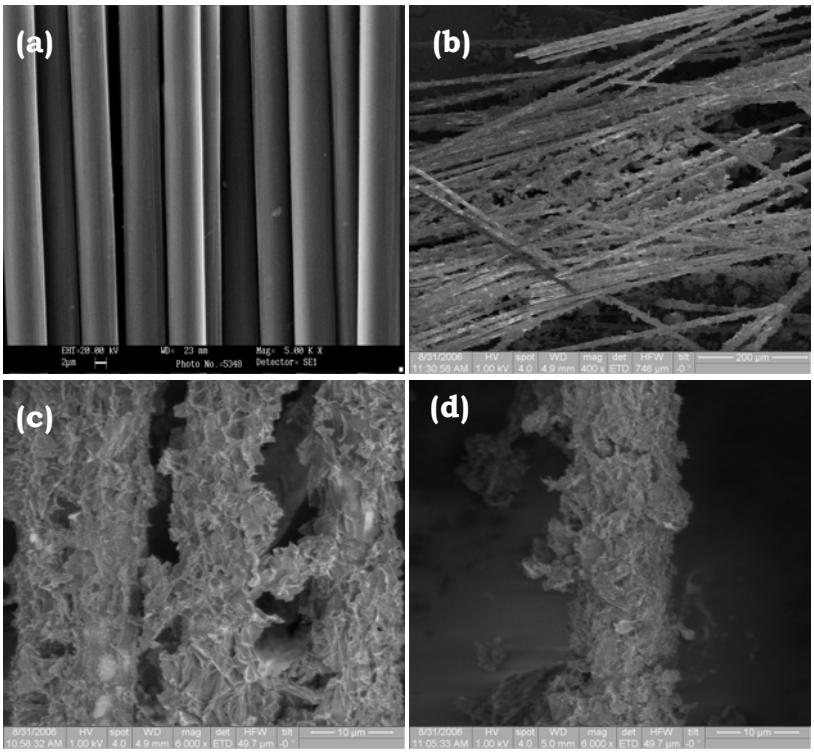

Figure 1.4.3.2: FESEM images of (a) acid-treated carbon fibers, (b) and (c) heavily BN-coated carbon fibers (d) heavily BN-coated single strand of the fiber.

Figure 1.4.3.3 (a) gives the FESEM image of the carbon fibers with thinner coating obtained by the reaction of the acid-treated carbon fibers with the 1:6 H_3BO_3-urea mixture for 1h and then heated at 1273 K for 3 h in an inert atmosphere. In Figure 1.4.3.3 (b) we show a FESEM image of a carbon fiber with thinner coating. The thickness of the coating here is around 1 μm.

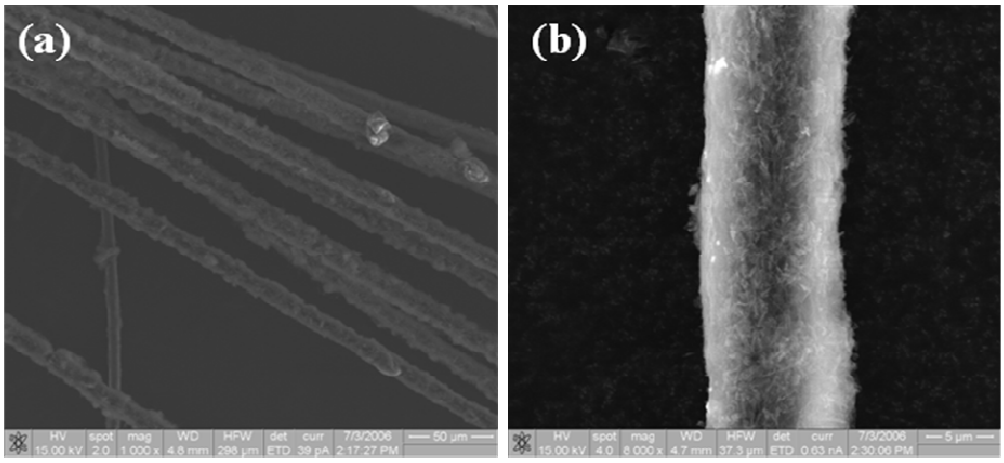

Figure 1.4.3.3: SEM images of (a) carbon fibers and (b) single strand with thinner coating

We have characterized the BN-coated carbon fibers by XPS. Figure 1.4.3.4 gives the XP spectrum of the-BN coated carbon fibers. The spectrum shows characteristic binding energies (BE) of 285 eV for C (1s), 190.3 eV for B (1s) and 397.4 eV for N (1s) corresponding to BN.

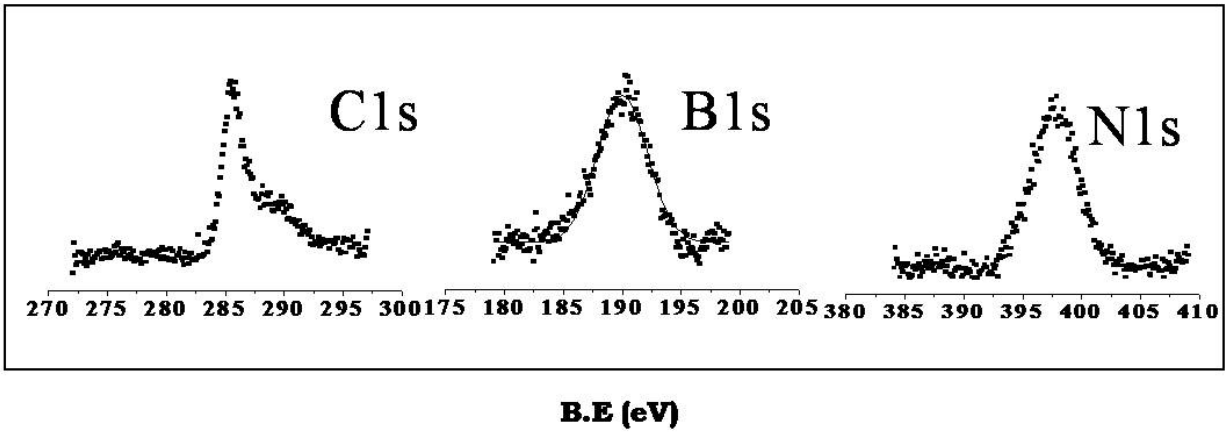

Figure 1.4.3.4: XP spectrum of the heavily BN-coated carbon fibers.

Treatment of acid-treated MWNTs with the 1:6 H_3BO_3-urea mixture for 1h followed by heating at 1273 K for 3 h in a N_2 atmosphere gave BN-coated MWNTs. In Figures 1.4.3.5 (a) and (b) are shown the TEM images of the BN-coated MWNTs. The thickness of the BN coating is around 10 nm. The inset in Figure 1.4.3.5 (b) is the high resolution electron

microscope (HREM) image of a BN-coated MWNT. The lattice spacing of the graphitic layers of the MWNT is 0.34 nm corresponding to the (002) planes.

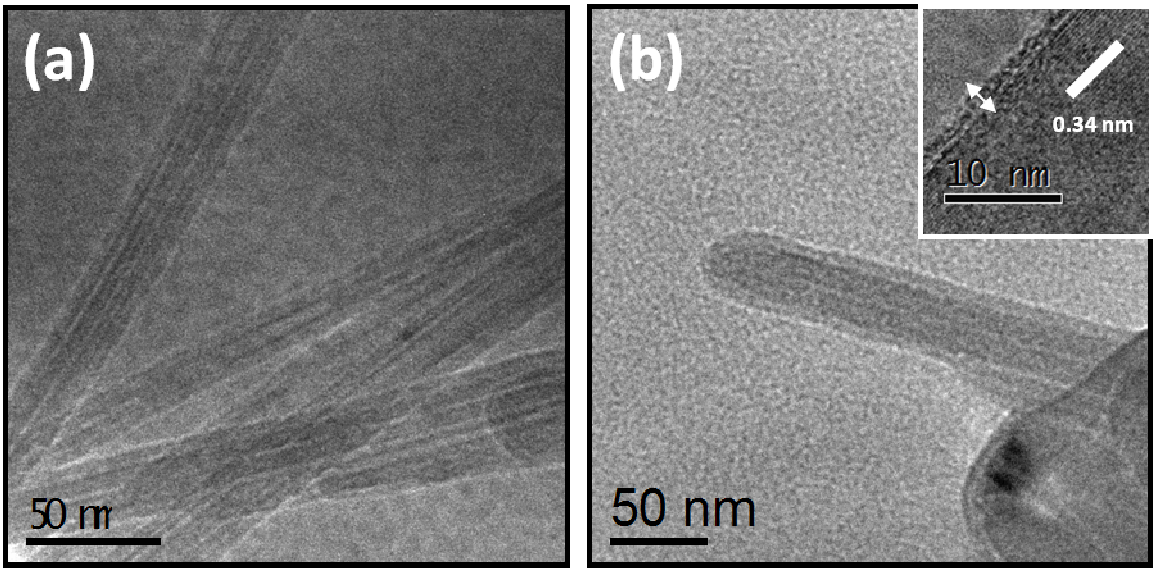

Figure 1.4.3.5: (a) and (b) are the TEM images of BN coated MWNTs with the inset in b) showing the HREM image of a BN coated MWNT.

In Figure 1.4.3.6 we have given the XP spectrum of the BN-coated MWNTs which gives characteristic BE of 285 eV for C (1s), 190 eV for B (1s) and 397.8 eV for N (1s) corresponding to BN.

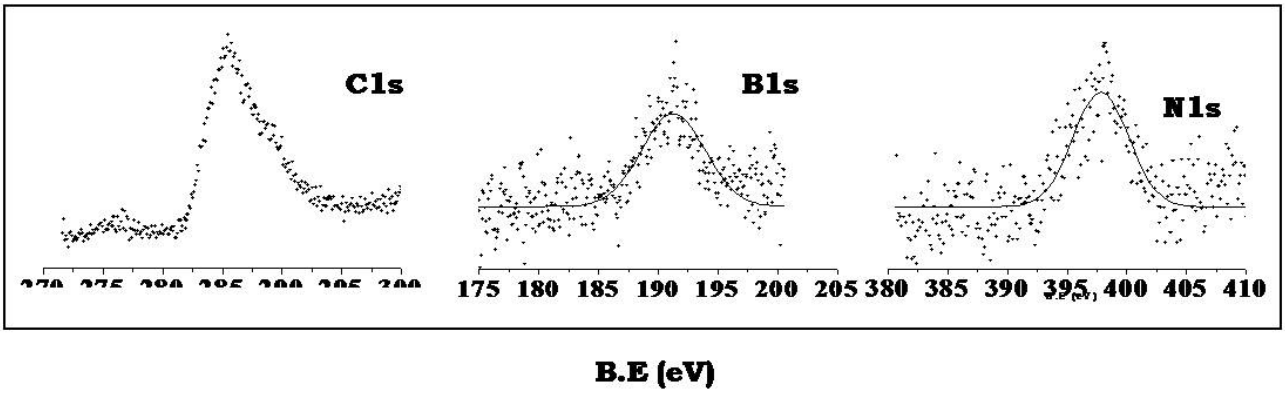

Figure 1.4.3.6: XP spectrum of BN-coated MWNTs.

Acid-treated inorganic nanowires were also reacted with the 1:6 H_3BO_3-urea mixture for 1h followed by a heat treatment at 1273 K for 3 h in a N_2 atmosphere. In Figure 1.4.3.7 (a) we give the TEM image of a BN-coated SiC nanowire. The coating thickness is ~10 nm. Figure 1.4.3.7 (b) is the HREM image of the BN-coated SiC nanowire. It shows a lattice spacing of 0.25 nm corresponding to the (111) planes of the SiC and a spacing of 0.34 nm corresponding to the (002) planes of the BN. The lattice image suggests BN to be turbostatic. The XP spectrum of the BN coated SiC nanowire gave the characteristic BE of 190 eV for B (1s) and 397.6 for N (1s) corresponding to BN.

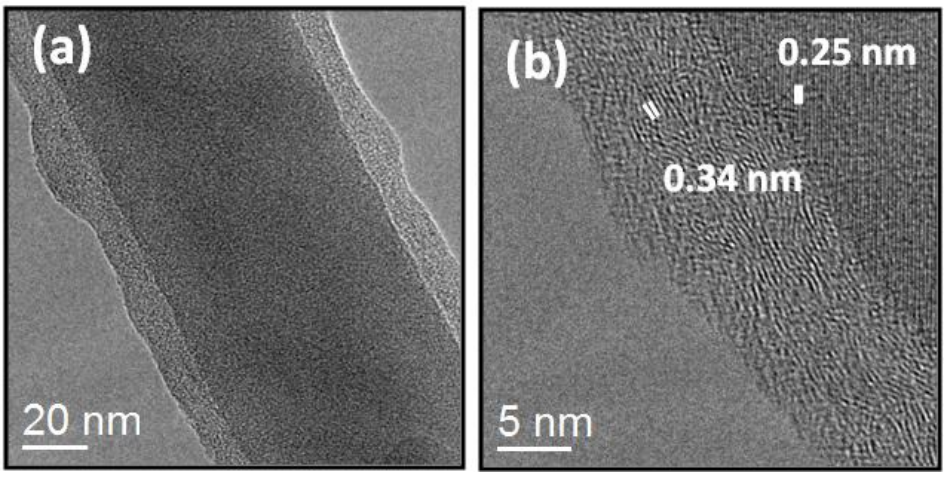

Figure 1.4.3.7: (a) TEM and (b) HREM images of a BN coated SiC nanowire

Figure 1.4.3.8 (a) gives a TEM image of a BN-coated Si_3N_4 nanowire. From the TEM image it is seen that the coating thickness is ~8 nm. The HREM image of the BN-coated Si_3N_4 nanowire in Figure 1.4.3.8 (b) shows a spacing of 0.66 nm corresponding to the (100) planes of Si_3N_4 and a spacing of 0.34 nm corresponding to the (002) planes of the BN. In Figure 1.4.3.9 (a) we show the TEM image of a BN-coated Al_2O_3 nanowire. The BN coating seems to be amorphous since the HREM image shown in Figure 1.4.3.9 (b) shows only lattice spacing of 0.25 nm corresponding to the (104) planes of Al_2O_3.

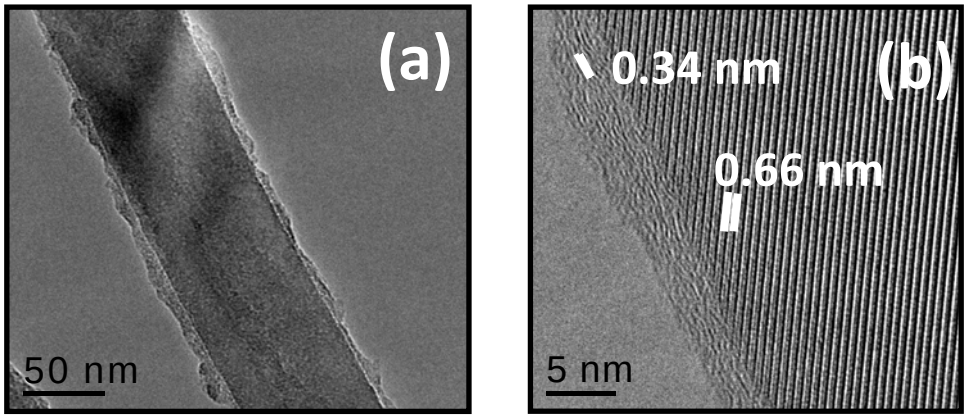

Figure 1.4.3.8: (a) TEM and (b) HREM images of a BN coated Si_3N_4 nanowire.

The HREM image shown as an inset of Figure 1.4.3.9 (d) gives a lattice spacing of 0.24 nm corresponding to the (110) planes of GaN and a spacing of 0.34 nm corresponding to the (002) planes of the BN.

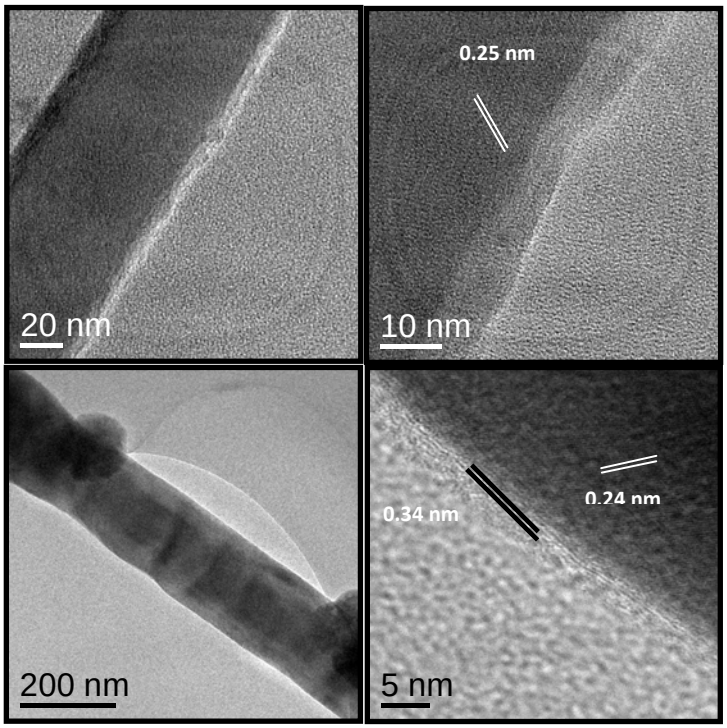

Figure 1.4.3.9: (a) TEM and (b) HREM images of a BN coated Al_2O_3 nanowire and (c) TEM and (d) HREM images of a BN coated GaN nanowire.

1.5 Conclusions

In conclusion, we have succeeded in preparing crystalline nanoparticles of BN, TiN NbN and γ-Mo_2N by heating mixtures of urea with H_3BO_3, $TiCl_4$, $NbCl_5$ and $MoCl_5$ respectively in the temperature range of 800-1273 K. In the case of TiN, nanowires have been obtained by carrying out the reaction of urea with $TiCl_4$ over Au islands deposited on Si substrates. The NbN and γ-Mo_2N nanoparticles showed a superconducting T_c around 8 and 7 K. It is also noteworthy that the γ-Mo_2N nanoparticles readily transform to δ-MoN nanoparticles on heating in NH_3 at a relatively low temperature. The δ-MoN so obtained seems to be somewhat disordered since the superconducting transition is around 5 K. It has also been found that the NbN and MoN_x nanoparticles show surface ferromagnetism.

We have been able to prepare three ternary nitrides of type M_nMo_3N (n=3 with M=Fe and Co and n=2 with M=Ni) by a simple reaction of the precursor molybdates with urea. All the nitrides were of sub-micron sized particles as revealed by the SEM micrographs.

The present study shows that the urea route provides a simple means of preparing ternary metal oxynitrides, wherein a mixture of the corresponding metal carbonates and metal oxides is heated with excess urea. The metal oxynitrides so obtained are generally stoichiometric and are in the form of nanoparticles.

We have also been able to develop a simple route involving the reaction of H_3BO_3 with urea to coat carbon nanotubes as well as nanowires of SiC, Si_3N_4, Al_2O_3 and GaN with BN, the coating thickness being generally few nanometers. We have been able to get the high resolution electron microscope images of the BN coating in most of the cases. Carbon fibers could also be coated with BN with a coating thickness of few microns by the urea route.

References

1. R. Marchand, Y. Laurent, J. Guyader, P. L'Haridon and P. Verdier, J. Eur. Ceram. Soc., 1991, 8, 197-213.
2. S. Wolfgang, Angew. Chem. , 1993, 32, 806-818.
3. N. Brese and M. O'Keeffe, in Crystal chemistry of inorganic nitrides, Editon edn., 1992, pp. 307-378.
4. G. V. Samsonov and I. M. Vinitskii, Handbook of Refractory Compounds, Academic Press, New York, 1980.
5. S. T. Oyama, The Chemistry of Transition Metal Carbides and Nitrides, Blackie Academic Professional, Glasgow 1996.
6. L. E. Toth, Transition Metal Carbides and Nitrides, Academic Press, New York,, 1971.
7. L. A. Chernozatonskii, E. G. Gal'pern, I. V. Stankevich and Y. K. Shimkus, Carbon, 1999, 37, 117-121.
8. D. Golberg, Y. Bando, M. Mitome, K. Kurashima, N. Grobert, M. Reyes-Reyes, H. Terrones and M. Terrones, Chem. Phys. Lett, 2002, 360, 1-7.
9. P. B. Mirkarimi, K. F. McCarty and D. L. Medlin, Mater. Sci. Eng., R, 1997, 21, 47-100.
10. S. P. S. Arya and A. D'Amico, Thin Solid Films, 1988, 157, 267-282.
11. M. Wittmer, B. Studer and H. Melchior, J. Appl. Phys., 1981, 52, 5722-5726.
12. R. Buhl, H. K. Pulker and E. Moll, Thin Solid Films, 1981, 80, 265-270.
13. R. A. Andrievski, I. A. Anisimova and V. P. Anisimov, Thin Solid Films, 1991, 205, 171-175.

14. J. Rivory, J. M. Behaghel, S. Berthier and J. Lafait, Thin Solid Films, 1981, 78, 161-165.

15. T. H. Geballe, B. T. Matthias, J. P. remeika, A. M. Glogston, V. B. Compton, J. P. Maita and H. J. Williams, Physics, 1966, 2, 293.

16. K. S. Lee, H. Abe, J. A. Reimer and A. T. Bell, J. Catal., 1993, 139, 34-40.

17. L. Volpe and M. Boudart, J. Phys. Chem., 1986, 90, 4874-4877.

18. S. T. Oyama, Catal. Today, 1992, 15, 179-200.

19. M. Saito and R. B. Anderson, J. Catal., 1980, 63, 438-446.

20. J. A. J. Rodriguez, G. M. Cruz, G. Bugli and M. Boudart, Catal. Lett. , 1997, 45, 1.

21. C. L. Bull, P. F. McMillan, E. Soignard and K. Leinenweber, J. Solid State Chem. , 2004, 177, 1488.

22. B. T. Matthias and J. K. Hulm, Phys. Rev., 1952, 87, 799.

23. C. L. Bull, T. Kawashima, P. F. McMillan, D. Machon, O. Shebanova, D. Daisenberger, E. Soignard, E. Takayama-Muromachi and L. C. Chapon, J. Solid State Chem., 2006, 179, 1762-1767.

24. D. A. Papaconstantopoulos, W. E. Pickett, B. M. Klein and L. L. Boyer, Phys. Rev. B, 1985, 31, 752.

25. Z. Altouninan, X. Chen, L. X. Liao, D. H. Ryan and J. O. Strom-Olsen, J. Appl. Phys., 1993, 73, 6017.

26. F. J. DiSalvo, Science, 1990, 247, 649.

27. L. Volpe and M. Boudart, J. Solid State Chem., 1985, 59, 332.

28. L. Volpe and M. Boudart, Catal. Rev. Sci. Eng., 1985, 27, 515.

29. R. B. Levy and M. Boudart, Science, 1973, 181, 547.

30. A. J. Perry, M. Georgson and W. D. Sproul, Thin Solid Films, 1988, 157, 255.

31. Y. Otani, . P. F. Hurley, H. Sun and J. M. D. Coey, J. Appl. Phys., 1991, 69, 5584.

32. S. Miraglia, J. L. Soubeyroux, C. Kolbeck, O. Ishard, D. Fruchart and M. Guillot, J. Less-Common Met., 1991, 171, 51.

33. H. J. Buschow, J. Magn. Magn. Mater., 1991, 100, 79.

34. D. P. F. Hurley, H. Sun and J. M. D. Coey, J. Magn. Magn. Mater., 1991, 99, 229.

35. K. H. J. Buschow, R. Coehoorn, D. B. de Mooij and T. H. J. K. de Waard, J. Magn. Magn. Mater., 1990, 92, 35.

36. M. Y. Chern and F. J. Disalvo, J. Solid State Chem., 1990, 88, 459-464.

37. H. Randhawa, P. C. Johnson and R. Cunningham, J. Vac. Sci. Technol., 1988, A6, 2136.

38. U. Konig, Surf. Coat Technol., 1987, 33, 91.

39. C. H. Jaggers, J. N. Michaels and A. M. Stacy, Chem. Mater., 1990, 2, 150.

40. C. C. Yu and S. T. Oyama, J. Solid State Chem., 1995, 116, 207.

41. G. Hitoki, T. Takata, J. N. Kondo, M. Hara, H. Kobayashi and K. Domen, Chem. Commun., 2002, 1698.

42. M. Jansen and H. P. Letschert, Nature, 2002, 404, 980.

43. A. Kasahara, K. Nukumizu, G. Hitoki, T. Takata, J. N. Kondo, M. Hara, H. Kobayashi and K. Domen, J. Phys. Chem. A, 2002, 106, 6750-6753.

44. Y.-I. Kim, P. M. Woodward, K. Z. Baba-Kishi and C. W. Tai, Chem. Mater., 2004, 16, 1267-1276.

45. S. Iijima, Nature, 1991, 354, 56.

46. J. T. Hu, M. Ouyang, P. D. Yang and C. M. Lieber, Nature, 1999, 399, 48.

47. L. J. Lauhon, M. S. Gudiksen, D. Wang and C. M. Lieber, Nature, 1999, 420, 57.

48. M. S. Gudiksen, L. J. Lauhon, J. Wang, D. C. Smith and C. M. Lieber, Nature, 2002, 415, 617.

49. Z. Yao, H. W. Ch. Postma, L. Balents and C. Dekker, Nature, 1999, 402, 273.

50. X. Blase, A. Rubio, S. G. Louie and M. L. Cohen, Europhys. Lett. , 1998, 28, 335.

51. M. J. Powers, M. C. Benjamin, L. M. Porter, R. J. Nemanich, R. F. Davis, J. J. Cuomo, G. L. Doll and S. J. Harris, Appl. Phys. Lett., 1995, 67, 3912.

52. C. Kimura, T. Yamamoto, T. Hori and T. Sugino, Appl. Phys. Lett. , 2001, 79, 4533.

53. N. Park and J. Ihm, Bull. Am. Phys. Soc. , 2002, 47, 1013.

54. T. Sugino, S. Kawasaki, K. Tanioka and J. Shirafuji, Appl. Phys. Lett. , 1997, 71, 2704

55. L. Volpe and M. Boudart, J. Solid State Chem. , 1985, 59, 332.

56. F. T. a. F. J. D. Roger Marchand, J. Mater. Chem., 1999, 9, 297 - 304.

57. A. Calka and A. P. Radlinski, Appl. Phys. Lett., 1991, 58, 119.

58. J. Ma, Y. Du and Y. Qian, J. Alloys Compd. , 2005, 389, 296-298.

59. H. Junqing, L. Qingyi, T. Kaibin, Y. Shuhong, Q. Yitai, Z. Guien and L. Xianming, J. Am. Ceram. Soc., 2000, 83, 430-432.

60. K. Sardar and C. N. R. Rao, Adv. Mater., 2004, 16, 425.

61. K. Sardar, M. Dan, B. Schwenzer and C.N.R.Rao, J. Mater. Chem., 2005, 15, 2175-2177.

62. N. G. Chopra, R. J. Luyken, K. Cherrey, V. H. Crespi, M. L. Cohen, S. G. Louie and A. Zettl, Science, 1995, 269, 966-967.

63. P. Cai, L. Chen, L. Shi, Z. Yang, A. Zhao, Y. Gu, T. Huang and Y. Qian, Solid State Commun., 2005, 133, 621-623.

64. F. L. Deepak, C. P. Vinod, K. Mukhopadhyay, A. Govindaraj and C. N. R. Rao, Chem. Phys. Lett., 2002, 353, 345.

65. U. A. Joshi, S. H. Chung and J. S. Lee, J. Solid State Chem., 2005, 178, 755-760.

66. G. Qixun, X. Yi, W. Xinjun, L. Shichang, H. Tao and B. Chuannan, J. Am. Ceram. Soc., 2005, 88, 249-251.

67. X. Feng, Y.-J. Bai, B. Lu, C.-G. Wang, Y.-X. Qi, Y.-X. Liu, G.-L. Geng and Li, Inorg. Chem., 2004, 43, 3558-3560.

68. R. A. Janes, M. Aldissi and R. B. Kaner, Chem. Mater., 2003, 15, 4431-4435.

69. L. Shi, Y. Gu, L. Chen, Z. Yang, J. Ma and Y. Qian, J. Nanosci. Nanotechnol., 2005, 5, 296-299.

70. W. Lengauer, J. Cryst. Growth, 1988, 87, 295-298.

71. N. S. Gajbhiye and R. S. Ningthoujam, Phys. Status Solidi C, 2004, 1, 3449-3454.

72. C. J. H. Jacobsen, Chem. Commun., 2000, 1057.

73. D. S. Bem, C. P. Gibson and H.-C. z. Loye, Chem. Mater., 1993, 5, 397.

74. D. S. Bem and H.-C. Z. Loye, J. Solid State Chem., 1993, 104, 467-469.

75. P. S. Herle, N. Y. Vasanthacharya, M. S. Hegde and J. Gopalakrishnan, J. Alloys Compd., 1995, 217, 22-24.

76. J. D. Houmes, S. Deo and H.-C. zur Loye, J. Solid State Chem., 1997, 131, 374-378.

77. K. S. Weil and P. N. Kumta, Mater. Sci. Eng., B, 1996, 38, 109-117.

78. R. N. Panda and N. S. Gajbhiye, J. Alloys Compd., 1997, 256, 102-107.

79. P. S. Herle, M. S. Hegde, K. Sooryanarayana, T. N. Guru Row and G. N. Subbanna, Inorg. Chem., 1998, 37, 4128-4130.

80. F. S. S. Alconchel, D. Beltrán, A. Beltrán, J. Mater. Chem., 1998, 8, 1901-1909.

81. S. K. Jackson, R. C. Layland and H.-C. zur Loye, J. Alloys Compd., 1999, 291, 94-101.

82. C. J. H. Jacobsen, J. J. Zhu, H. Lindelov and J. Z. Jiang, J. Mater. Chem., 2002, 12, 3113-3116.

83. R. Marchand, Y. Laurent, J. Guyader, P. L'Haridon and P. Verdier, J. Eur. Ceram. Soc. , 1991, 8, 197.

84. S. J. Clarke, K. A. Hardstone, C. W. Michie and M. J. Rosseinsky, Chem. Mater., 2002, 14, 2664-2669.

85. P. Maillard, F. Tessier, E. Orhan, F. Chevire and R. Marchand, Chem. Mater., 2004, 17, 152-156.

86. F. Tessier, R. Assabaa and R. Marchand, J. Alloys Compd., 1997, 262-263, 512-515.

87. N. Diot, R. Marchand, J. Haines, J. M. Léger, P. Macaudière and S. Hull, J. Solid State Chem., 1999, 146, 390-393.

88. G. Tobias, D. Beltran-Porter, O. I. Lebedev, G. Van Tendeloo, J. Rodriguez-Carvajal and A. Fuertes, Inorg. Chem., 2004, 43, 8010-8017.

89. S. J. Clarke, B. P. Guinot, C. W. Michie, M. J. C. Calmont and M. J. Rosseinsky, Chem. Mater., 2001, 14, 288-294.

90. S. J. Clarke, C. W. Michie and M. J. Rosseinsky, Chem. Mater., 2000, 12, 863-865.

91. J. I.-M. R. Pastrana-Fábregas, R. Sáez-Puche J. Mater. Res, 2006, 21, 2255-2260.

92. P. Antoine, R. Assabaa, P. L'Haridon, R. Marchand, Y. Laurent, C. Michel and B. Raveau, Mater. Sci. Eng., B 1989, 5, 43-46.

93. S. J. Clarke, P. R. Chalker, J. Holman, C. W. Michie, M. Puyet and M. J. Rosseinsky, J. Am. Chem. Soc., 2002, 124, 3337-3342.

94. F. Cheviré, F. Tessier and R. Marchand, Mater. Res. Bull., 2004, 39, 1091-1101.

95. P. Antoine, R. Marchand, Y. Laurent, C. Michel and B. Raveau, Mater. Res. Bull. , 1988, 23, 953.

96. P. S. Herle, M. S. Hegde and G. Subbanna, J. Mater. Chem., 1997, 7, 2121.

97. S. H. Elder, F. J. DiSalvo, J. B. Parise, J. A. Hriljac and J. J. W. Richardson, J. Solid State Chem., 1994, 108, 73.

98. I. D. Fawcett, K. V. Ramanujachary and M. Greenblatt, Mater. Res. Bull., 1997, 32, 1565.

99. D. Logvinivich, R. Aguiar, R. Robert, M. Trottmann, S. G. Ebbinghaus, A. Reller and A. Weidenkaff, J. Solid State Chem., 2007, 180, 2649.

100. S. Alconchel, F. Sapiña, D. Beltrán and A. Beltrán, J. Mater. Chem., 1998, 8, 1901.

101. C. Linlin, Y. Haihui and G. Yury, J. Am. Ceram. Soc. , 2004, 87, 147-151.

102. J. B. Yoo, J. H. Han, S. H. Choi, T. Y. Lee, C. Y. Park, T. W. Jeong, J. H. Lee, S. Yu, G. Park, W. K. Yi, H. S. Kim, Y. J. Baik and J. M. Kim, Physica B, 2002, 323, 180-181.

103. Y. Li, P. S. Dorozhkin, Y. Bando and D. Golberg, Adv. Mater., 2005, 17, 545-549.

104. L. Gao, X. Jin, J. Li, Y. Li and J. Sun, Mater. Sci. Eng., A, 2006, 415, 145-148.

105. Y.-H. K. T. Kusunose, T. Sekino, T. Matsumoto, N. Tanaka, T. Nakayama, K. Niihara,, J. Mater. Res., 2005, 20, 183-190.

106. W. S. Jang, S. Y. Kim, J. Lee, J. Park, C. J. Park and C. J. Lee, Chem. Phys. Lett., 2006, 422, 41-45.

107. J. Zhang, L. Zhang, F. Jiang and Z. Dai, Chem. Phys. Lett., 2004, 383, 423-427.

108. Q. Yu and G. Lian, J. Am. Ceram. Soc., 2004, 87, 352-357.

109. S. Podsiadlo, Thermochim. Acta, 1995, 256, 367-373.

110. S. Podsiadlo, Thermochim. Acta,, 1995, 256, 375.

111. A. G. B. C. Satishkumar, E. M. Vogl, L. Basumallick, C.N.R. Rao, J. Mater. Res, 1997, 12, 604-606.

112. A. G. F. L. Deepak, and C. N. R. Rao, J. Nanosci. Nanotechnol., 2001, 1, 303-308.

113. G. Gundiah, F. L. Deepak, A. Govindaraj and C. N. R. Rao, Top. Catal. , 2003, 24, 137-146.

114. G. Gundiah, G. V. Madhav, A. Govindaraj, M. M. Seikh and C. N. R. Rao, J. Mater. Chem., 2002, 12, 1606-1611.

115. B. T. Matthias and J. K. Hulm, Phys. Rev., 1952, 87, 799.

116. C. L. Bull, T. Kawashima, P. F. McMillan, D. Machon, O. Shebanova, D. Daisenberger, E. Soignard, E. T. Muromachi and L. C. Chapon, J. Solid State Chem. , 2006, 179, 1762.

117. Ram Seshadri, Curr. Opin. Solid State Mater. Sci. , 2005, 9, 1.

118. M. Venkatesan, C. B. Fitzgerald and J. M. D. Coey, Nature, 2004, 430, 630.

119. A. Zyweitz, J. Furthmuller and F. Bechstedt, Phys. Rev. B, 2000, 62, 6854.

120. I. S. Elfimov, S. Yunoki and G. A. Sawatzky, Phys. Rev. Lett., 2002, 89, 216403.

121. R. Monnier and B. Delley, Phys. Rev. Lett., 2001, 87, 157204.

122. J. M. D. Coey, M. Venkatesan, P. Stamenov, C. B. Fitzgerald and L. S. Dorneles, Phys. Rev. B 2005, 72, 024450.

123. A. Sundaresan, R. Bhargavi, N. Rangarajan, U. Siddesh and C. N. R. Rao, Phys. Rev. B, 2006, 74, 161306.

124. N. H. Hong, J. Sakai, N. Poirot and V. Breze, Phys. Rev. B, 2006, 73, 132404.

125. Nanowires and Nanobelts: Materials, Properties and Devices (Ed: Z. L. Wang), Kluwer Academic, Boston, MA 2003.

126. R. C. Haddon, Acc. Chem. Res., 2002, 35, 997-997.

127. C. N. R. Rao, B. C. Satishkumar, A. Govindaraj and N. Manashi, ChemPhysChem, 2001, 2, 78-105.

PART 2

Functionalization and Solubilization of Inorganic Nanomaterials

Summary[*]

In view of the important need to generate well-dispersed inorganic nanostructures in various solvents, we have explored the dispersion of nanostructures of metal oxides such as CeO_2, TiO_2, Fe_3O_4 and ZnO in solvents of differing polarity in the presence of several surfactants. The solvents used are water, dimethylformamide (DMF) and toluene. The surfactant-solvent combinations yielding the best dispersions are reported along with some of the characteristics of the nanostructures in the dispersions.

Covalent functionalization of nanowires of TiO_2, ZnO and Al_2O_3 has been carried out by employing the organosilicon reagents, γ-aminopropyltriethoxysilane and hexadecyltrimethoxysilane (HDTMS). The presence of the organosilane coating was confirmed by electron microscopy, EDAX analysis and IR spectroscopy. HDTMS-coated oxide nanowires give stable dispersions in CCl_4 and toluene. Nanoparticles of these metal oxides as well as of CeO_2 and Fe_3O_4 could be solubilized in non-polar solvents by functionalizing with HDTMS. Nanotubes and nanoparticles of BN could also be functionalized and solubilized with HDTMS. Organotin reagents have also been used to covalently functionalize oxide nanostructures and multi-walled carbon nanotubes, thereby producing stable dispersions in CCl_4 and toluene. The organotin reagents used were dibutyldimethoxytin and trioctyltinchloride. Covalent functionalization of nanostructures using organosilane and organotin reagents provides a general method applicable to large class of inorganic materials as well as carbon nanotubes and is likely to be useful in practice.

Polyoctasilsesquioxane (POSS) has been synthesized and has been used to coat nanostructures so as to enable their dispersion in polar solvents. POSS-coated nanoparticle were employed to make polymer composites of PVA and nylon 6,6. Use of POSS-coated

TiO_2 nanoparticles in combination with other pigments such Fe_2O_3 resulted in lightening of the color exhibited by the pigment.

* Papers based on above studies have been published in *J. Clust. Sci.* ***(2008)***, *J. Nanosci. Nanotech.* ***(2009)*** *and J. Mater. Chem.* ***(2009)***.

2.1. Introduction

Nanotechnology is almost a household word now-a-days, or at least some word with ‘‘nano’’ in it, such as nanoscale, nanoparticle, nanophase, nanocrystal, or nanomachine. The concept of nanotechnology was first introduced by Nobel laureate Richard Feynman [1] in 1959 at the annual meeting of the American Physical Society at the California Institute of Technology (Caltech). In his classic lecture entitled: "*There is a plenty room at the bottom*", Feynman stated, "*The principles of physics, as far as I can see, do not speak against the possibility of manoeuvring things atom by atom*". Later, Notio Taniguchi from the Tokyo Science University first defined the nanotechnology as: (1) the creation of useful materials, devices, and systems through the control matter at the nanometer length scale and (2) the exploitation of novel properties and phenomena developed at that scale [2]. Thus nanoscience and nanotechnology primarily deal with the synthesis, characterization, exploration, and exploitation of nanostructured materials. These materials are characterized by at least one dimension in the nanometer range. A nanometer (nm) is one billionth of a meter, or 10^{-9} m. Nanoscale microstructural features are not new, either in the natural world or in materials engineering. There are examples of nanoscale ferromagnetic particles found in microorganisms, e.g., 50 nm Fe_3O_4 in the organism *A. magnetotactum* [3]. A number of examples exist of improvement in mechanical properties of structural materials when a fine microstructure was developed. The performance of materials depends on their properties. The properties in turn depend on the atomic structure, composition, microstructure, defects, and interfaces, which are controlled by thermodynamics and kinetics of the synthesis. Nanostructured materials, often characterized by a significant amount of surfaces and interfaces, have been attracting much interest because of their demonstrated or anticipated unique properties compared to conventional materials [4]. This can be explained as follows.

One nanometer is approximately the length equivalent to 10 hydrogen or 5 silicon atoms aligned in a line. Small features permit more functionality in a given space, but nanotechnology is not only a simple continuation of miniaturization from micron meter scale down to nanometer scale. Materials in the micrometer scale mostly exhibit physical properties the same as that of bulk form; however, materials in the nanometer scale may exhibit physical properties distinctively different from that of bulk. Materials in this size range exhibit some remarkable specific properties; a transition from atoms or molecules to bulk form takes place in this size range. In other words nanostructures thus constitute a bridge between molecules and infinite bulk systems. For example, crystals in the nanometer scale have a low melting point and reduced lattice constants, since the number of surface atoms or ions becomes a significant fraction of the total number of atoms or ions and the surface energy plays a significant role in the thermal stability. Crystal structures that are stable at elevated temperatures might not be stable at much lower temperatures in nanometer sizes, so ferroelectrics and ferromagnetics may lose their ferroelectricity and ferromagnetism when the materials are shrunk to the nanometer scale. On the other hand non-magnetic materials tend to show ferromagnetism at nano regime due to surface defects. Bulk semiconductors become insulators when the characteristic dimension is sufficiently small (in a couple of nanometers). Although bulk gold does not exhibit catalytic properties, Au nanocrystal demonstrates to be an excellent low temperature catalyst. This unique phenomenon of varying the properties exhibited by the materials by tuning their size has resulted in the enormous growth in the field of synthesis of various nanostructures with a control in their size and morphology.

Obviously there are two approaches to the synthesis of nanomaterials and the fabrication of nanostructures: top-down and bottom-up. Attrition or milling is a typical top-down method in making nanoparticles, whereas the colloidal dispersion is a good example of

bottom-up approach in the synthesis of nanoparticles. Both the approaches have their advantages and disadvantages and both are widely used in the synthesis of nanomaterials [5-7].

One way to distinguish nanostructured materials is based on their dimensionality, i.e. according to the number of spatial dimensions in which the materials are *not* nanoscaled. In recent years, much attention has been devoted to zero-, one- and two-dimensional nanostructures, e.g. nanoparticles (0-D), nanotubes and nanowires (1-D) or thin films and multilayer systems (2-D). Given below are the various nanostructures of different dimensionalities and their approximate size range [5].

Nanostructures and Their Assemblies

Nanostructure	Size	Material
Clusters, nanocrystals Quantum dots	Radius, 1–10 nm	Insulators, semiconductors, metals, magnetic materials
Other nanoparticles	Radius, 1–100 nm	Ceramic oxides
Nanobiomaterials, Photosynthetic reaction center	Radius, 5–10 nm	Membrane protein
Nanowires	Diameter, 1–100 nm	Metals, semiconductors, oxides, sulfides, nitrides
Nanotubes	Diameter, 1–100 nm	Carbon, layered Chalcogenides, BN, GaN
Nanobiorods	Diameter, 5 nm	DNA
Two-dimensional arrays of nanoparticles	Area, several nm^2–μm^2	Metals, semiconductors, magnetic materials
Surfaces and thin films	Thickness, 1–100 nm	Insulators, semiconductors, metals, DNA
Three-dimensional superlattices of nanoparticles	Several nm in three dimensions	Metals, semiconductors, magnetic materials

0-D nanomaterials encompasses nanoparticles which are in the range 1-100 nm which could be noncrystalline, an aggregate of crystallites or a single crystallite, nanocrystals that are single crystals in nanometer size and quantum dots which exhibit size quantification effect in at least one dimension. Among the various nanoparticles, gold nanoparticles have, in particular, been the subject of considerable attention over the ages and enjoy an interesting history dating back to the pioneering work of Faraday on the synthesis of gold hydrosols (gold nanoparticles dispersed in water) [8]. Gold nanoparticles find application in a variety of fields such as catalysis [9], as electron microscopy markers [10] and in DNA sequence

determination. The procedures for synthesis of gold hydrosols include, (1) reduction of aqueous chloroaurate ions by a variety of reducing agents such as citric acid [11], sodium borohydride [12], and alkaline tetrakis(hydroxymethyl)phosphonium chloride [13]; (2) radiation-induced reduction of gold ions [14, 15] and (3) sonochemical reduction of gold ions [16], to name just a few. The synthesis of gold nanoparticles in non-polar organic media is a considerably newer area of research whose origin may be traced to the seminal work of Brust and co-workers [17]. In this report, the authors have demonstrated the phase transfer of chloroaurate ions into toluene using a phase transfer molecule such as tetra-alkylammonium bromide. Thereafter, the gold ions were reduced using sodium borohydride to yield gold nanoparticles of excellent monodispersity capped with alkanethiol molecules. Brust and co-workers used thiolate chemistry to cap the gold nanoparticles with alkanethiols present in the organic phase during phase transfer and reduction of the gold ions, thus rendering them hydrophobic and soluble in the organic phase. Such surfactant stabilized gold nanoparticles behave like new compounds and can be easily separated out of solution in the form of a powder and re-dissolved in different organic solvents without significant variation in the particle size distribution.

Nanotubes and nanowires are designated as 2-D nanostructures. Nanowires are called by variety of names such as whiskers, fibers or fibrils and nanorods depending upon their aspect ratio. Although whiskers and nanorods are in general considered to be shorter than fibers and nanowires, the definition is often a little arbitrary. As far as 1-D nanostructures next to silicon there has been considerable interest in the synthesis of 1-D nanostructures of ZnO due to its potential application in various fields [18]. Using a vapour-solid process and without the use of metal catalyst nanobelts and various other nanostructures of ZnO were formed [19]. Aligned growth of ZnO nanorods has been successfully achieved on solid substrates using vapour-liquid-solid (VLS) or vapour-solid-solid (VSS) processes with the use of Au nanoparticles as

catalysts [20, 21], in which the catalyst initiates and guides growth, and the epitaxial orientation relationship between the nanorods and the substrate leads to aligned growth [22]. Nanorods of Single crystalline ZnO has been synthesized by solvothermal method [23].

Of all the nanostructures, carbon nanotube (CNT) is one of the widely studied systems because of its unique properties which in turn make it commercially important. After the discovery by Iijima [24], several new methods were devised for the synthesis of CNTs. Multi-walled carbon nanotubes (MWNTs) can be produced in high yields by the catalytic combustion of polypropylene in the presence of an organically-modified clay and a Ni catalyst [25]. Carbon nanotubes prepared by the catalytic decomposition of methane over Mo/Ni/MgO catalysts turn out to be fairly thin with 2–4 graphitic walls due the formation of small Ni-Mo catalyst particles (2–16 nm in diameter) [26]. Alignment of MWNTs can be achieved by making use of Fe_2O_3 nanoparticles and magnetic fields [27]. A controlled synthesis of aligned MWNTs can be achieved by a layer-by-layer assembly of multilayer catalyst precursor films with the desired number of layers and composition [28]. Single-walled carbon nanotubes (SWNTs) have been grown using small catalytic iron nanoparticles synthesized within protein cages as catalysts [29]. A low-temperature method for the growth of SWNTs by water plasma chemical vapor deposition (CVD) has been reported [30]. Vertical growth of SWNTs of small diameter has been accomplished by heating small iron nanoparticles in the presence of an activated gas [31].

Thin films which are classified as 2-D nanomaterials have thickness in the nano regime while their length can be few microns. Film growth methods can be generally divided into two groups: vapor-phase deposition and liquid-based growth. The former includes, for example, evaporation, molecular beam epitaxy (MBE), sputtering, chemical vapor deposition (CVD), and atomic layer deposition (ALD). Examples of the latter are electrochemical

deposition, chemical solution deposition (CSD), Langmuir-Blodgett films and self-assembled monolayers (SAMs). Thin films of various metal and metal chalcogenides have also been prepared by means of liquid-liquid interface. Recently studies on 2-D graphene has created quite a sensation because of the unusual properties exhibited by graphene and its potential applications [32]. During the initial studies, graphene was mainly prepared by means of micromechanical cleavage which unfortunately cannot be used for large-scale applications. The other methods employed to synthesize graphene include (a) pyrolysis of camphor under reducing conditions [33], (b) exfoliation of graphitic oxide [34], and (c) conversion of nanodiamond [35].

After reviewing the various nanostructures of different dimensionality by taking one material for each case and its general approaches employed for their synthesis, it is clear that these nanostructures with their unique properties can play major role in the development of future technology. While a number of suitable methods have been developed for the synthesis of various nanostructures of different dimensionality, successful application of such nanostructures is highly dependent on the stability of the particles under a range of different conditions. One among the conditions is to have a stable dispersion of the nanoparticles in desired solvent. Consequently, it may be necessary to modify the surface of materials. The most common way to do so is to attach suitable groups to the surface atoms. Other than to provide solubility, surface modifications are also carried out to stabilize nanoparticles against agglomeration. The modification can avoid homogeneity and compatibility problems between the two phases and thus improve the mechanical properties of the composite. A third interest in structures modification is to enable their self-organization. Thus functionalization of nanostructures is a field that is as important as the synthesis or application oriented research.

Surface modification of nanostructures can be done either by covalent functionalization or non-covalent interactions. Wrapping of polymers around nanostructures

is an example for non-covalent interactions. Covalent functionalization of nanostructures in turn can be done in two ways. In method one, the functionalization of the nanostructures can be achieved during the synthesis itself, leading to *in-situ* surface modification. This is usually achieved by using complexing agents which can bind to the surfaces thereby stabilizing the nanostructures during their formation. In the post-synthesis-modification method, nanostructures are synthesized and the surface of the pre-synthesized nanostructures modified with ligands which posses the desired functionality. The extent of surface modification and the choice of ligands depend upon the ease with which the material can interact with the ligand. For example noble metal nanoparticles are mainly modified by thiols, disulfides, amines, nitriles, carboxylic acids and phosphines whereas metal oxide nanostructures are usually functionalized with carboxylates, phosphonates and silanes. Nitride nanostructures are functionalized by exploiting the presence of surface amino groups which can be reacted with an acid chloride. In all cases, it must be duly noted that functionalization of the particles necessarily yields a drastic change of their surfaces. Hence care should be taken, so that the choice for the functionalization function must be a compromise between having the maximum number of desirable functional groups for having the stability of the particles in their dispersion media and not to exceed the threshold limit, so that the inherent properties of the nanostructure under investigation are preserved.

2.2. Scope of the present investigations

Among the various one-dimensional nanostructures, carbon nanotubes (CNTs) have been the most fascinating and have been studied extensively ever-since their discovery in 1991 [24]. Interest in CNTs stems from the fact that they possess exceptional mechanical and electrical properties [36]. However, a number of significant problems are to be addressed before

they can measure upto their full potential as practical, functional nanomaterials. Difficulties associated with their lack of solubility and homogeneity have long been causing hindrance to some of the practical applications. CNTs are insoluble in all known solvents and this is a serious problem limiting our ability to carry out solution-based processing or characterization. CNTs have been rendered soluble by covalent functionalization, [37] but this is not a favoured route as it strongly modifies their chemical and physical properties. The only possible way to suspend CNTs in solution, without perturbing their electronic or mechanical properties, is by the use of a surfactant [38] or a polymer [39, 40]. Such research efforts have stimulated and enabled the exploitation of the properties and applications that are not otherwise accessible in the solid state, through dispersions of CNTs in polymeric nanocomposites [41].

Owing to their novel properties and potential applications, interest in the synthesis and properties of one-dimensional (1D) nanostructures such as nanowires and nanorods is increasing enormously [42-44]. In particular, nanostructures of metal oxides and other inorganic materials have been the subject of extensive research due to their possible use in catalysis and mesoscopic physics as well as in the fabrication of nanoscale electronic, optical, optoelectronic, electromechanical and sensing devices [45, 46]. Nanostructures of ZnO, CdO, Ga_2O_3, In_2O_3, TiO_2 and SnO_2 and other oxides have been explored in this regard [47, 48]. Processing metal oxide nanostructures often requires their dispersion or dissolution in appropriate solvents. Since the as-synthesized metal oxide nanostructures do not form stable dispersions and generally settle down rapidly, it becomes necessary to functionalize surfaces of the oxide nanostructures appropriately to enable their dispersion or solubilization in the desired solvents. There are reports of the use of surfactants [49] and oligomeric ligands [50] to obtain stable dispersions of oxide nanowires.

The presence of residual amino groups on the surface of metal nitride nanostructures have been exploited in their functionalization. Xie et al. [51] have functionalized BNNTs with oligomeric diamine-terminated PEG in which the amino groups on the polymer interact with the surface of BNNT and thereby enable their dispersion in aqueous media. Pal et al. [52] have obtained a stable hydrocarbon dispersions of BNNTs functionalized with Lewis bases such as a trialkylamine or a trialkylphosphine. These authors suggest that BNNTs act as Lewis acids because of the inherent electron deficiency of the boron in BNNT. Reports on the surface functionalization of GaN nanostructures are scarce. Estephan et al.[53] have functionalized GaN nanocrystals with a peptide which has specific recognition for GaN.

We considered it most useful to explore newer and better methods of functionalizing and solubilizing the inorganic nanostructures as well as carbon nanotubes. For this purpose, we have explored the use of organosilicon and organotin reagents. Organosilanes are used as lubricants and in a wide range of situations including the formation of self-assembled monolayers [54-56]. Coating inorganic nanocrystals with silica using organosilanes and functionalization of silica gel using allylsilanes has been reported in the literature [57-62]. Silica coatings are generally obtained either by the sol-gel reaction involving silanes in an alcohol-water mixture or by the use of reverse microemulsions [63]. Modification of silica or glass slides is often carried out by the reaction with a silane in toluene solution [59]. Byrne et al [64] have used alkoxysilanes to prepare titania-reinforced polystyrene nanocomposites.

Herein we have tried to solubilize nanoparticles of metal oxides in toluene and water by employing surfactants like PEO, TX-100, PVA, PEG, SDS and AOT. We have also attempted a detailed investigation of the covalent functionalization of various nanostructures by organosilicon and organotin reagents in order to obtain stable dispersions in non-polar solvents. POSS has been synthesized and lab which in turn was used to functionalize

nanostructures to solubilize them in polar solvents. We have investigated nanowires and nanoparticles of several metal oxides which include TiO_2, ZnO, Al_2O_3, CeO_2 and Fe_3O_4 because of their importance in various applications. For example, it is useful to have dispersions of Fe_3O_4 nanoparticles for magnetic resonance imaging. Similarly, dispersions of TiO_2 and ZnO nanostructures are useful not only for preparing composites but also in applications such as photovoltaics. We have investigated nanostructures of BN because of its high mechanical strength and of GaN because of its useful optical and electrical properties. In addition, we examined dispersions of multiwalled carbon nanotubes (MWNTs) because of their wide utility.

For the covalent functionalization of the nanostructures we have used organosilane, POSS or organotin reagents. Organosilanes find use as cross linking agents, enhanced substrate adhesives and moistures absorbents. A coating of organosilane will provide nanostructures with good water dispersibility, biocompatibility, and surface functionality, as the silanol group on the silica shell offers versatile possibilities for covalently functionalizing their surface. The octa(tetramethylammonium)-polyhedral oligomeric silsesquioxane or TMA-POSS is an anionic silicate species with the double eight-membered Si_4O_4 ring, $Si_8O_{20}^{8-}$, the cubic octamer, is formed selectively by adding tetramethylammonium ions or other organic quaternary ammonium ions with three methyl groups to silicate solutions. These octasilsesquixanes are 1.2–1.4 nm in diameter and can have functional groups in each octant in Cartesian space, either opposite or completely orthogonal to each other. This symmetry allows their assembly in one, two or three dimensions nm by nm, selectively with complete control of periodicity over very long length scales. In Figure 2.2.1, we show the structure of POSS. We have exploited the surface functionalities present on the inorganic nanostructures for functionalizing them. In the case of metal oxide nanostructures, they

generally possess surface hydroxyl groups while we can generate carboxyl and hydroxyl groups on MWNTs, graphene and nanodiamond by acid treatment.

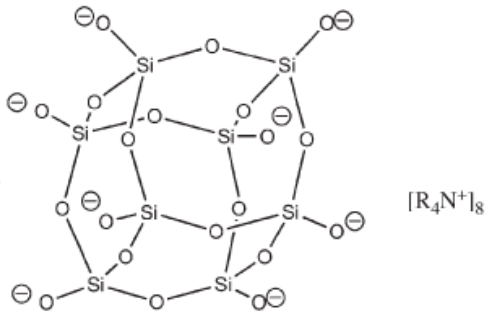

Figure 2.2.1: Structure of TMA-POSS

Though the nitride nanostructures on the other hand have surface amino groups, they are enough quantitatively for the functionalization. We therefore tried to create a very minimal surface oxide layer by treating the nanostructures with dilute nitric acid so as to make their surface reactive. We have employed organosilane, organotin reagents and POSS to react with the surface hydroxyl groups resulting in the organometallic coating. The routes to functionalize with organosilanes can generally be classified into two groups, i.e., the Stöber process-based approaches and the reverse (water-in-oil) microemulsion method. In our procedure we have carried out the reaction in toluene to slower the reaction rate of silanes in toluene compared to aqueous media. In Figure 2.2.2, we show a schematic depicting the functionalization of nanostructures with organosilicon or organotin reagents. Upon functionalization the surface of the nanostructures can be rendered hydrophobic or hydrophilic depending on reagents which in turn would enable their dispersion in solvents of corresponding polarity. Organosilane- or organotin-functionalized nanostructures on heating under air/oxygen resulted in silica- or tin oxide-coated nanostructures. Water soluble POSS-coated nanoparticles of TiO_2, Fe_2O_3 and activated graphite were employed to prepare composites of PVA and Nylon-6,6. Part of the purpose was to get polymer composites with colors bestowed by the inorganic nanoparticles in combination with TiO_2 nanoparticles

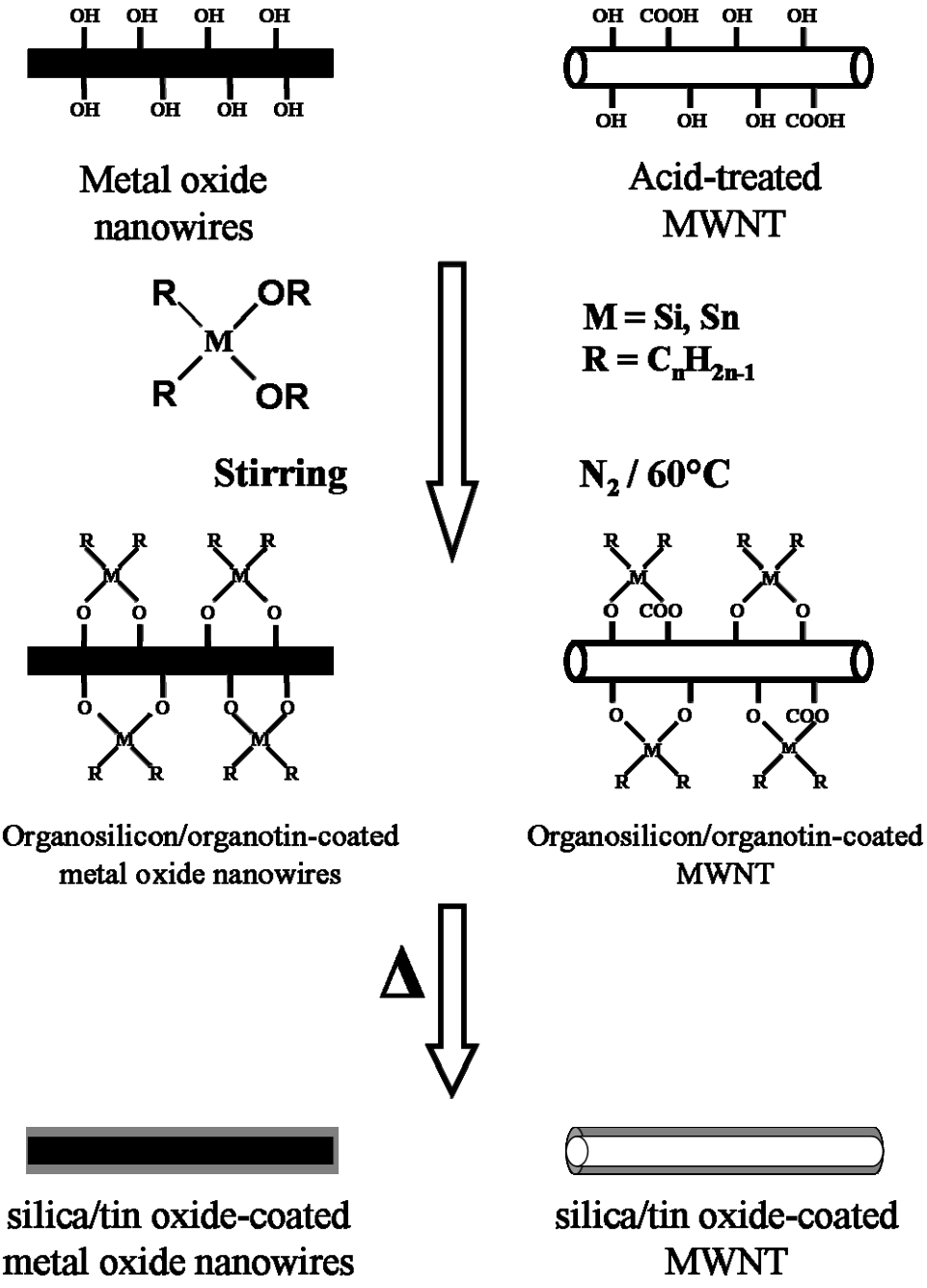

Figure 2.2.2: Scheme showing the typical procedure employed for coating oxide nanostructures and MWNTs with organosilicon or organotin reagents.

2.3. Experimental and related aspects

2.3.1. Metal Oxide nanostructures

- ***Synthesis***

The nanoparticles of TiO_2 ZnO, Fe_3O_4, Fe_2O_3 and CeO_2 were prepared following slight modifications of the solvothermal procedures already reported in the literature. The solvothermal procedure is favoured over the other known methods because of its low cost, versatility and potential large scale production capability. The synthetic methodologies employed are as outlined below.

TiO_2 nanoparticles were synthesized by employing a sol-gel method with titanium isopropoxide [65] as raw material. 10 ml of titanium isopropoxide was mixed with 40 ml of anhydrous ethanol in a dry atmosphere. The mixed titanium isopropoxide/ethanol solution was then hydrolyzed by adding it to another mixture comprising 10 ml of water, 10 ml of anhydrous ethanol and 2 ml of 70% HNO_3 at room temperature dropwise under stirring. A yellowish transparent sol was obtained subsequently after continuous stirring for 2 h. The sol was then allowed to stand for 6 h at room temperature and was dried at 343 K for 24 h to yield the dry gel precursor. Finally, TiO_2 nanoparticles were obtained by calcining the gel precursor at 450 °C for 2 h. The average diameter of the TiO_2 nanoparticles is ~13 nm

In the case of ZnO nanoparticles, 0.25 mmol of zinc acetate was dissolved in 42 ml of isopropanol with constant stirring at 323 K and then quenched in ice. To this solution, 0.32 mmol of NaOH in 8 ml of isopropanol was added, and the solution was maintained at 338 K in a water bath. The precipitate formed was washed with distilled water and collected by centrifugation [66].

To prepare Fe_3O_4 nanoparticles, we used the method due to Kang et al. [67]. The synthetic methodology involves successive dissolution of 5.2 g of $FeCl_3$ and 2.0 g of $FeCl_2$ in 25 ml of distilled water containing 0.85 ml of 12.1 N HCl. The resulting solution was then added dropwise into 250 ml of 1.5 M NaOH solution under vigorous stirring. The last step generated an instant black precipitate. The precipitate was isolated in the magnetic field, and the supernatant was removed from the precipitate by decantation. The average diameter of the Fe_3O_4 nanoparticles is ~17 nm.

α-Fe_2O_3 was synthesized by precipitation process in basic media in which a 0.5 M acidic solution of ferric nitrate $Fe(NO_3)_3$.9H2O was added into a beaker containing 7.2 M NH_4OH solution in order to precipitate the hydroxide form, $Fe(OH)_3$. The pH was maintained at about 9.5. The resultant brown precipitate was dried overnight at 373 K followed by a thermal treatment at 673 K for 6 h in ambient atmosphere to obtain α-Fe_2O_3 nanoparticles [68].

CeO_2 nanoparticles were prepared by the addition of 0.1 M of 100 mL $Ce(NO_3)_3$ to 100 mL of 0.5 M of hexamethylenetetramine at 343 K under constant stirring. The pale yellow precipitate formed was filtered and calcined to give CeO_2 nanoparticles [69].

TiO_2 nanowires crystallizing in the anatase phase were synthesized through a slight modification of the solvothermal route reported by Wen et al. [70] using the mixed solvent aqueous NaOH-ethanol. In a typical synthesis, 0.115 g of commercial Degussa P25 powder was mixed with 3.5 ml of 10 M NaOH and 3.5 ml of ethanol. The mixed solution was then transferred into a 35 ml Teflon-lined stainless-steel autoclave. The autoclave was maintained at 453 K under autogenous pressure for 24 h and then cooled to room temperature naturally. The sample so obtained was filtered off, washed several times with dilute HCl aqueous solution and water until the pH value of the washing solution was about 7. The sample was

dried and annealed at 723 K for 2 h. The TiO_2 nanowires so obtained have diameters in the 60-150 nm range and are a few microns in length.

ZnO nanowires were obtained by a slight modification of the method reported in the literature [71]. The synthetic protocol involves the hydrolysis of zinc acetate under solvothermal conditions. In a typical synthetic procedure, 0.29 g (1.32 mmol) zinc acetate dihydrate ($Zn(Ac)_2.2H_2O$) was first dissolved in 50 ml ethanol and then 1.6 g (0.04 mol) NaOH was added and stirred for 1.5 h to make it dissolve at room temperature. The resulting cloudy solution was sealed in a 70 ml Teflon-lined stainless-steel autoclave and heated at a temperature of 373 K for 24 h. The autoclave was then allowed to cool down to room temperature. White or yellow precipitates were collected and washed with water and ethanol several times until the washing solution was free of NaOH. The average diameter of the ZnO nanowires is ~14 nm with lengths going up to a few microns.

Al_2O_3 nanowires and nanotubes were synthesized by a carbothermal procedure involving the use of a mixture of aluminum and graphite or active carbon powders [72]. In a typical procedure, a finely ground intimate mixture of aluminum and graphite powders (molar ratio 1 : 1) was placed in an alumina boat kept and heated under the flow of Ar (50 standard cubic centimeters per minute, sccm) and oxygen (10 sccm). The temperature was maintained at 1573 K for 6 h. The Al_2O_3 nanowires obtained by this method have an average diameter 150-200 nm.

- ***Functionalization with surfactants***

The dispersions of metal oxide nanoparticles were obtained as follows. Surfactant solutions of 1% (weight/volume) strength were prepared in different solvents. A known quantity of the nanoparticles (5 mg in each case) was dispersed in 20 ml of the solutions and

sonicated in a water bath for 1 h. The dispersion was allowed to stand for 24 h and then characterized.

- ***Functionalization with organosilane or organotin reagents***

γ-Aminopropyltriethoxysilane (APTES), hexadecyltrimethoxysilane (HDTMS), chlorotriethoxysilane, dibutyldimethoxytin and trioctyltinchloride were purchased from Sigma Aldrich and used without any further purification. The solvents used were distilled and stored over sodium. All air and moisture sensitive compounds were handled under a nitrogen atmosphere.

In a typical experiment to coat the oxide nanostructures with the organosilicon or an organotin reagent, about 30 mg of the oxide nanoparticles were ground into a fine powder using an agate mortar and pestle and placed in a clean and dry round-bottomed flask. To this 20 ml of dry toluene was added and the mixture was placed in a sonic bath for 30 minutes. Organosilane or organotin reagent was then added to the nanoparticles at a 1:1 (organosilane or organotin : metal oxide) molar ratio by micropipette in a nitrogen atmosphere. The mixture was refluxed at 373 K for 12 h after which the mixture was cooled down and the residue washed with dry hexane and then with water–acetone mixture (20% of H_2O). The functionalized nanoparticles were dried in vacuum for one day under ambient temperature.

To coat the metal oxide nanowires with an organosilicon or an organotin reagent, typically about 30 mg of the nanowires were ground into powder in an agate mortar and placed in a clean and dry round-bottom flask. To this 20 ml of dry toluene was added and the mixture placed in a sonic bath for 30 minutes. The organosilicon or organotin reagent was added to the nanowires at a 1:1 molar ratio (organosilane or organotin : metal oxide) from a micropipette in a nitrogen atmosphere. The mixture was stirred at 333 K for 12 h after which

the mixture was cooled down and the residue washed with dry toluene and then with water–acetone mixture (20% of H_2O). The functionalized nanowires were dried in vacuum for one day under ambient temperature.

- ***Functionalization with polyoctasilsesquioxane (POSS)***

Synthesis of TMA-POSS

Tetramethylammonium silicate methanolic solutions were prepared by stirring a mixture of tetraethoxysilane, water and a methanolic solution of TMA hydroxide for 2 days at room temperature. Air in the vessels was substituted by nitrogen gas after adding deionized water for the hydrolysis of tetraethoxysilane to the mixtures, and the vessels were sealed. The mixtures were kept for 2 days at room temperature under stirring**.** The conditions of the solutions were such that the $Si0_2$ concentration was 1.0 mol dm^3, the TMA ions-to-SiO_2, molar ratio was 1.0, and the water-to-SiO_2, molar ratio was 10.0. After stirring, the cubic octameric silicate species formed in the solutions were separated, washed and dried under vacuum [78].

To functionalize nanostructures with POSS, for about 30 mg of the nanostructures 150 mg of POSS was taken resulting in 1:5 weight ratio of POSS/nanostructures. The nanostructures were taken in a round bottom flask and dispersed in absolute ethanol by ultra sonication followed by addition of required amount of POSS. The system was then purged with nitrogen for 10 min and then sealed. The reaction was allowed to continue for 24 h under constant vigorous stirring. After the completion of the reaction, the POSS-functionalized nanostructures were washed with ethanol and dried under vacuum.

2.3.2. Metal Nitride nanostructures

- ***Synthesis***

In the synthesis BN, 100 mg of H_3BO_3 and 600 mg of urea, taken in the molar ratio 1:6 was ground to give an intimate mixture. The mixture was then taken in an alumina boat and heated in a tube furnace at 1273 K for 3 h in a N_2 atmosphere [73].

GaN nanocrystals were prepared by a simple route based on the single source precursor, gallium–urea complex $[Ga(H_2NCONH_2)_6]Cl_3$, as reported in the literature [74]. The gallium–urea complex was prepared by dissolving 2 g of Ga_2O_3 in conc. HCl to give $GaCl_3$ and the excess HCl was removed by heating. Urea (15.37 g) and isopropanol (20 ml) were added to the $GaCl_3$ and stirred for two hours. A white precipitate was obtained which was filtered and washed. GaN nanocrystals were obtained by refluxing the gallium urea complex (500 mg) in n-trioctylamine (20 ml) for 24 h. The nanocrystals were precipitated by the addition of isopropanol after cooling the reaction mixture. GaN nanocrystals were also annealed in an ammonia atmosphere at 723 K for 24 h to improve their crystallinity and are designated as annealed GaN nanocrystals.

In order to prepare BN nanotubes, an intimate mixture of finely 0.36 g of multi-walled carbon nanotubes and 0.62 g boric acid (mole ratio 3:1) was taken in an 8 mm quartz tube closed at one end, and held vertically inside a larger quartz tube placed in a tubular furnace. NH_3 gas was passed through the quartz tube (flow rate 10 sccm) and the temperature of the furnace, maintained initially at 473 K for 2 h, was slowly raised to 1273 K and maintained at that temperature for 3 h. The product obtained was light grey powders formed at the bottom of the inner quartz tube. White deposits formed at the mouth of the inner quartz tube and also at the outlet of the outer quartz tube. The white product was identified as pure BN. The grey

product had some carbon depending on the carbon content in the starting composition. The average outer diameter of the nanotubes varied from 50 to 150 nm [75].

- ***Functionalization with organosilane or organotin reagents***

To coat the metal nitride nanostructures such as the nanoparticles and nanotubes of BN and nanoparticles of GaN with organosilane or organotin reagents, the nanostructures were first treated with dilute HNO_3 and then treated with the organosilane or organotin reagent, employing a procedure similar to that mentioned before.

2.3.3. Carbon nanostructures

- ***Synthesis***

Multi-walled carbon nanotubes were prepared by the pyrolysis of ferrocene [76]. Pyrolysis of the ferrocene was carried out in a quartz tube located in a two-stage furnace system. In a typical experiment, a weighed quantity of a ferrocene was taken in a quartz boat, placed inside a furnace and a mixture of Ar (75%)-H_2 (25%) was passed through the quartz tube. The furnace temperature was increased to 473 K and the ferrocene vapour so generated was carried by the Ar-H_2 stream, into a quartz tube maintained at 1173 K in a second furnace. The decomposition of the ferrocene occurs in the second furnace. The as-synthesized MWNTs synthesized were refluxed with conc. HCl to remove the metal nanoparticles. The MWNTs were acid-treated to have surface carboxyl and hydroxyl groups. For this 100 mg of the MWNTs were refluxed with 30 ml conc. HNO_3 for 12 h after which 10 ml conc. H_2SO_4 was added followed by refluxing for another 12 h. The acid-treated MWNTs were washed with distilled water and dried under vacuum.

Graphene samples utilized in the present studies were prepared by the thermal exfoliation of graphitic oxide and are designated as EG [77]. In this method, graphitic oxide was

prepared by reacting graphite (Alfa Aesar, 2–15 *m*m) with a mixture of conc. nitric acid and sulfuric acid with potassium chlorate at room temperature for 5 days. Enough care was taken to cool down the experimental set up at the initial stages as the reaction is highly exothermic. The graphitic product obtained washed and dried under ambient conditions. Thermal exfoliation of graphitic oxide was carried out in a long quartz tube at 1323 K under an Argon atmosphere. The acid-treatment of EG samples was done as follows. Initially conc. nitric acid (2 mL), conc. sulfuric acid (2 mL) and water (16 mL) were added to graphene (50 mg) and subsequently heated in a microwave oven for 10 min under hydrothermal conditions. Further, the sample was heated at 373 K for 12 h. The product was washed with distilled water and centrifuged repeatedly to remove traces of acid. This yielded graphene that was functionalized with –OH and –COOH groups.

- ***Functionalization with organosilane or organotin reagents***

In order to coat the MWNTs or EG with an organosilane or organotin reagent, about 20 mg of the acid-treated MWNTs or EG were placed in round-bottom flask and to this was added 20 ml of dry toluene. To this the organosilane or organotin reagent was added at 1:1 molar ratio in the presence of nitrogen atmosphere. The mixture was then stirred at 333 K for 12 h after which it washed with the same procedure as that of nanowires.

- ***Functionalization with POSS***

To functionalize carbon nanostructures with POSS, a procedure similar to that used for metal oxide nanostructures was employed. Acid-treated carbon nanostructures were treated with POSS (1:5 weight ratio) in absolute ethanol in a nitrogen atmosphere. The reaction was carried out for 24 h and the products obtained were washed with ethanol to remove excess unreacted POSS and dried under ambient conditions.

- ***Dispersion studies***

Dispersion studies were carried by sonication of the functionalized nanostructures in desired solvents for 5 minutes. THE APTES-, HDTMS-, dibutyldimethoxytin-, trioctyltinchloride-coated nanostructures were dispersed in toluene and CCl_4 whereas the nanostructures functionalized with POSS were dispersed in ethanol. The excess nanostructures were removed by centrifugation and the dispersion was kept undisturbed to check the stability of the coated nanoparticles in the solvent.

2.3.4. Composites of PVA and Nylon-6,6 with POSS-functionalized inorganic nanoparticles

Synthesis of Nylon 6, 6

Nylon 6,6 was synthesized by an interfacial polycondensation reaction between hexamethylenediamine and freshly prepared adipoyl chloride. For this purpose, 10 g of adipic acid was taken in a clean round bottom flask. To this 12 mL of thionyl chloride was added followed by an addition of few drops of DMF and the mixture was refluxed for 3 h. The excess thionyl chloride was removed by rotary evaporation. The obtained product was dissolved in hexane. 1 g of hexamethylenediamine was dissolved in 25 mL distilled water in a 100 mL beaker. To this 0.2 g of sodium hydroxide was added. Then 1 g of adipoyl chloride dissolved in 25 mL of hexane was added carefully to hexamethylenediamine using a glass rod along the sides of the beaker. Nylon 6, 6 formed at the interface was taken out using a copper hook and it was rinsed with distilled water several times.

Synthesis of PVA composites

In a typical preparation of PVA-nanoparticles composite, required amount of POSS-treated nanoparticles were dispersed in warm water and stirred for 2 h. Followed by this

appropriate amount of PVA was added to the mixture and the solution was heated at 343 K with vigorous stirring until the polymer dissolved forming a dispersion of the nanoparticles. The polymer-nanoparticles dispersion was dried in Petri dishes at 310 K over period of 3 days. Composites of PVA with different weight ratios of nanoparticles of TiO_2, Fe_2O_3 and graphite were prepared to study the variation in color induced by varying the amount of TiO_2 nanoparticles in the composites.

Synthesis of nylon-6,6 composites

To prepare nylon 6,6-nanoparticles composites of various ratios (see Table 1), calculated amount of nanoparticles were taken in 100 ml beaker containing distilled water. To this solution, 0.5 g of hexamethylenediamine and 0.25 g of NaOH were added. This mixture was stirred for 2 h to enable uniform dispersion of the nanoparticles in water. Followed by this 0.5 g adipoyl chloride taken in another beaker containing 20 mL of hexane was slowly added to the above mixture along the sides of the beaker. The nylon composite formed at the interface of the two layers was removed, washed with distilled water several times and kept for drying.

• *Characterization Techniques*

X-ray Diffraction: X-ray diffraction (XRD) patterns of the nitrides were recorded using Cu Kα radiation on a Rich-Siefert XRD-3000-TT diffractometer.

Scanning electron microscopy: Scanning electron microscope (SEM) images were obtained using a LEICA S440i SEM.

Field emission scanning electron microscopy: Field emission scanning electron microscopy (FESEM) images were obtained using a FEI NOVA NANOSEM 600.

Transmission electron microscopy: For transmission electron microscopy, the nitrides were dispersed in CCl_4 and dropped on to the holey carbon-coated copper grids. The grids were allowed to dry in the air. Transmission electron microscope (TEM) images were obtained with a JEOL JEM 3010, operating with an accelerating voltage of 300 kV.

Thermogravimetric analysis: Thermogravimetric analysis (TGA) was carried out on a Mettler-Toledo-TG-850 instrument

Raman spectroscopy: Raman spectra were recorded with a LabRAM HR with the 633 nm line from HeNe laser. The excitation wavelength is 632.8 nm.

Infrared spectroscopy: Infrared spectra were recorded using Bruker IFS 66v/S spectrometer.

2.4. Results and Discussion

2.4.1. Metal Oxide nanostructures

- ***Characterization of nanostructures***
- ***Metal oxide nanoparticles***

TiO_2 nanoparticles prepared by sol-gel method gave a XRD pattern as shown in the Figure 2.4.1 with peak $2\theta = 25.34$ ° characteristic of the anatase phase whereas the rutile phase will have the corresponding peak at $2\theta = 27.4$ °. The broad peaks indicate the nanocrystalline nature of the particles and from Scherrer formula average size was calculated to be 8 nm. In Figures 2.4.2, we show the electron microscope images of the as-prepared TiO_2 nanoparticles. Figure 2.4.2 (a) is the FESEM image of the nanoparticles while the TEM image of the TiO_2 nanoparticles is given in Figure 2.4.2 (b) with the particle size distribution as its inset. From the TEM image particle size distribution the average size of the

nanoparticles were calculated to be ~ 8 nm. TEM image showed that the particle distribution was appreciable uniform.

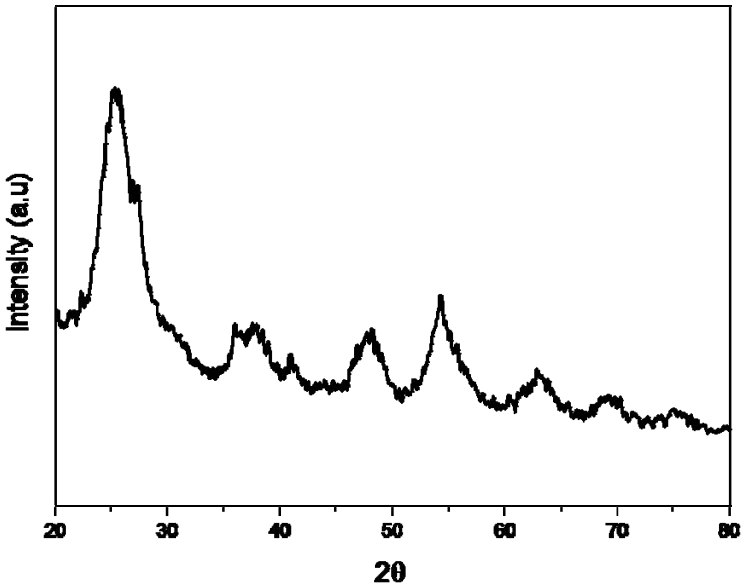

Figure 2.4.1: XRD pattern of TiO_2 nanoparticles.

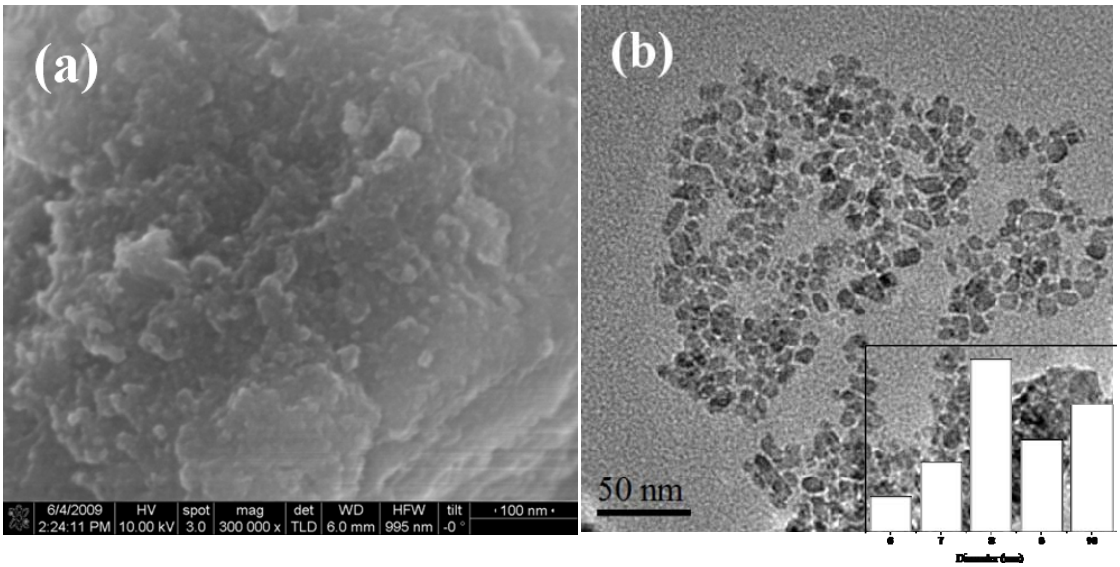

Figure 2.4.2: Electron microscope images of TiO_2 nanoparticles: (a) FESEM and (b) TEM.

In Figure 2.4.3 we show the XRD pattern of the ZnO nanoparticles from which the particle size is calculated to be ~ 20 nm. The pattern could be indexed as the hexagonal wurtzite structure and no crystalline hydroxide phase was observed. In Figure 2.4.4 (a), we show the FESEM image of the ZnO nanoparticles. From the TEM image of the ZnO

nanoparticles shown in Figure 2.4.4 (b) which is fairly monodisperse, the average size of the nanoparticles were found to be around 17 nm from particle size distribution histogram shown as inset.

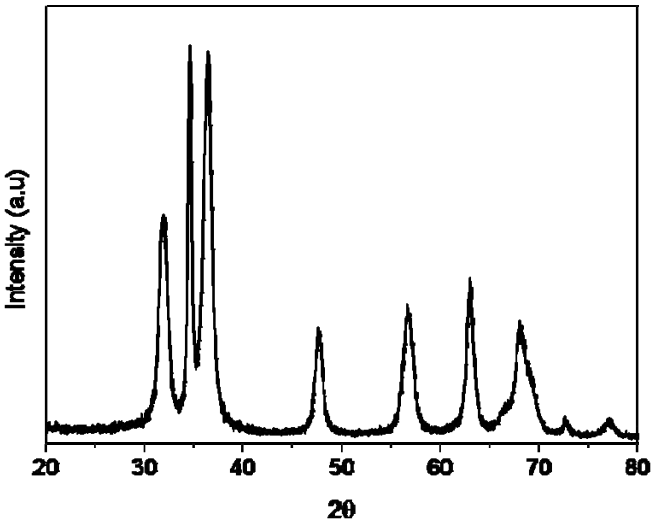

Figure 2.4.3: XRD pattern of ZnO nanoparticles.

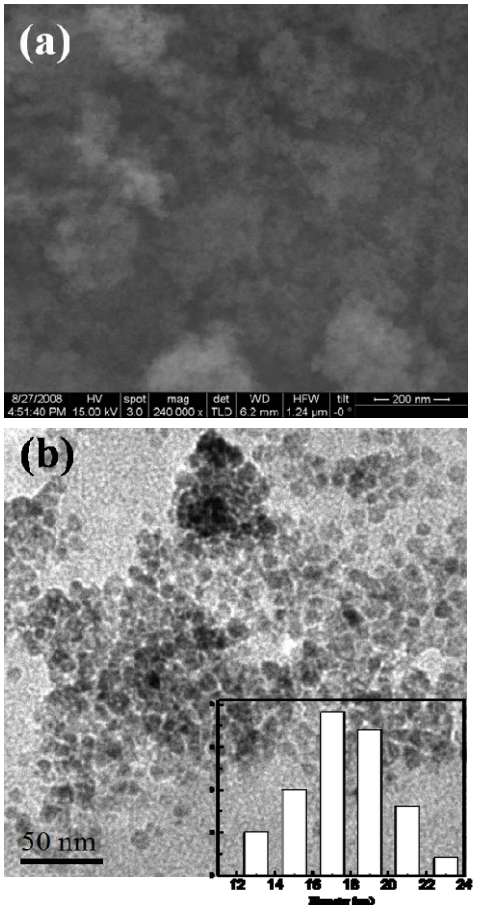

Figure 2.4.4: (a) FESEM and (b) TEM images of ZnO nanoparticles.

Fe_3O_4 nanoparticles were prepared by the coprecipitation of $FeCl_2$ and $FeCl_3$ in NaOH in which the molar ratio of Fe(II)/Fe(III) = 0.5 and a pH = 11-12 was maintained which is a prerequisite to synthesize nanoparticles which are homogeneous both in size and composition. The as-synthesized nanoparticles gave a XRD pattern as shown in Figure 2.4.5 (a). From XRD pattern particle size was calculated to be ~ 11 nm. The peaks could be indexed to the cubic magnetite and it also indicates that the product is nanocrystalline single phase Fe_3O_4 without any impurities. In Figure 2.4.5 (b) is shown the TEM image of the nanoparticles with particle size distribution histogram as inset which shows the average particle size to be ~ 13 nm.

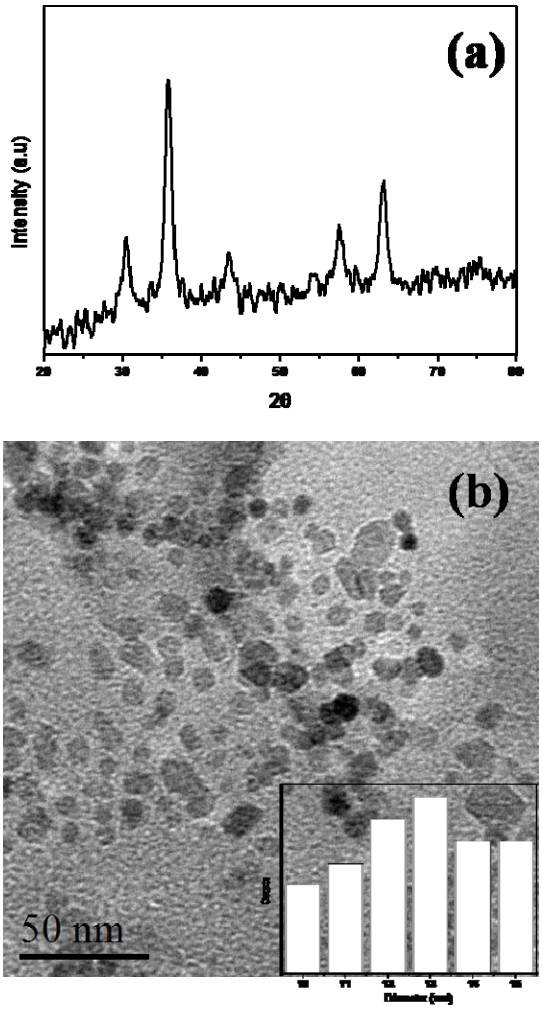

Figure 2.4.5: (a) XRD pattern and (b) TEM image of Fe_3O_4 nanoparticles.

Fe_2O_3 nanoparticles prepared by the precipitation method gave an XRD pattern as shown in the Figure 2.4.6 (a). From the XRD pattern it can be ascertained that the compound formed is pure hematite without any impurities with average particle size around 80 nm.

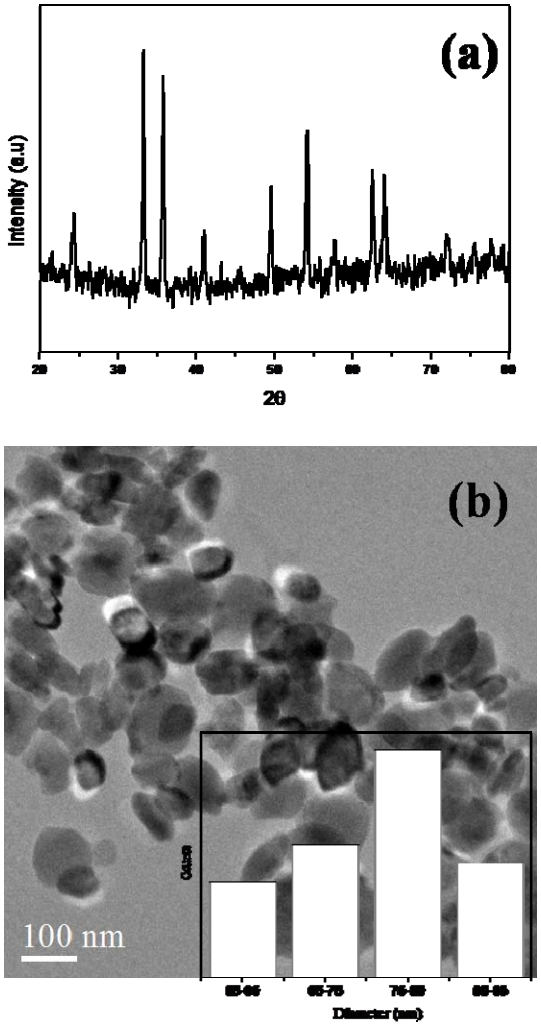

Figure 2.4.6: (a) XRD pattern and (b) TEM image of Fe_2O_3 nanoparticles.

The TEM image of the Fe_2O_3 nanoparticles is shown in the Figure 2.4.6 (b) with inset showing its particle size distribution histogram. From the TEM image it can be seen that the Fe_2O_3 nanoparticles have average particle size around 75-80 nm. Fe_2O_3 nanoparticles upon annealing became a fine powder of red brown color.

The XRD pattern of the ceria nanoparticles is shown in the Figure 2.4.7 (a). The diffraction peaks could be indexed to the fluorite-structured ceria phase.

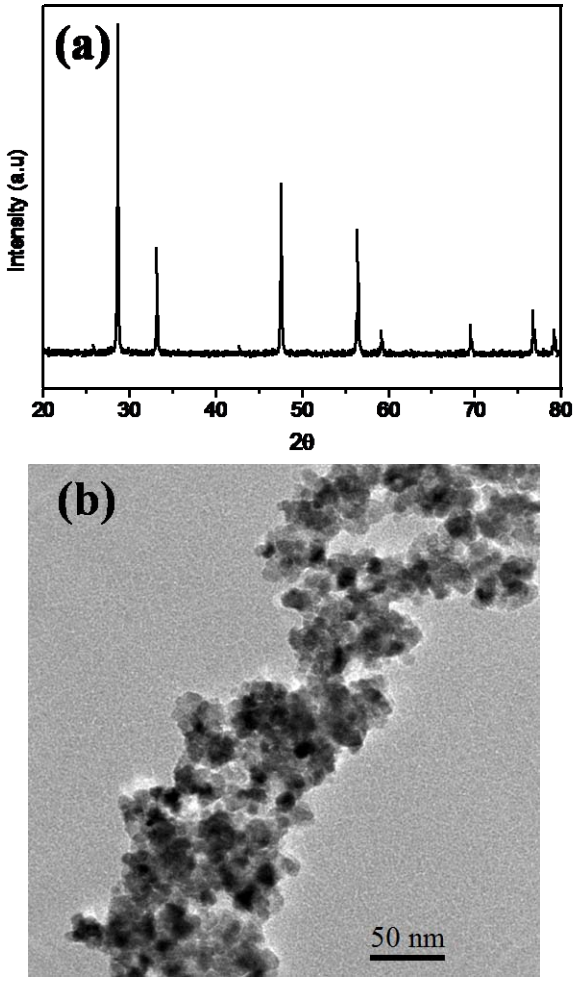

Figure 2.4.7: (a) XRD pattern and (b) TEM image of CeO_2 nanoparticles.

The TEM image of the ceria nanoparticles given in Figure 2.4.7 (b) shows that the particles are agglomerated.

All the above mentioned nanoparticles prepared were in powder form and air stable. The nanoparticles were prepared with or without slight modification of the reported procedure and were characterized to ensure the absence of any impurity phase. The

nanoparticles which were prepared at room temperature were used as such. On the other hand the annealed nanoparticles were treated with dilute nitric acid so as to generate and ensure the presence of surface -OH groups that are necessary for the functionalization. After the mild acid treatment the nanoparticles were analyzed again to make sure the purity and morphology of the sample is retained.

- ***Metal oxide nanowires***

Nanowires of TiO_2 and ZnO were prepared by the hydrothermal method. The nanowires obtained were washed and dries under ambient conditions for further characterizations. In Figure 2.4.8, we show the XRD pattern of the as-synthesized TiO_2 nanowires. The peaks can be indexed to the anatase phase of the titania.

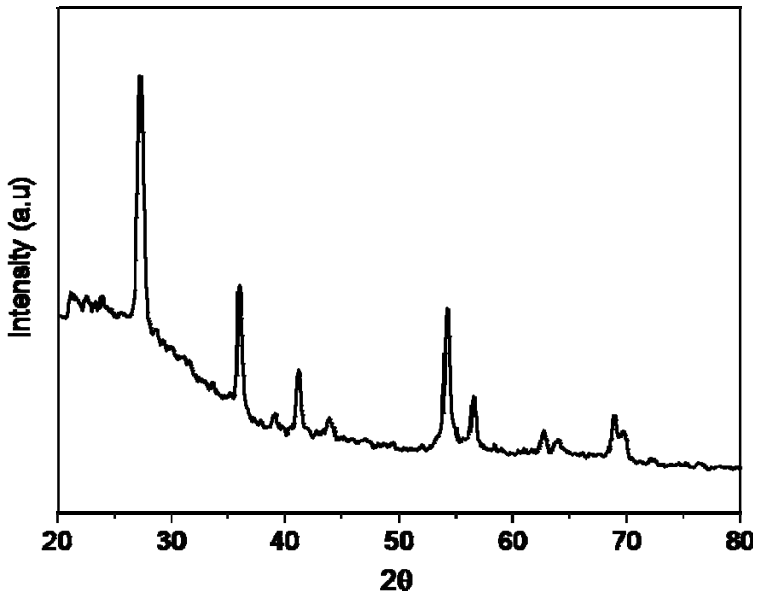

Figure 2.4.8: XRD pattern of TiO_2 nanowires.

The product is mainly composed of nanowires as can be seen from the FESEM image shown in Figure 2.4.9 (a). From the TEM image shown in Figure 2.4.9 (b), the as-synthesized TiO_2 nanowires are found have an average diameter over a range of 60-150 nm. The IR spectrum

of the TiO_2 nanowires show a band at 3500 cm^{-1} which can be attributed to the surface hydroxyl groups.

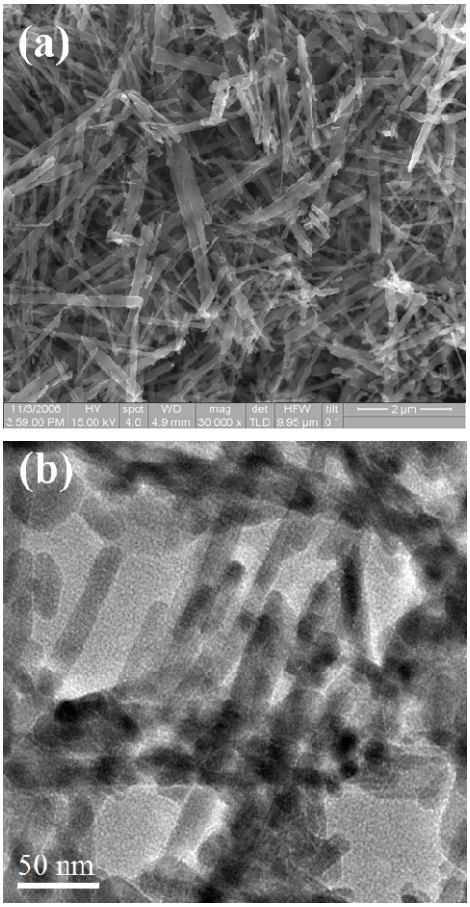

Figure 2.4.9: (a) FESEM and (b) TEM images of TiO_2 nanowires.

Figure 2.4.10 shows the XRD pattern of the as-synthesized ZnO nanowires and the peaks are the typical reflections from wurtzite-type ZnO. The XRD pattern ascertains the purity of the sample as there are no peaks other than those that correspond to the hexagonal ZnO. In Figure 2.4.11 (a), we show a representative FESEM image of the as-synthesized ZnO nanowires and the TEM image is show in Figure 2.4.11 (b). From the TEM image it is seen that the nanowires are reasonably monodisperse with the average diameter around ~14 nm

and with lengths going up to a few microns. As in the case of TiO_2 nanowires the IR spectrum of ZnO nanowires also shows a peak corresponding to the surface –OH groups.

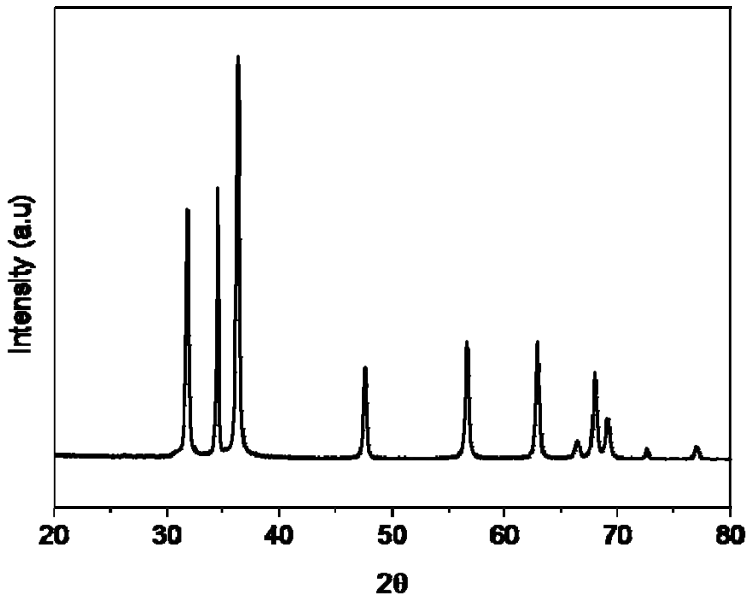

Figure 2.4.10: XRD pattern of ZnO nanowires.

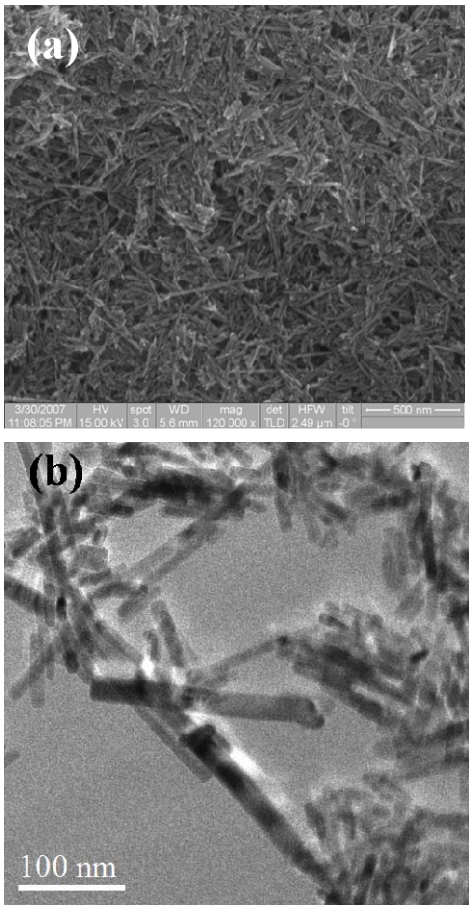

Figure 2.4.11: (a) FESEM and (b) TEM images of ZnO nanowires.

Nanowires of Al_2O_3 have been synthesized by carbothermal method. The XRD pattern of the Al_2O_3 nanowires is shown in the Figure 2.4.12 which corresponds to the cubic phase of the Al_2O_3.

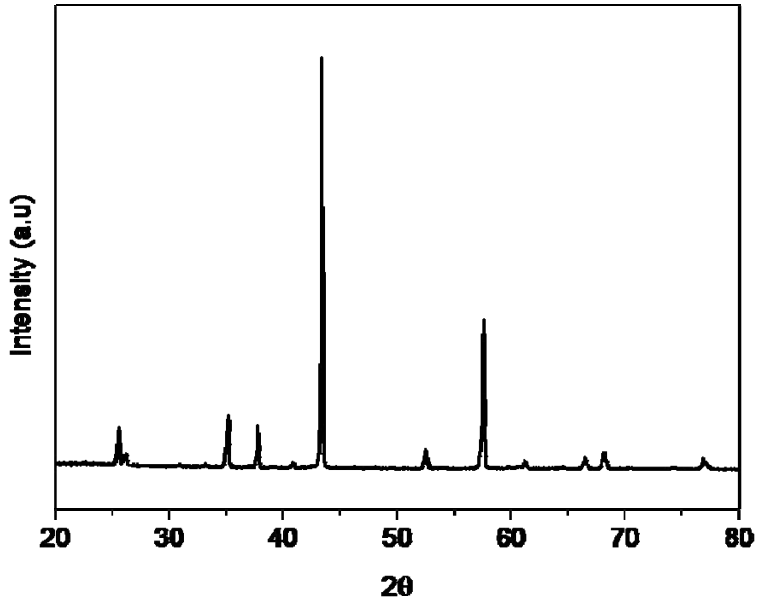

Figure 2.4.12: XRD pattern of Al_2O_3 nanowires.

The nanostructures synthesized by the carbothermal methods mainly comprise nanowires with high aspect ratio in good yield. Along with nanowires other network-type structures, with a radial outgrowth from a stem-like structure are also observed. In Figure 2.4.13 (a) is shown the SEM image of the alumina nanowires. From the TEM images it was seen that the average diameter of the Al_2O_3 nanowires were in the range 150-200 nm. In Figure 2.4.13 (b) we show the TEM image of a single Al_2O_3 nanowire. The nanowire is highly crystalline which can be seen from the SAED pattern of the same shown as inset in 2.4.13 (b). Since the nanowires of Al_2O_3 were prepared at high temperature, in order generate surface hydroxyl

groups the nanowires were treated with dilute nitric acid prior to the functionalization procedure.

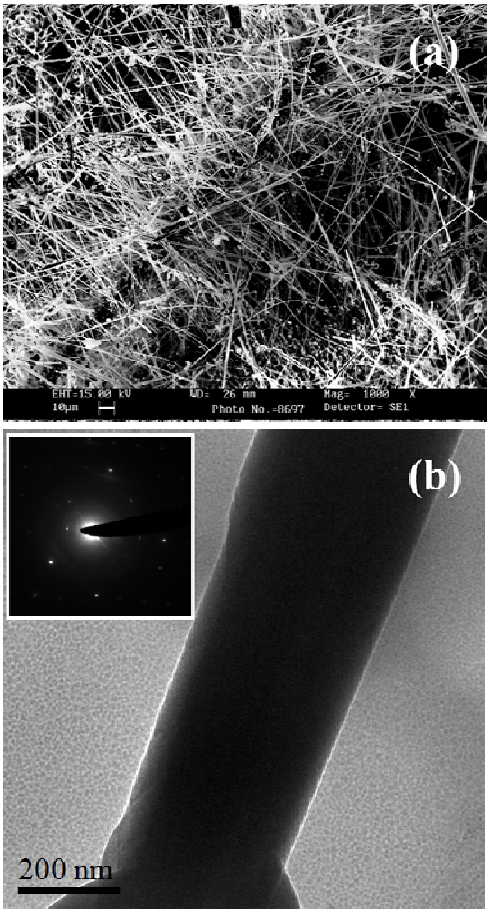

Figure 2.4.13: (a) FESEM and (b) TEM images of Al_2O_3 nanowires.

- ***Solubilization by surfactants***

We have investigated how nanoparticles of metal oxides can be dispersed in different solvents. We have employed several surfactants and polymers for the study which include cetyltrimethylammonium bromide (CTAB), sodium dodecyl sulphate (SDS), polyethylene

glycol (PEG), polyethylene oxide (PEO), Triton X-100 (TX-100), polyvinyl alcohol (PVA) and sodium bis(2-ethylhexyl) sulphosuccinate (AOT).

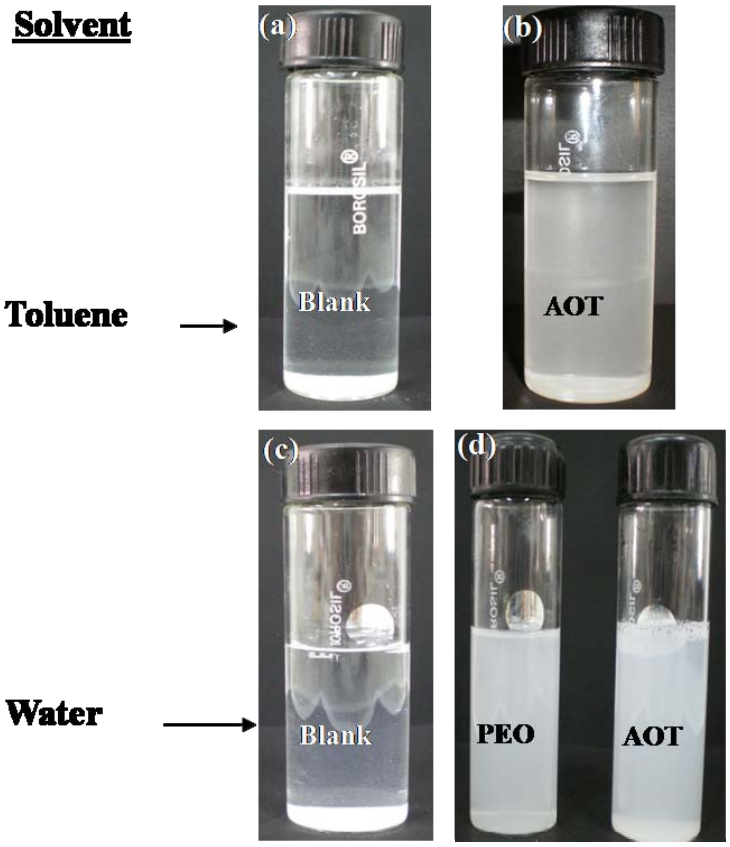

Figure 2.4.14: Photographs of suspensions of TiO_2 nanoparticles in different surfactant-solvent combinations (a) and (b) show the suspensions in toluene and (c) and (d) show the suspensions in water.

In Figures 2.4.14 (a) and (c), we show the photographs of the dispersions of the as-synthesized TiO_2 nanoparticles in toluene and water respectively. Stable dispersions of the TiO_2 nanoparticles shown in Figure 2.4.14 (b) and (d) were enabled by the addition of surfactants. Figure 2.4.14 (b) is the photograph of the dispersion of the TiO_2 nanoparticles in toluene with AOT and Figure 2.4.14 (d) shows the dispersions of the nanoparticles in water

in the presence of PEO and AOT. The dispersions were stable for upto 1-2 weeks. The TiO_2 nanoparticles dispersed in water and toluene do not show much change from the starting material as evidenced from the PL spectrum.

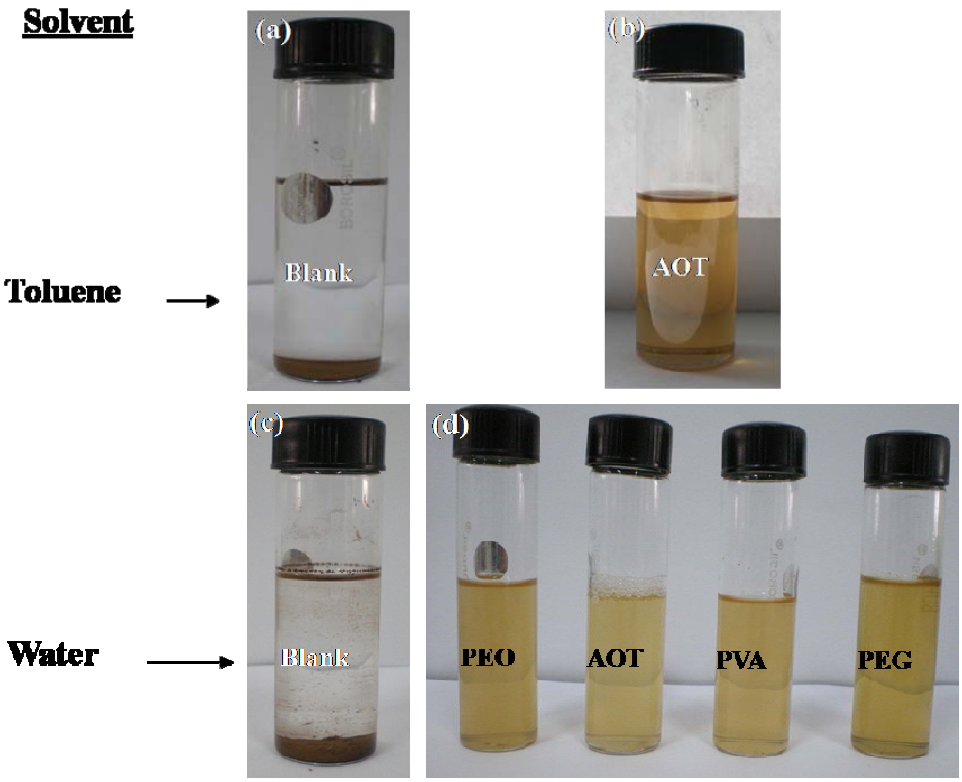

Figure 2.4.15: Photographs of suspensions of Fe_3O_4 nanoparticles in different surfactant-solvent combinations (a) and (b) show the suspensions in toluene and (c) and (d) show the suspensions in water.

Figure 2.4.15 shows photographs of dispersions of Fe_3O_4 nanoparticles (average nanoparticles ~17 nm). All these photographs were taken after the dispersions were allowed to stand for 24 h. Figures 2.4.15 (a) and (c), show the dispersions of the as-synthesized Fe_3O_4 nanoparticles in toluene and water respectively whereas Figures 2.4.15 (b) and (d) show the dispersions of the nanoparticles in toluene and water respectively in the presence of surfactants. From the photographs, it is evident that the as-synthesized Fe_3O_4 nanoparticles are not stable for longer duration while the surfactant-held nanoparticles were stable for 4-5

weeks. The surfactant which held the nanoparticles of Fe_3O_4 in toluene for long periods was AOT as shown in Figure 2.4.15 (b). PEO, AOT, PVA and PEG held the nanoparticles of Fe_3O_4 in water for long durations as can be seen from Figure 2.4.15 (d).

In the case of TiO_2 nanoparticles stable dispersions could be obtained when AOT and PEO were used in water. In case of toluene, AOT produced stable dispersions. Similarly, nanoparticles of Fe_3O_4 could be stabilized in toluene by AOT while in water PEO, AOT, PVA and PEG held the nanoparticles for longer durations. All the dispersions exhibit the remarkable property that the physical properties of the nanowires in the solution are not perturbed by the presence of surfactants or polymers around them. The surfactants/polymers bind to the surfaces of the nanostructures through weak non-covalent interactions. In summary, PEO and AOT generally disperse oxide nanostructures in water while AOT disperses them in toluene.

- ***Functionalization of nanostructures with organosilane reagents***

Another approach through which stable dispersions could be obtained in non polar solvents is to coat the nanoparticles with a hydrophobic or organic coating. We were interested in dispersing the metal oxide nanostructures in hydrocarbon solvents. For this purpose we have employed organo-silane hydrophobic coating on the surface of the nanostructures. We have, therefore, attempted to disperse nanoparticles of metal oxides such as CeO_2, Fe_3O_4, TiO_2 and ZnO and nanowires of TiO_2, ZnO and Al_2O_3 in organic solvents by coating the oxide nanostructures with APTES and HDTMS. Metal oxide nanostructures get coated by hexadecyltrimethoxysilane on refluxing the nanostructures and the organosilane in a hydrocarbon solvent. The organosilane-coated metal oxide nanostructures give stable dispersions in hydrocarbon solvents due to their hydrophobic surface.

The functionalization of nanoparticles with HDTMS has been characterized using electron microscopy and infrared spectroscopy. TEM sampling was done by dispersing the functionalized nanoparticles in toluene by ultra sonication and then placing a drop of the dispersion on the carbon coated copper grid followed by evaporation. In Figure 2.4.16 (a) we show a TEM image of the CeO_2 nanoparticles reacted with HDTMS to reveal how the nanoparticles are coated by the organosilane. The EDX spectrum in Figure 2.4.16 (b) of the HDTMS-coated CeO_2 nanoparticles shows the presence of Si along with cerium. The TEM image of the HDTMS-coated Fe_3O_4 nanoparticles in Figure 2.4.16 (c) shows the presence of the coating of HDTMS reagent. The EDX spectrum of the HDTMS-coated Fe_3O_4 nanoparticles in Figure 2.4.16 (d) shows the presence of Si.

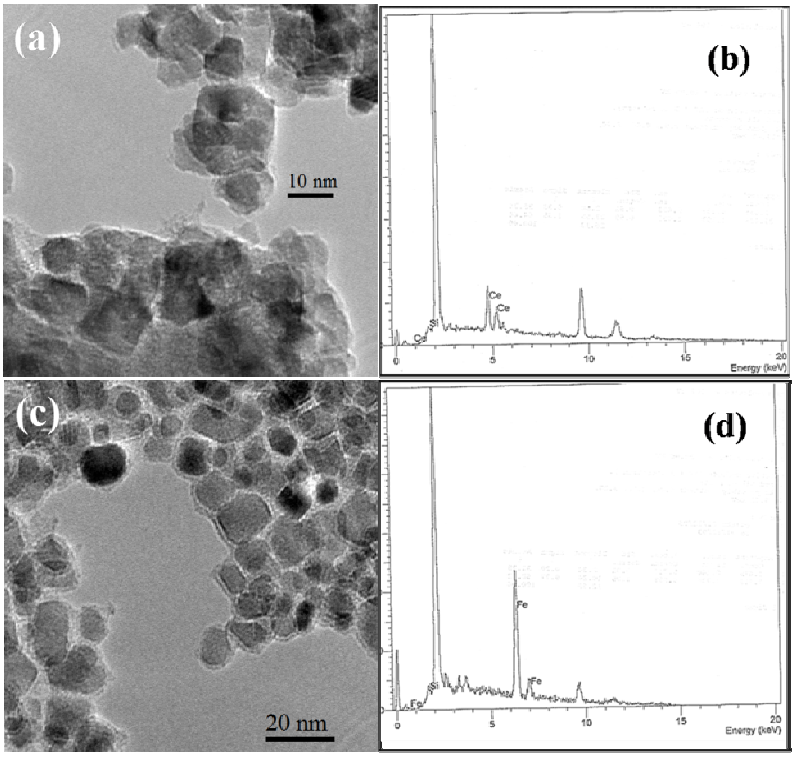

Figure 2.4.16: (a) TEM image and (b) EDX spectrum of HDTMS-coated CeO_2 nanoparticles; (c) TEM image and (d) EDX spectrum of HDTMS-coated Fe_3O_4 nanoparticles.

The presence of the organosilane coating on the CeO_2 and Fe_3O_4 nanoparticles was also ascertained by infrared spectroscopy. In Figures 2.4.17 (a) and (c), we show the infrared spectra of the as-synthesized CeO_2 and Fe_3O_4 nanoparticles respectively. The IR spectra of HDTMS-coated nanoparticles of CeO_2 and Fe_3O_4 shown in Figures 2.4.17 (b) and (d) show characteristic bands due alkyl groups at 2850 and 2950 cm^{-1} and a band due to Si-O groups at 1100 cm^{-1} [79].

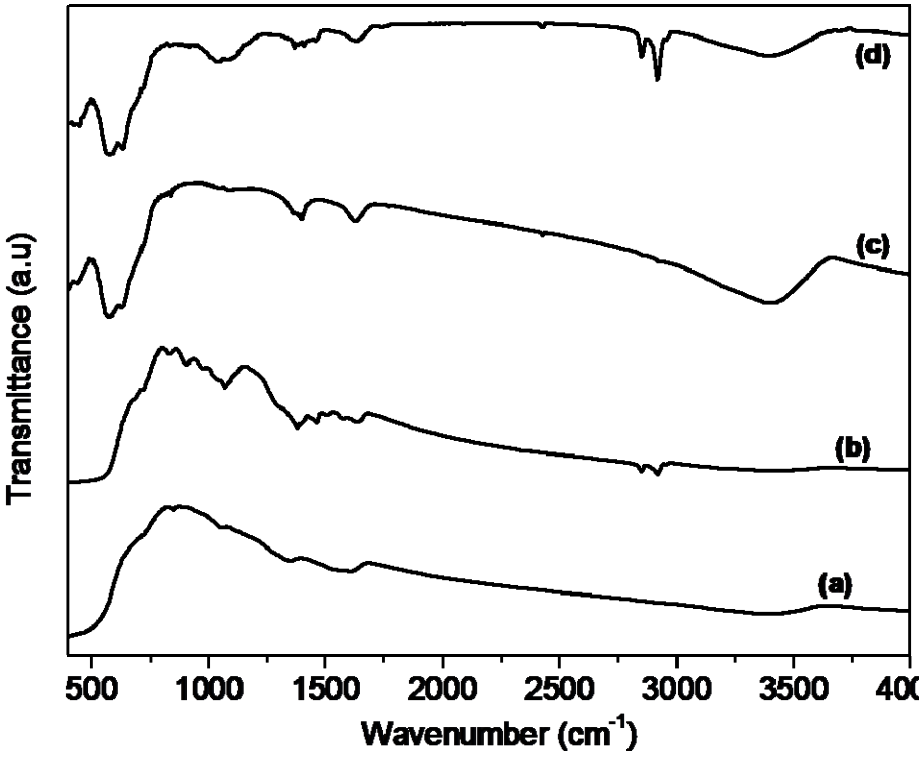

Figure 2.4.17: IR spectra (a) of the as-prepared and (b) of the HDTMS-coated CeO_2 nanoparticles. IR spectra (c) of the as-prepared and (d) of the HDTMS-coated Fe_3O_4 nanoparticles.

The TEM image in Figure 2.4.18 (a) shows the HDTMS-coated TiO_2 nanoparticles. The presence of the organosilane coating is evident from the EDX spectrum of the coated TiO_2 nanoparticles as in 2.4.18 (b) showing presence of Si in addition to Ti. Figure 2.4.18 (c) represents the TEM image of the HDTMS-coated ZnO nanoparticles. The EDX spectrum of the organosilane-coated ZnO nanoparticles in Figure 2.4.18 (d) clearly shows the presence of

Si. Similar to the HDTMS-coated CeO_2 and Fe_3O_4 nanoparticles, HDTMS-coated nanoparticles of TiO_2 and ZnO also gave IR spectra showing characteristic bands due alkyl groups at 2850 and 2950 cm^{-1} and a band due to Si-O groups at 1100 cm^{-1}. On heating the HDTMS-coated nanoparticles in air or oxygen at 873 K, silica-coated nanoparticles are obtained. This was confirmed by EDX analysis and IR spectra which showed the absence of the organic residue. The silica coating is, however, X-ray amorphous.

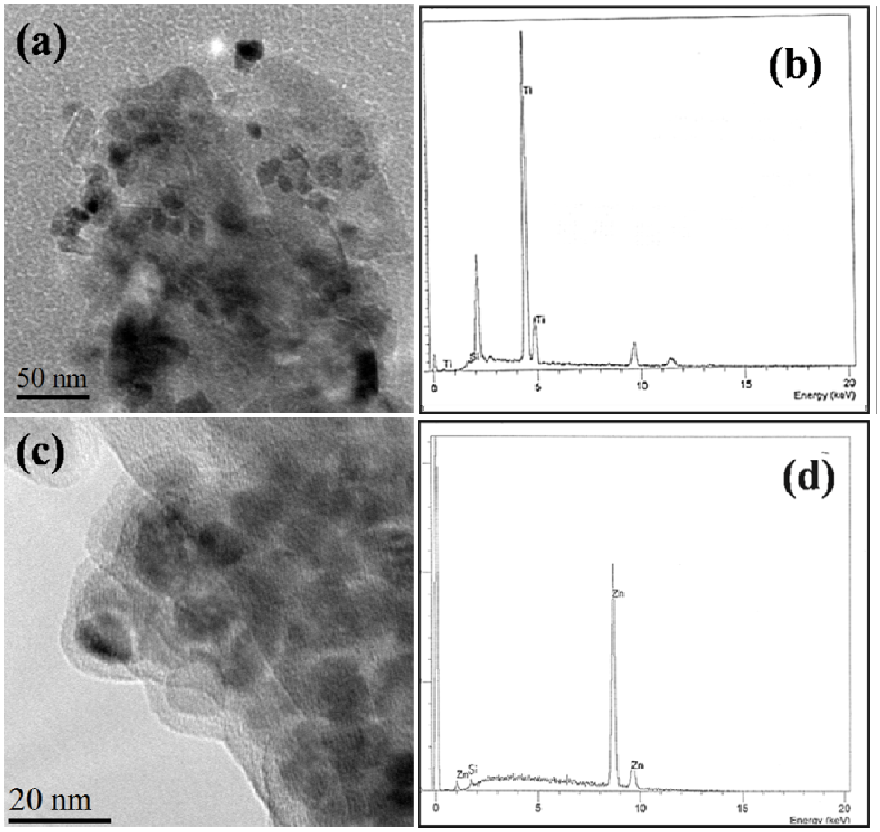

Figure 2.4.18: (a) TEM image and (b) EDX spectrum of HDTMS-coated TiO_2 nanoparticles; (c) TEM image and (d) EDX spectrum of HDTMS-coated ZnO nanoparticles.

Figure 2.4.19 (a) is a photograph of the as-synthesized CeO_2 nanoparticles in toluene showing that the particles just settle down at the bottom of the liquid. The photographs of the dispersions of the silane-functionalized CeO_2 nanoparticles in toluene and n-hexane are shown in Figure 2.4.19 (b) and (c) respectively. Figure 2.4.19 (d) is a photograph of the as-prepared Fe_3O_4 nanoparticles in toluene whereas Figure 2.4.19 (e) and (f) are photographs of the silane-coated Fe_3O_4 nanoparticles in toluene and n-hexane respectively. The fact that the photographs were taken 48h after the preparation of the dispersions shows that the nanoparticles of the silane-coated CeO_2 are stable in hydrocarbon solvents. To check the effect of the silane concentration on the nature of dispersions, we carried out a reaction in which the silane : metal oxide ratio was 0.25 : 1. We found that the organosilane-coated CeO_2, Fe_3O_4, TiO_2 and ZnO nanoparticles so prepared gave dispersions in hydrocarbon solvents stable for more than 48h. TEM studies however, showed that the coating thickness was considerably reduced. The agglomeration of the organosilane-coated nanoparticles occurred to a lesser extent compared to the nanoparticles coated with the higher concentrations of the HDTMS.

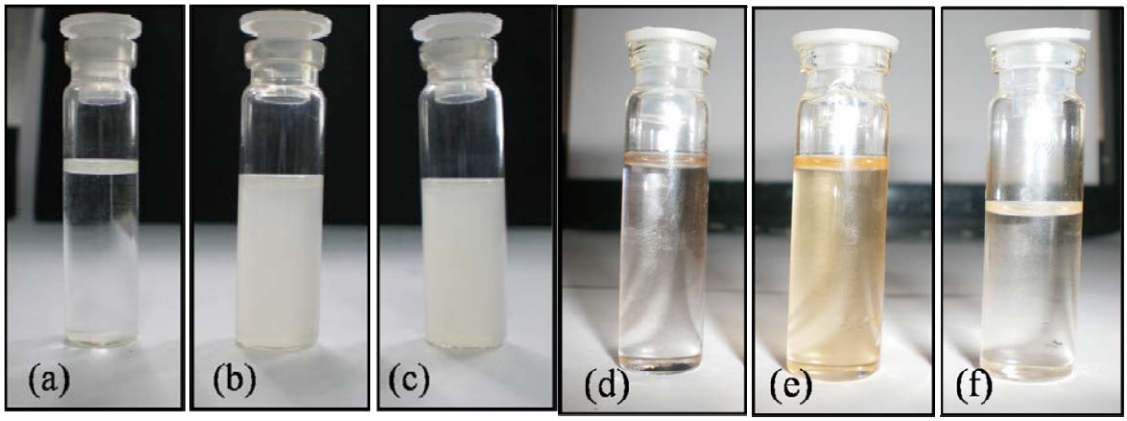

Figure 2.4.19: Photographs of (a) as-prepared CeO_2 nanoparticles in toluene, HDTMS-coated CeO_2 nanoparticles in (b) toluene and (c) n-hexane (d) as-prepared Fe_3O_4 nanoparticles in toluene, (e) HDTMS-coated Fe_3O_4 nanoparticles in (e) toluene and (f) hexane.

In Figure 2.4.20, we show the TEM images of organosilane-coated metal oxide nanowires. Figures 2.4.20 (a), (b) and (c) show the TEM images of the APTES-coated TiO_2, ZnO and Al_2O_3 nanowires. The coating thickness is 10-15 nm as can be seen from the TEM images. Figures 2.4.20 (d), (e) and (f) show the TEM images of the HDTMS-coated TiO_2, ZnO and Al_2O_3 nanowires. The silane coating on the surface of the nanowires is around 15 nm.

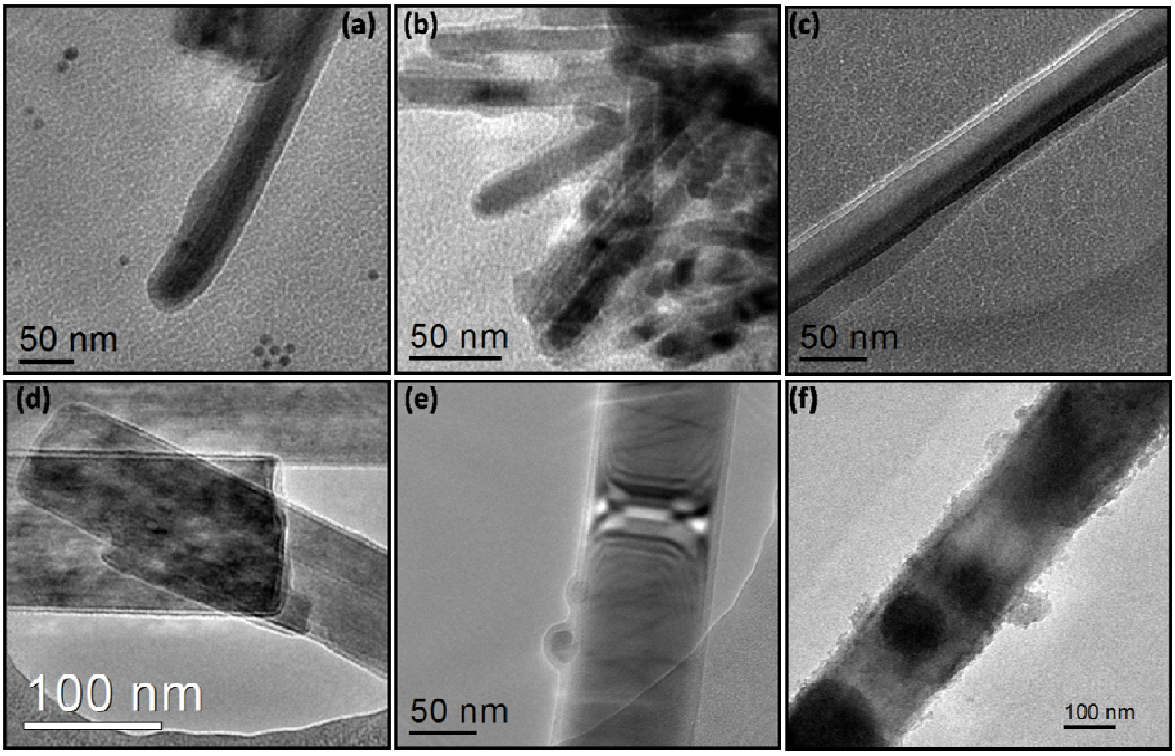

Figure 2.4.20: TEM images of the APTES-coated (a) TiO_2, (b) ZnO and (c) Al_2O_3 nanowires and the HDTMS-coated (d) TiO_2, (e) ZnO and (f) Al_2O_3 nanowires.

The presence of the organosilane coating was ascertained by EDAX analysis, by indicating the presence of silicon in addition to the corresponding metal. The nanowires coated with the two organosilane reagents gave similar EDAX spectra. The EDAX spectra of the APTES-coated TiO_2, ZnO and Al_2O_3 nanowires are given as Figures 2.4.21 (a), (b) and (c).

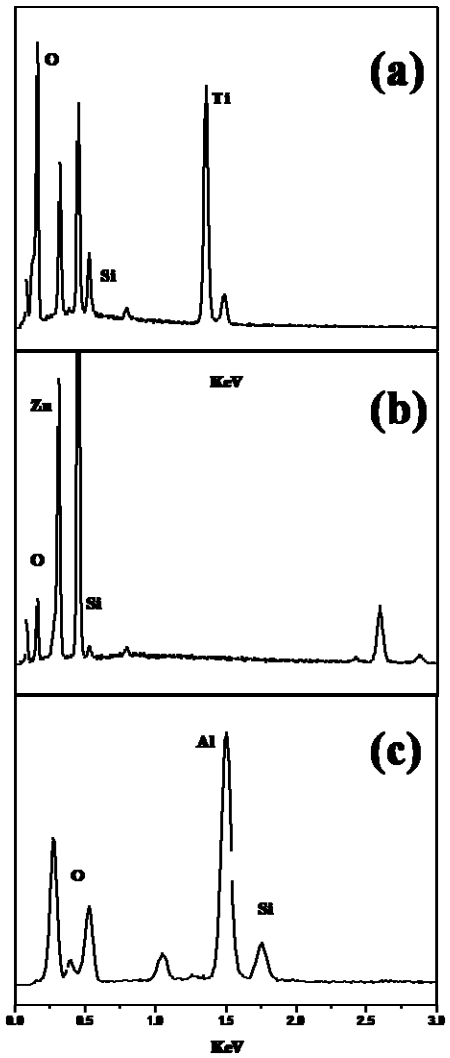

Figure 2.4.21: EDX spectra of the organosilane-coated (a) ZnO, (b) TiO_2 and (c) Al_2O_3 nanowires.

We have also confirmed the presence of the organosilane coating by means of IR spectroscopy. Sampling of IR spectroscopy was done by making pellets of washed and dried functionalized nanowires with dry KBr. In Figure 2.4.22, we show the IR spectra of the as-synthesized and APTES-coated metal oxide nanowires. From the figures it can be seen that in the APTES-coated nanowires' IR spectra, there are additional bands at 1100 cm^{-1} due to the Si-O-Si stretching vibration along with bands due to the alkyl groups around 2850 and 2950 cm^{-1}.

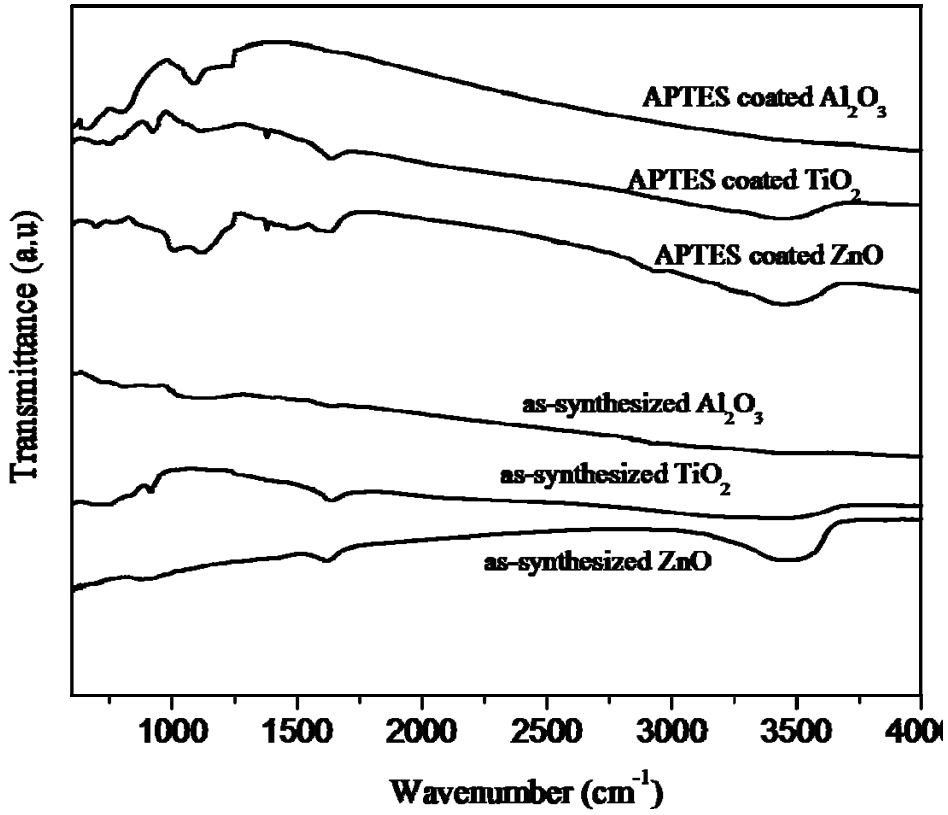

Figure 2.4.22: IR spectra of as-synthesized and APTES-coated nanowires of ZnO, TiO_2 and Al_2O_3

In Figure 2.4.23 are shown the IR spectra of the HDTMS-coated nanowires of ZnO, TiO_2 and Al_2O_3. As in the case of APTES-coated nanowires IR spectra of HDTMS-coated nanowires of ZnO, TiO_2 and Al_2O_3 show bands due to the Si-O-Si stretching vibration at 1100 cm^{-1} along with bands due to the alkyl groups around 2850 and 2950 cm^{-1}. The band at ~950 cm^{-1} is due to the Ti-O-Si bond [80]. Since in HDTMS the length of hydrocarbon chain is longer than that of in APTES, the contribution towards bands due to the alkyl groups is more which can be seen from the more prominent nature of the same in HDTMS-coated nanowires. Thus it can be said that HDTMS coating on the nanowires makes surface of the nanowires more hydrophobic than in the case of APTES-coating.

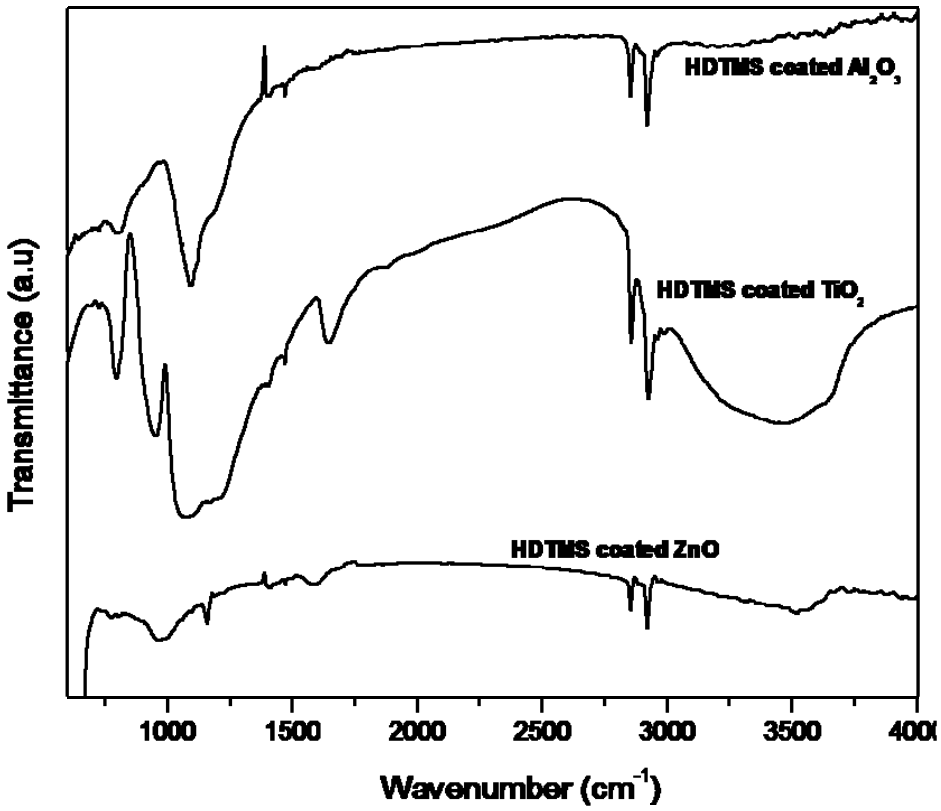

Figure 2.4.23: IR spectra of HDTMS-coated nanowires of ZnO, TiO_2 and Al_2O_3.

Dispersions of APTES-coated metal oxide nanowires were not stable irrespective of the nature of the solvent while the HDTMS-coated nanowires gave stable dispersions in toluene and CCl_4. Among the two solvents, CCl_4 gave dispersions stable over longer duration than toluene. In Figures 2.4.24 (a) and (c) we show the photographs of the dispersions of the as-prepared nanowires of TiO_2 and ZnO in toluene. The as-prepared nanowires do not get dispersed and settle down soon sonication. Figures 2.4.24 (b) and (d) show the photographs of CCl_4 and toluene dispersions of HDTMS-coated TiO_2 and ZnO nanowires respectively 12 hours after the dispersions were prepared. The dispersions of the organosilane-coated nanowires were generally stable for more 24 h. Functionalization of the oxide nanowires by HDTMS renders the surface of the nanowires hydrophobic which in turn induces the dispersion of nanowires in non-polar solvents.

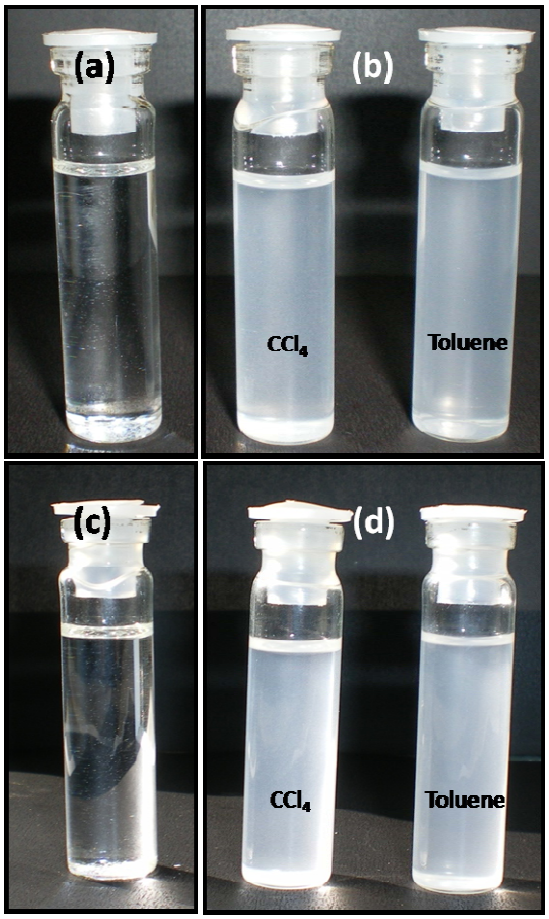

Figure 2.4.24: Photographs of dispersions of (a) as-prepared TiO_2 nanowires in toluene, (b) HDTMS-coated TiO_2 nanowires in non-polar solvents, (c) as-prepared ZnO nanowires in toluene and (d) HDTMS-coated ZnO nanowires in non-polar solvents

On heating the silane-coated metal oxide nanowires in air or oxygen at 873 K, silica-coated nanowires were obtained. Figures 2.4.25 (a), (b) and (c) are the TEM images and the EDAX spectra of the silica-coated nanowires of TiO_2, ZnO and Al_2O_3 respectively, obtained after heating the respective HDTMS-coated nanowires. The EDAX spectra show the presence of Si along with the respective elements. The presence of silica coating was confirmed by IR spectroscopy. In Figure 2.4.26 we show the IR spectra of the silica-coated nanowires of TiO_2, ZnO and Al_2O_3 obtained after the heat treatment of the respective HDTMS-coated nanowires. From the spectrum it can be seen that the Si-O-Si band at 1100 cm^{-1} is retained while the bands due to the alkyl groups have disappeared. The silica coating was, however, X-ray amorphous.

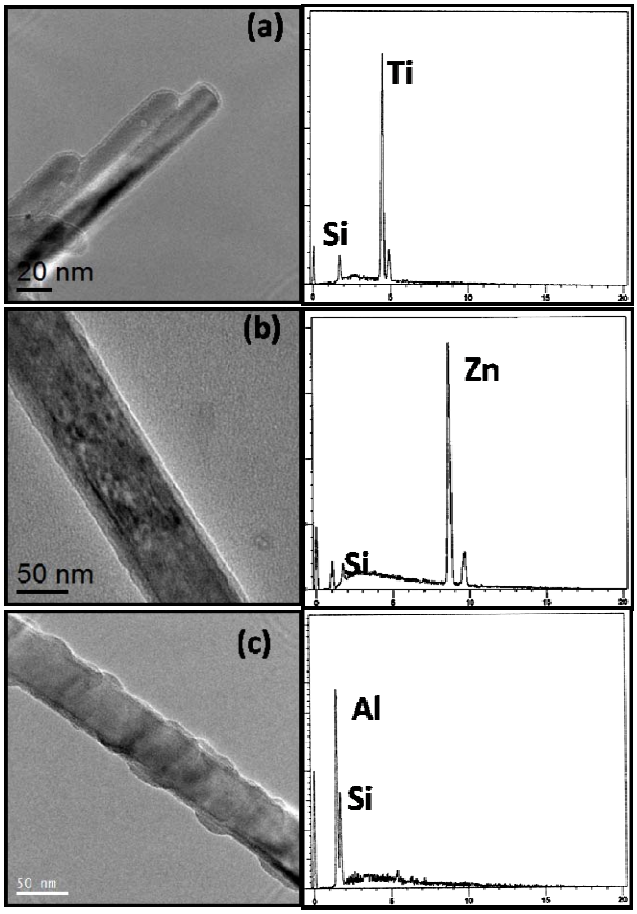

Figure 2.4.25: TEM images and EDAX spectra of the silica-coated nanowires of (a) TiO_2, (b) ZnO and (c) Al_2O_3 obtained by the heat treatment of the respective HDTMS-coated nanowires.

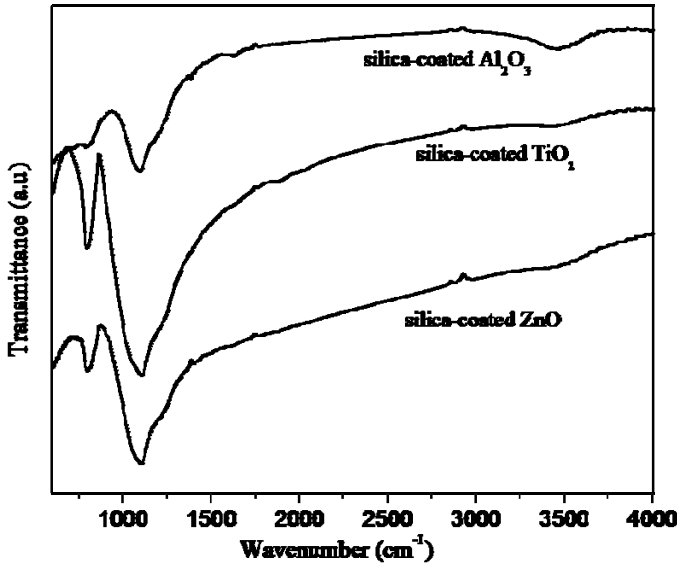

Figure 2.4.26: IR spectra of silica-coated nanowires of ZnO, TiO_2 and Al_2O_3.

- ***Functionalization of nanostructures with organotin reagents***

We have tried to functionalize the metal oxide nanoparticles with organotin reagents. For this purpose we have treated the nanoparticles of CeO_2 and Fe_3O_4 with dibutyldimethoxytin. In Figures 2.4.27 (a) and (b) we show the TEM image and EDAX spectrum of the dibutyldimethoxytin-coated nanoparticles of CeO_2. TEM image and EDAX spectrum of the dibutyldimethoxytin-coated nanoparticles of Fe_3O_4 are shown in Figures 2.4.27 (c) and (d). EDAX spectrum confirmed the coating by the presence of tin along with the presence of corresponding metal.

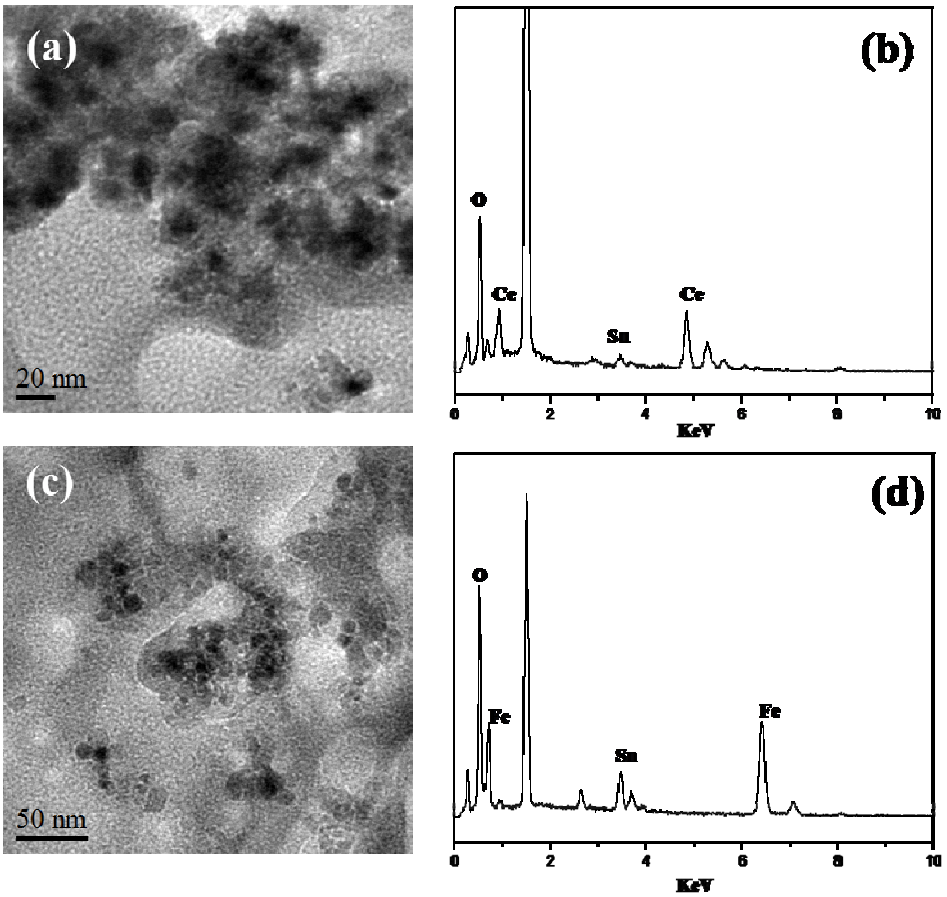

Figure 2.4.27: (a) TEM image and (b) EDAX spectrum of dibutyldimethoxytin-coated CeO_2 nanoparticles and (a) TEM image and (b) EDAX spectrum of dibutyldimethoxytin-coated Fe_3O_4 nanoparticles.

Unlike organosilane-coated metal oxide nanoparticles dispersions which were stable for more than 24 h, the organotin-coated CeO_2 and Fe_3O_4 nanoparticles dispersions were stable for only1-2 h in non-polar solvents. Metal oxide nanoparticles of CeO_2 and Fe_3O_4 treated with an excess of organotin reagents (for example 1:4), gave good dispersions. These dispersions were as good as those of the organosilane-functionalized oxide nanoparticles.

We have employed organotin reagents to functionalize inorganic nanowires to obtain good dispersions in non-polar solvents. The organotin reagents used for this purpose were dibutyldimethoxytin and trioctyltinchloride. In Figures 2.4.28 (a) and (b), we show the TEM images of nanowires of TiO_2 and ZnO coated with dibutyldimethoxytin. TEM images of trioctyltinchloride coated nanowires of TiO_2 and ZnO are shown in Figures 2.4.28 (c) and (d). The average coating thickness is around 2-3 nm.

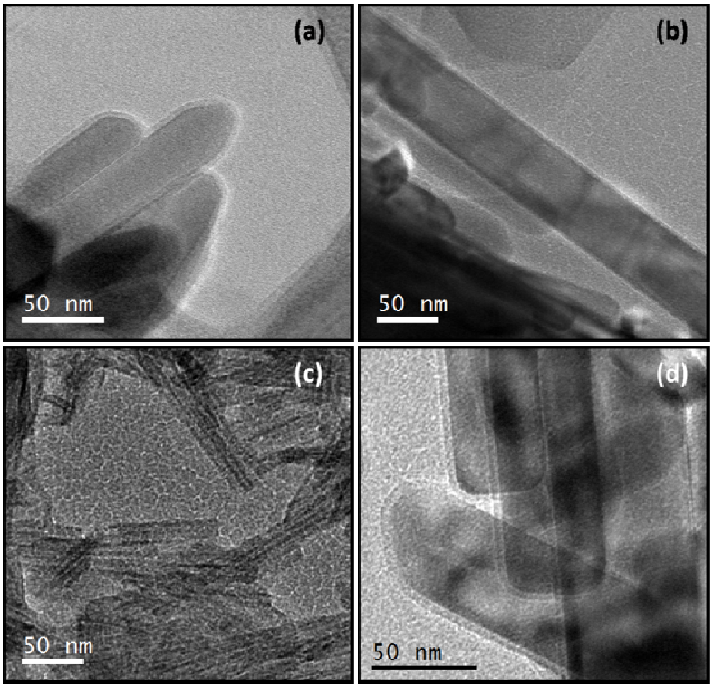

Figure 2.4.28: TEM images of dibutyldimethoxytin-coated (a) TiO_2 and (b) ZnO and trioctyltinchloride-coated (d) TiO_2 and (e) ZnO nanowires.

The presence of tin in the organotin-coated ZnO and TiO_2nanowires was confirmed by the EDAX spectra. A typical EDAX spectrum of organotin-coated nanowires of ZnO and TiO_2 is Figures 2.4.29 (a) and (b) respectively.

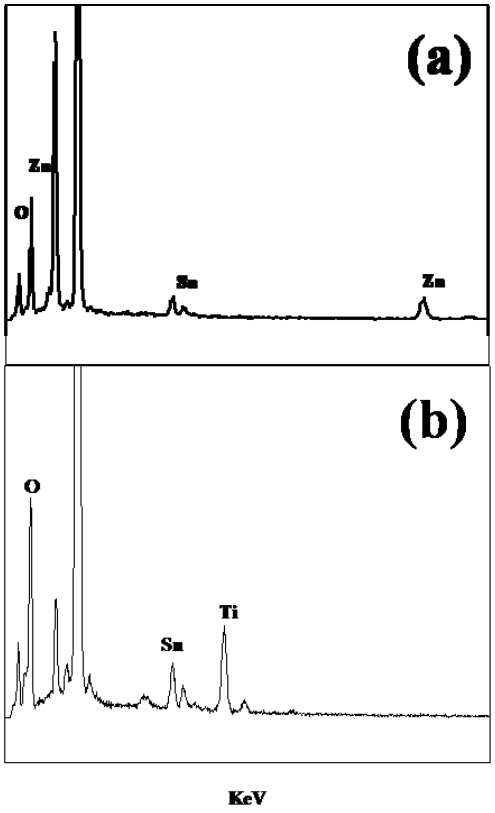

Figure 2.4.29: EDAX spectrum of dibutyldimethoxytin-coated (a) ZnO and (b) TiO_2 nanowires.

The IR spectra also demonstrate the presence of the organotin coating. Figures 2.4.30 (a), (b) and (c) show the IR spectra of the as-synthesized, dibutyldimethoxytin-coated and trioctyltinchloride-coated nanowires of TiO_2. The spectra of the organotin-coated nanowires show bands in the region 500-600 cm^{-1} which can be attributed to the Sn-O bond [81] and the bands due to the presence of alkyl groups at 2850 and 2950 cm^{-1}.

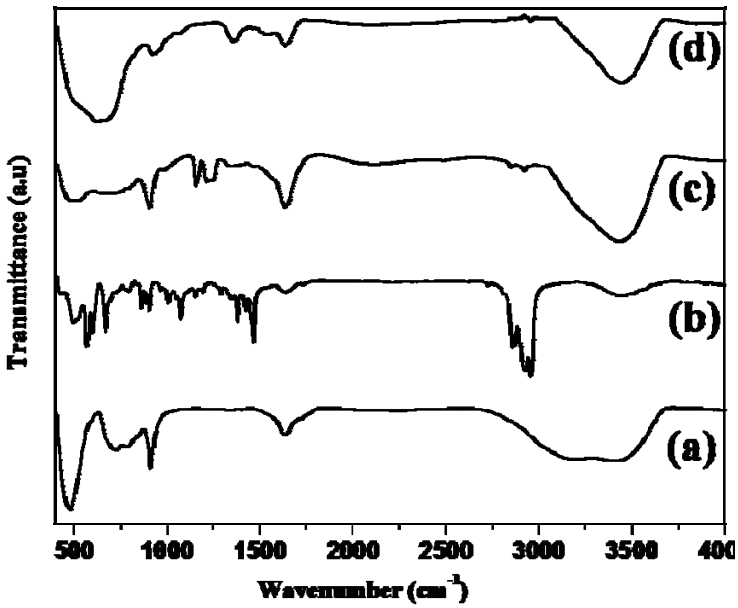

Figure 2.4.30: IR spectra of the (a) as-prepared, (b) dibutyldimethoxytin-coated, (c) trioctyltinchloride-coated and (d) tin oxide-coated TiO_2 nanowires.

Similar to organosilane functionalized nanowires, organotin-coated nanowires gave stable dispersions in non-polar solvents, with dibutyldimethoxytin-coated nanowires and nanotubes giving dispersions which were stable for longer durations than those with trioctyltinchloride. In Figures 2.4.31 (a) and (b), we show the photographs of the dispersions given by the dibutyldimethoxytin-coated nanowires of TiO_2 and ZnO respectively. Photographs in Figures 2.4.31 (c) and (d) show the dispersions of trioctyltinchloride-coated nanowires of TiO_2 and ZnO. All the photographs were taken 6 h after the preparations, and the dispersions were generally stable for more than 10 h. Here also the dispersions of organotin-coated nanowires were stable for a longer duration in CCl_4 than the dispersions in toluene.

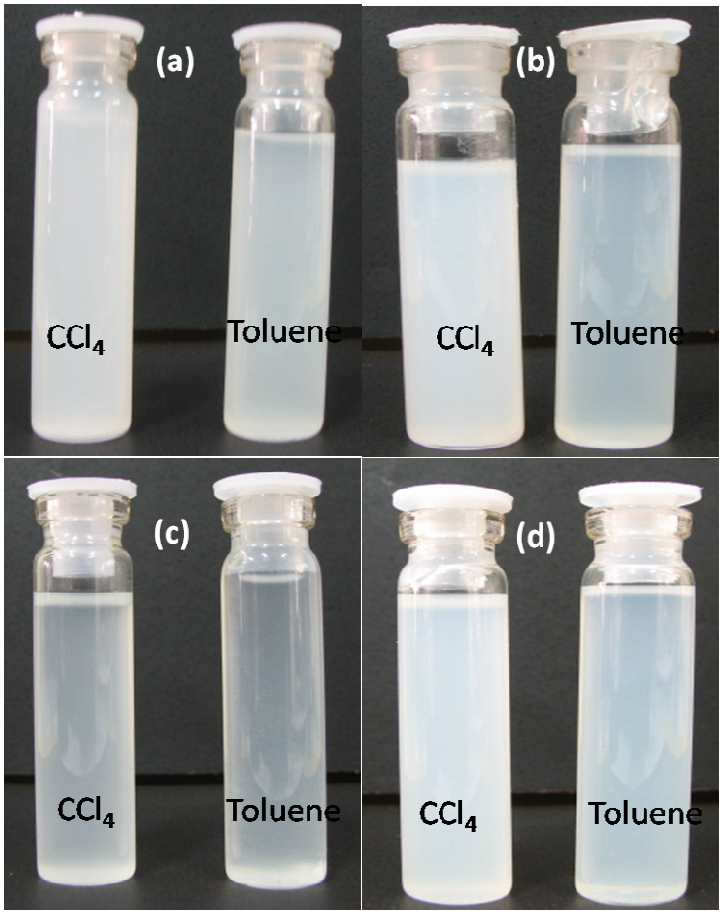

Figure 2.4.31: Photographs of dispersions of dibutyldimethoxytin-coated (a) TiO_2 and (b) ZnO and trioctyltinchloride-coated (d) TiO_2 and (e) ZnO nanowires.

Organotin-coated nanowires when heated in air or oxygen at 400 °C resulted in SnO_2 coated nanowires. The SnO_2 layer is crystalline as confirmed by the XRD pattern. From the TEM images it was seen that unlike the silica coating which was amorphous polycrystalline SnO_2 nanoparticles coat the nanostructures. In Figures 2.4.32 (a) and (b) we show the TEM images of tin oxide coated TiO_2 and ZnO respectively. The IR spectrum of the SnO_2 coated nanowires of TiO_2 obtained after the heat treatment of the dibutyldimethoxytin-coated nanowires of TiO_2 at 400 °C is given in the Figure 2.4.30 (d). From the spectrum it is seen that the band due to Sn-O bond around 500-600 cm^{-1} is retained and the bands due the alkyl groups have disappeared.

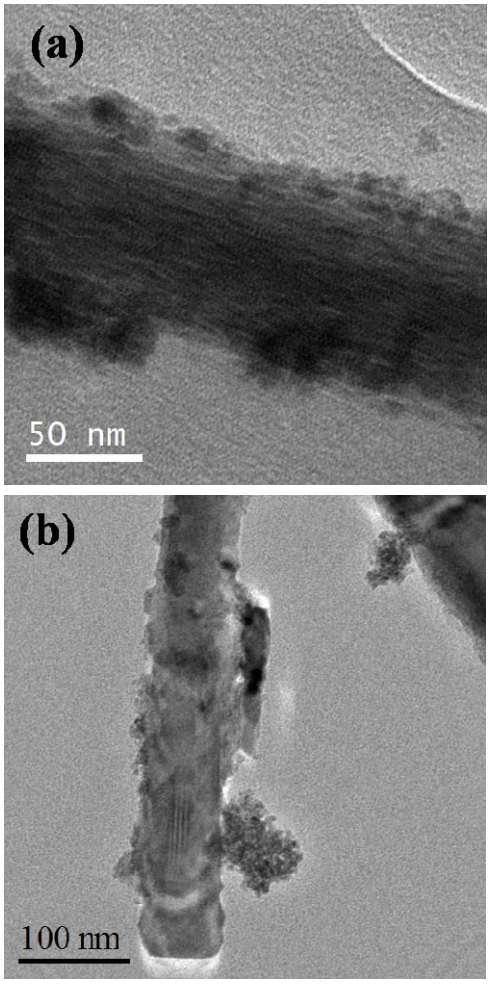

Figure 2.4.32: TEM images of tin oxide coated (a) TiO_2 and (b) ZnO nanowires.

- ***Functionalization of nanostructures with POSS***

POSS was synthesized by the hydrolysis of tetraethylorthosilicate in the presence of tetramethylammonium hydroxide under optimum pH. Depending upon the ratio between silica, water and ammonium ions, it is possible to synthesize selective silicates. Herein reaction conditions were maintained in such a way that the cubic octamer ($Si_8O_{20}^{8-}$) POSS is selectively synthesized. The POSS thus prepared is readily soluble in water. In Figures 2.4.33 (a) and (b) are given the FESEM and the corresponding EDAX spectrum of the POSS synthesized.

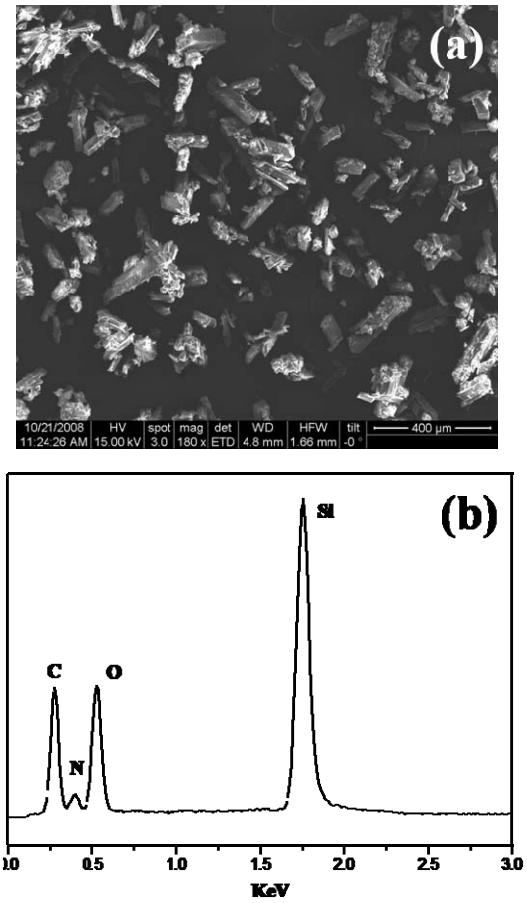

Figure 2.4.33: (a) FESEM image and (b) EDAX spectrum of as-synthesized POSS.

To obtain stable dispersions of inorganic nanostructures in polar solvents we have employed POSS. Herein the nanostructures were stirred with POSS for 24 h which in turn will enable covalent attachment of POSS on the surface of nanostructures. In Figure 2.4.34 (a) we show the FESEM image of the POSS-coated TiO_2 nanowires. The EDAX spectrum of the functionalized nanowires showed the presence of Si along with the respective elements. Figure 2.4.34 (b) is the TEM image of POSS-coated TiO_2 nanowires with a average coating thickness around 2-3 nm.

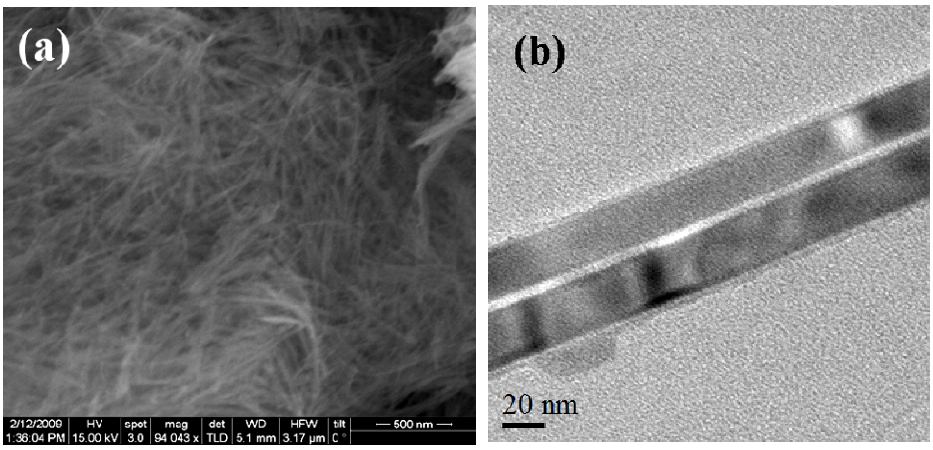

Figure 2.4.34: (a) FESEM and (b) TEM image of POSS-coated TiO_2 nanowires.

We have also characterized the POSS coating by IR spectroscopy. In Figure 2.4.35 we show the IR spectrum of the as-synthesized and POSS-coated TiO_2 nanowires with the latter showing the characteristic bands due to Si-O-Si vibration at 1100 cm^{-1}. Upon heating the POSS-coated nanowires in air/oxygen, we could obtain silica-coated nanowires. This can be seen from the IR spectrum of the silica-coated nanowires shown in Figure 2.4.35 in which the bands due to Si-O-Si vibration is retained.

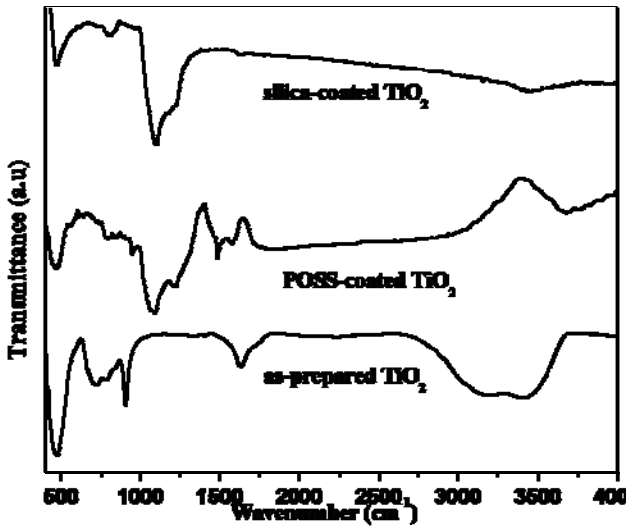

Figure 2.4.35: IR spectra of as-synthesized, POSS-coated and silica-coated TiO_2 nanowires.

In Figures 2.4.36 (a) and (b) we show the FESEM and TEM images of the ZnO nanowires treated with POSS. EDAX spectrum of POSS-coated ZnO nanowires showed presence of Si while the IR spectrum of the functionalized nanowires shows a band around 1100 cm^{-1} confirming the coating. Similar to POSS-coated TiO_2 nanowires, ZnO nanowires also gave silica coating upon heat treatment. TEM images of so obtained silica-coated nanowires of TiO_2 and ZnO are given in Figures 2.4.37 (a) and (b) respectively.

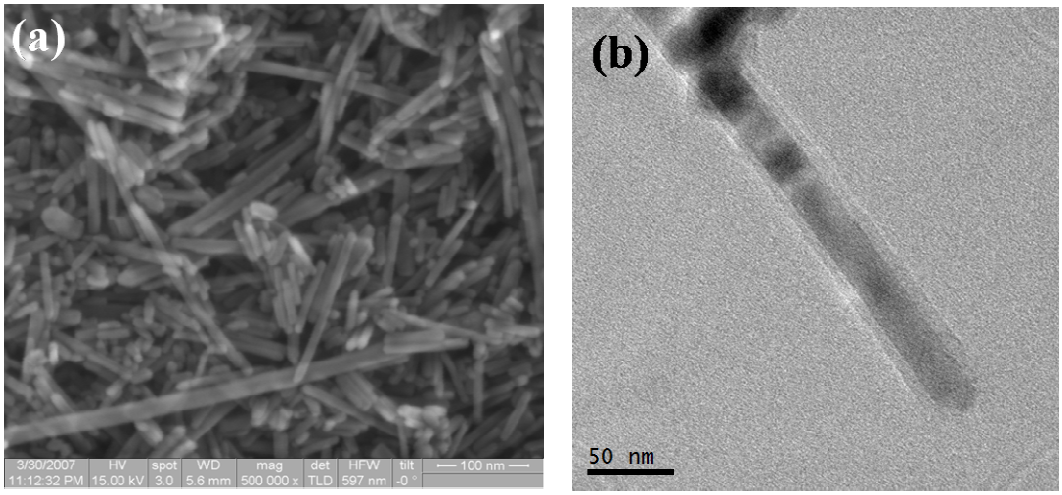

Figure 2.4.36: (a) FESEM and (b) TEM image of POSS-coated ZnO nanowires.

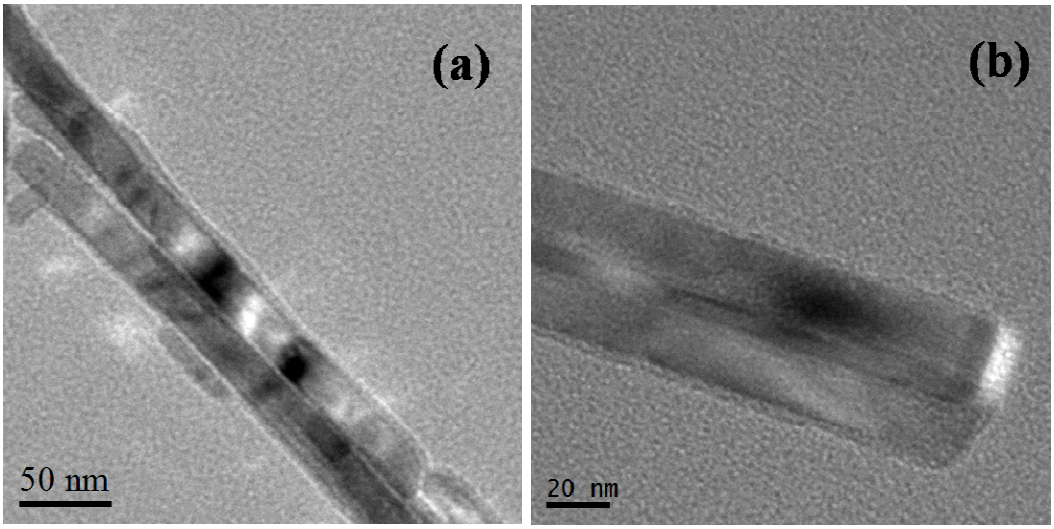

Figure 2.4.37: TEM images of silica-coated (a) TiO_2 and (b) ZnO nanowires.

2.4.2. Metal Nitride nanostructures

- ***Characterization of nanostructures***
- ***Metal nitride nanoparticles***

The nanoparticles of BN and GaN were prepared by means of urea route. The as-synthesized nanoparticles of BN gave an XRD pattern with broad peaks corresponding to the hexagonal BN and indicating smaller particle size. In Figure 2.4.38 (a) we show the TEM image of the as-synthesized BN nanoparticles. Unlike BN nanoparticles, the XRD pattern given by the as-synthesized GaN nanoparticles were amorphous which upon annealing in NH_3 atmosphere gave crystalline nanoparticles whose XRD patters corresponds to the hexagonal phase of GaN. The TEM image of annealed GaN nanoparticles is shown in Figure 2.4.38 (b).

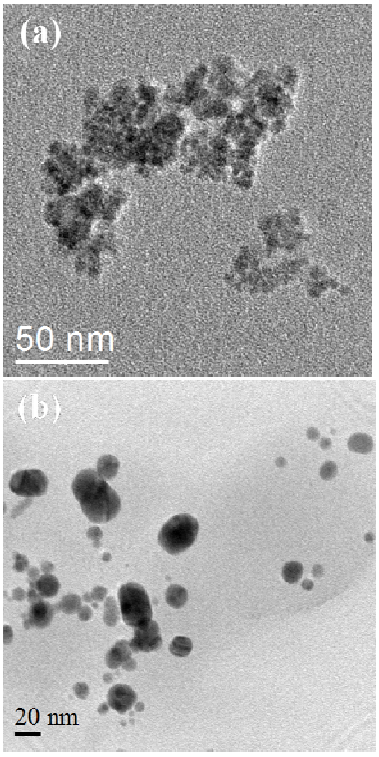

Figure 2.4.38: TEM images of (a) BN and (b) GaN nanoparticles.

- ***Metal nitride nanotubes***

The white product obtained during the synthesis of BN gave an XRD pattern as that of pure hexagonal phase of BN. The BN prepared nanotubes has an average diameter ranging from 50 to 150 nm. In Figure 2.4.39 (a), we show the FESEM image of the as-prepared BN nanotubes and in Figure 2.4.39 (b) is shown the TEM image of the same. Though the nanoparticles and nanotubes of metal nitride were treated with dilute nitric acid before functionalization, the IR spectra of the acid-treated samples did not show the band due to –OH groups.

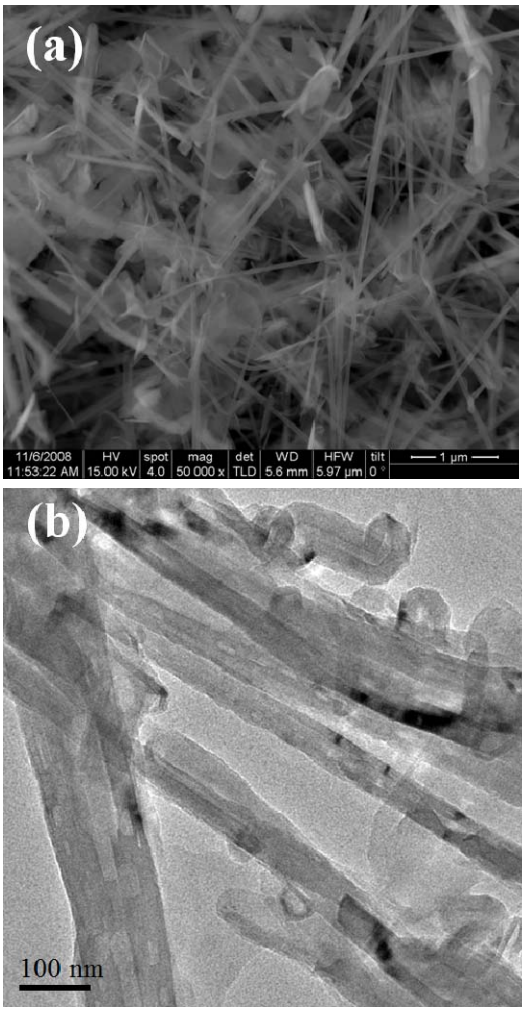

Figure 2.4.39: (a) FESEM and (b) TEM images of BN nanotubes.

- ***Functionalization of nanostructures with organosilane reagents***

We have attempted to coat nanoparticles and nanotubes of BN with HDTMS to enable the dispersion of BN nanostructures in non-polar solvents. Figures 2.4.40 (a) and (c) show TEM images of the HDTMS-coated nanoparticles and nanotubes of BN while Figures 2.4.40 (b) and (d) show the EDAX spectra of the HDTMS-coated BN nanoparticles and nanotubes respectively. The presence of the organosilane coating was ascertained by the presence of silicon in the EDAX spectrum IR spectra of the HDTMS-coated BN nanoparticles and nanotubes also confirm the presence of the organosilicon coating.

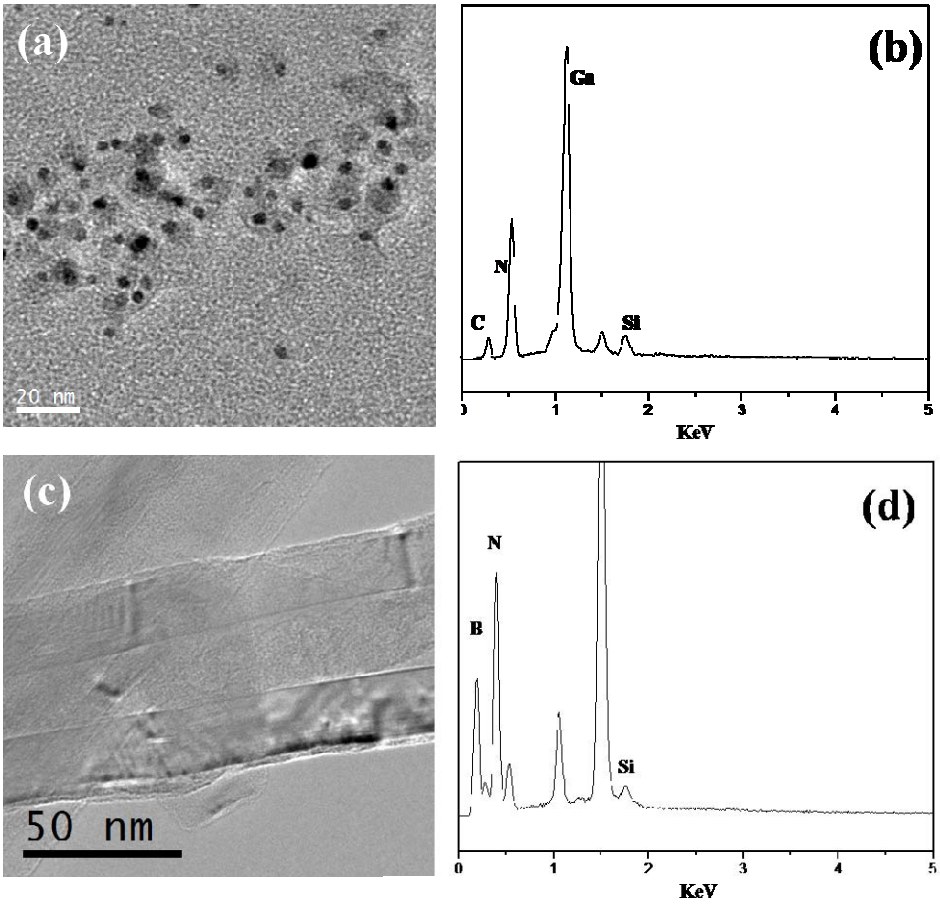

Figure 2.4.40: (a) TEM image and (b) EDAX spectrum of HDTMS-coated BN nanoparticles and (a) TEM image and (b) EDAX spectrum of HDTMS-coated BN nanotubes.

Photographs of the dispersions of as-prepared nanoparticles and nanotubes of BN in toluene are given in Figures 2.4.41 (a) and (c). Figures 2.4.41 (b) and (d) show the photographs of the dispersions of HDTMS-coated BN nanoparticles and nanotubes in CCl_4 and toluene, the former giving better dispersions. The photographs were taken 4 h after the dispersions were prepared. The dispersions were stable upto 8 h and the solids settle down after this period. These precipitates of HDTMS-coated BN nanostructures gave stable dispersions in CCl_4 and toluene on sonication.

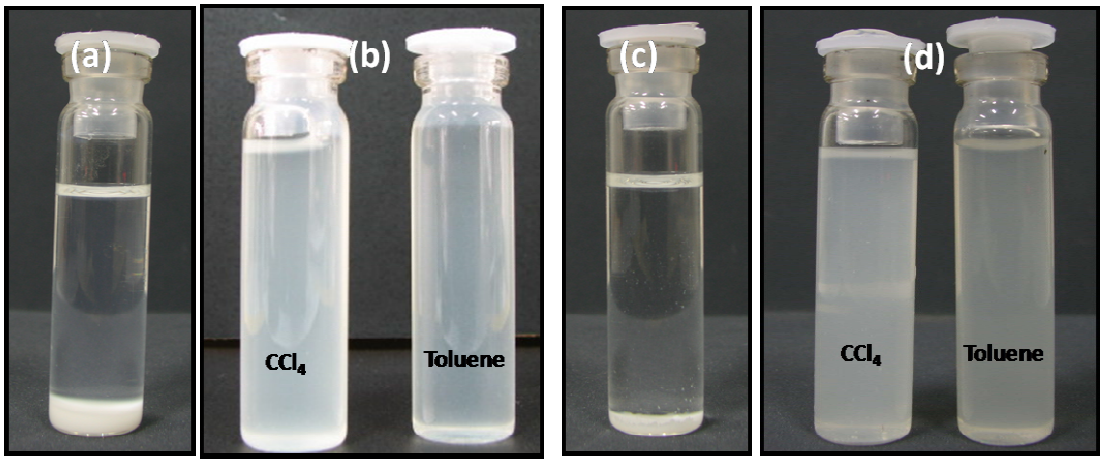

Figure 2.4.41: Photographs of dispersions of (a) as-prepared BN nanoparticles in toluene, (b) HDTMS-coated BN nanoparticles in non-polar solvents, (c) as-prepared BN nanotubes in toluene and (d) HDTMS-coated BN nanotubes in non-polar solvents.

We could coat GaN nanoparticles with HDTMS. When GaN nanoparticles treated with dilute HNO_3 were treated with HDTMS, we could not see any obvious organosilicon coating on the particles in the TEM images. The as-synthesized GaN nanoparticles were therefore, treated first with chlorotriethoxysilane and refluxed under nitrogen atmosphere for 12 h. After lowering the temperature, HDTMS was added and the mixture was refluxed for 12 h. After the reaction, the product was washed with dry toluene and water-acetone mixture. The TEM image of organosilane-coated GaN nanoparticles so obtained is given in Figure

2.4.42 (a). The EDAX spectrum of the organosilane-coated GaN nanoparticles shown in Figure 2.4.42 (b) indicates the presence of silicon. Unlike the BN nanoparticles, the dispersions of the HDTMS-coated GaN nanoparticles were not stable for more than 1 h.

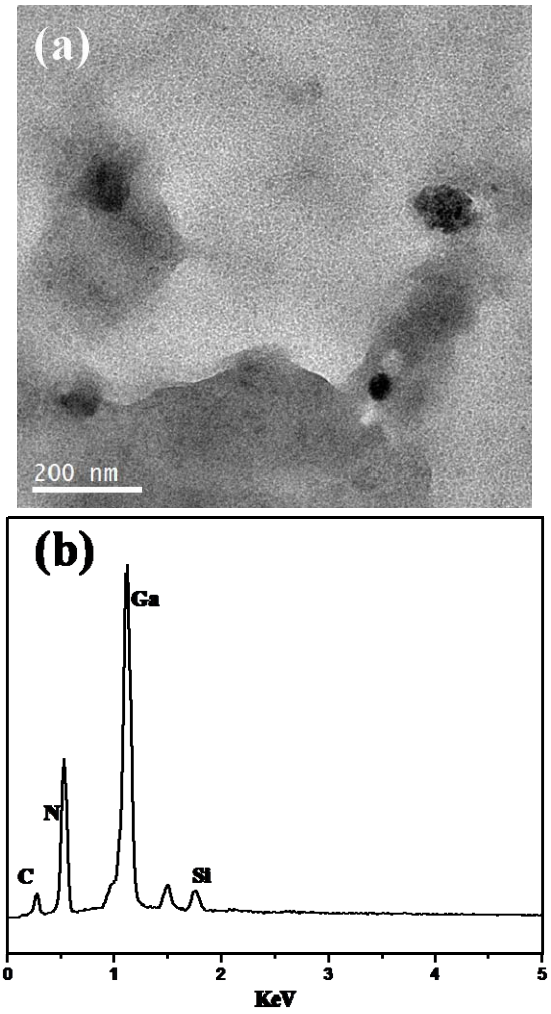

Figure 2.4.42: (a) TEM image and (b) EDAX spectrum of HDTMS-coated GaN nanoparticles.

- ***Functionalization of nanostructures with organotin reagents***

We show the TEM images of the dibutyldimethoxytin-coated nanoparticles and nanotubes of BN in Figures 2.4.43 (a) and (b). The organotin coating on BN nanoparticles and nanotubes were characterized by EDAX analysis and IR spectroscopy. The presence of tin in the EDAX spectrum shown as an inset in Figure 2.4.43 (a) confirms the organotin coating. The IR spectra of the dibutyldimethoxytin-coated BN nanoparticles and nanotubes showed the presence of Sn-O band at 500-600 cm^{-1} and alkyl bands at 2850 and 2950 cm^{-1} confirming the organotin coating.

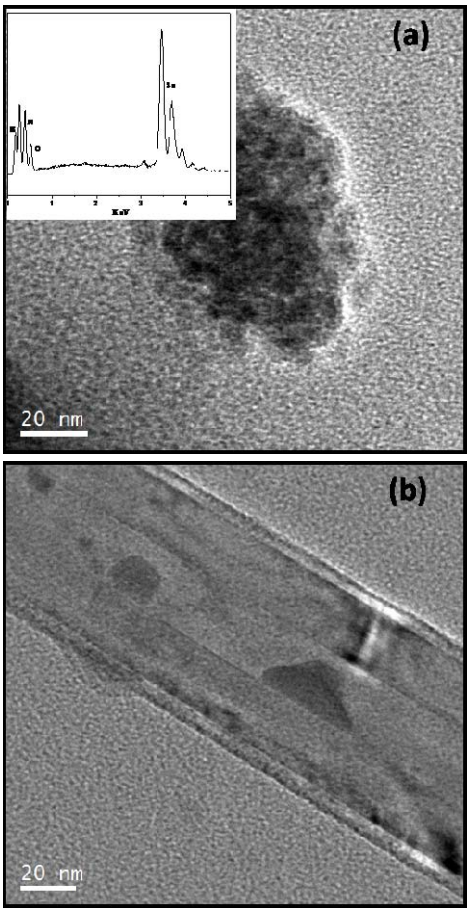

Figure 2.4.43: TEM images of dibutyldimethoxytin-coated BN (a) nanoparticles and (d) nanotubes. Inset in Figure (a) shows the EDAX spectrum.

In Figures 2.4.44 (a) and (b) are shown the photographs of the dispersions of dibutyldimethoxytin-coated nanoparticles and nanotubes of BN in non-polar solvents. The dispersion of the organotin-functionalized BN nanostructures were stable for more than 4 hours, with the dispersions in CCl_4 being more stable than those in toluene.

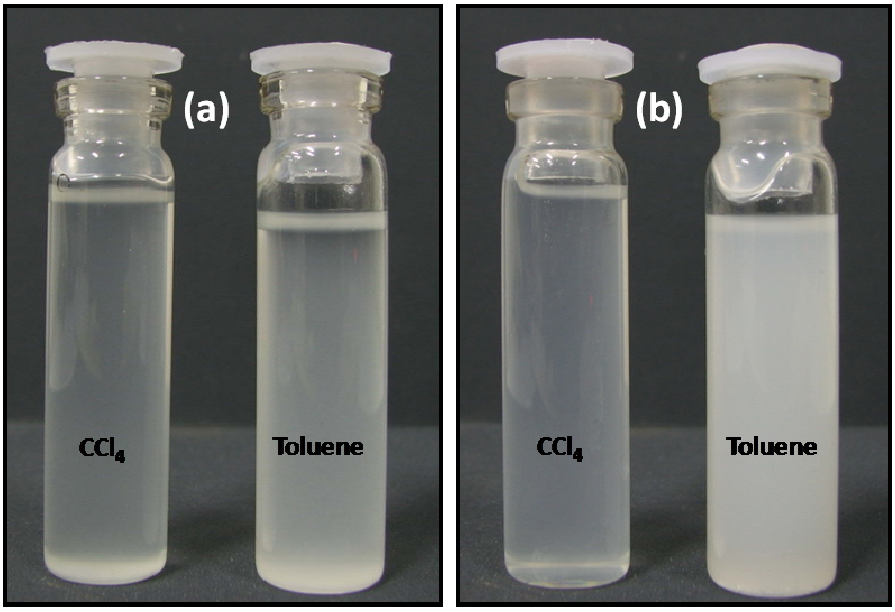

Figure 2.4.44: Photographs of dispersions of dibutyldimethoxytin-coated (a) BN nanoparticles and (b) BN nanotubes in non-polar solvents.

2.4.3. Carbon nanostructures

- ***Characterization of nanostructures***
- ***Carbon nanotubes***

A typical FESEM image of the MWNTs prepared by the pyrolysis of ferrocene is given in Figure 2.4.45 (a). The TEM image of the same is given in Figure 2.4.45 (b). The diameter of the nanotubes prepared by this method is in the range of 50-100 nm. The MWNTs upon acid-treatment were surface functionalized with –COOH and –OH groups which can be seen from the IR spectrum of the acid-treated sample which has bands around

3500 and 1700 cm^{-1}. The samples were dried in vacuum before functionalization with reagents.

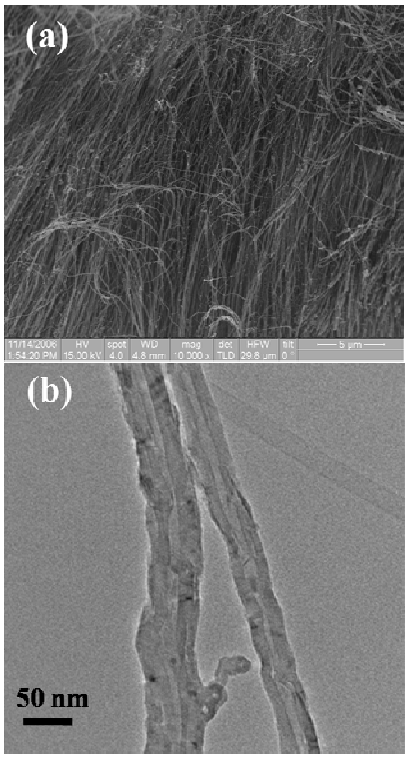

Figure 2.4.45: (a) FESEM and (b) TEM images of MWNTs.

- ***Graphene***

EG sample prepared by thermal exfoliation of graphite oxide generally comprises of 3-4 layers of graphene. Nanodiamond with phase purity higher than 98% and an average particle size of around 5 nm was purchased from Tokyo Diamond Tools, Tokyo, Japan. In Figures 2.4.46 (a) and (b), we show the TEM images of the nanodiamond and EG samples used in this study. The inset in Figure 2.4.46 (a) is the particle size distribution histogram of the pristine nanodiamond which has an average diameter of 5 nm. Both the graphene and nanodiamond samples were acid treated by using microwave followed by hydrothermal treatment. The morphology of the acid-treated samples as analysed by electron microscopic studies did not show change. The IR spectra of the samples show bands due to –OH and –COOH groups at 3500 and 1690 cm^{-1} respectively.

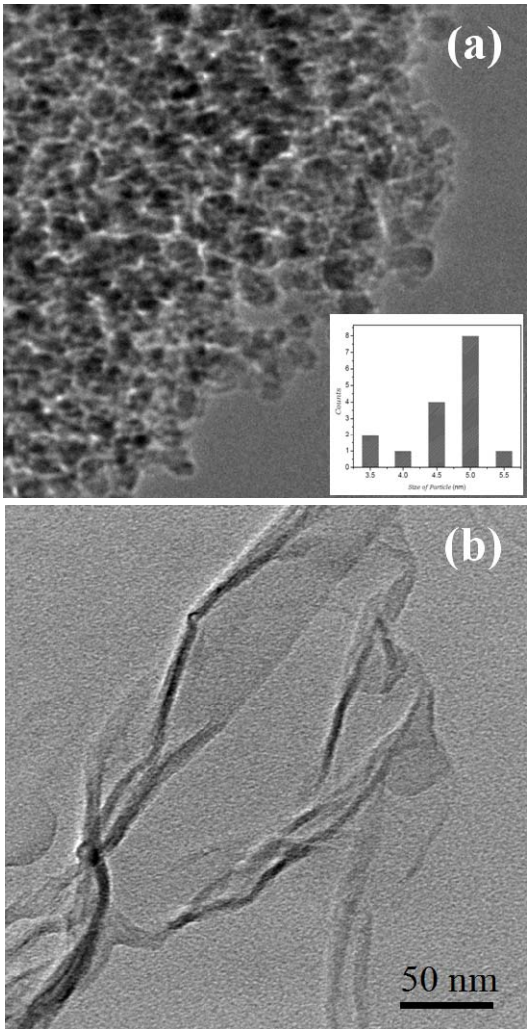

Figure 2.4.46: TEM images of (a) pristine nanodiamonds with the inset showing the particle size distribution and (b) EG samples.

- ***Functionalization of nanostructures with organosilane reagents***

We have functionalized MWNTs with HDTMS. For this purpose, acid-treated MWNTs were reacted with HDTMS employing a procedure similar to that of metal oxide nanowires. The presence of the organosilane coating was confirmed by TEM images, EDAX and IR spectroscopy. A TEM image of HDTMS-coated MWNT is given in Figure 2.4.47 (a). The HDTMS-coated MWNTs gave stable dispersions in toluene and CCl_4. In Figure 2.4.47

(b), we show a photograph of the dispersion of HDTMS-coated MWNTs in toluene taken 12 h after the preparation.

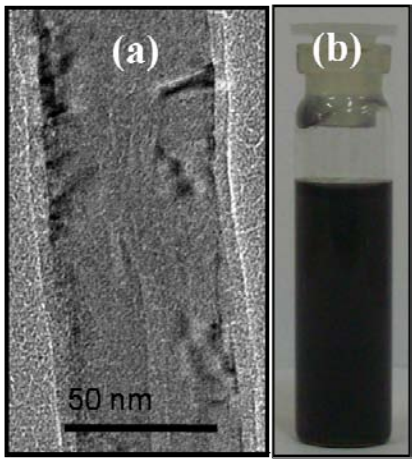

Figure 2.4.47: (a) TEM image and (b) photograph showing dispersion in toluene of HDTMS-coated MWWNTs.

- ***Functionalization of nanostructures with organotin reagents***

We have functionalized MWNTs with dibutyldimethoxytin and trioctyltinchloride. For this purpose, acid-treated MWNTs were reacted with the tin reagents employing a procedure similar to that used for the metal oxide nanowires. In Figures 2.4.48 (a) and (b), we show the TEM images of the dibutyldimethoxytin-coated and trioctyltinchloride-coated MWNTs respectively. From the TEM images it seen that the coating thickness is around 2-5 nm. The EDAX spectrum of the MWNTs functionalized with an organotin reagent show the presence of tin along with carbon. The organotin coating on MWNTs was analyzed by IR spectroscopy. The spectrum showed band due to Sn-O bond stretching at 500-600 cm^{-1} and bands due to organic residue at 2850 and 2950 cm^{-1}. In Figures 2.4.49 (a) and (b), we show photographs of the dispersions in non-polar solvents given by dibutyldimethoxytin-coated and trioctyltinchloride-coated MWNTs respectively.

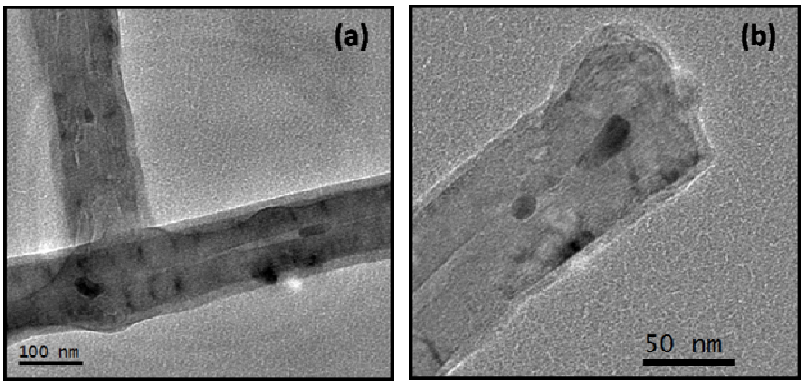

Figure 2.4.48: TEM images of (a) dibutyldimethoxytin-coated and (b) trioctyltinchloride-coated MWNTs.

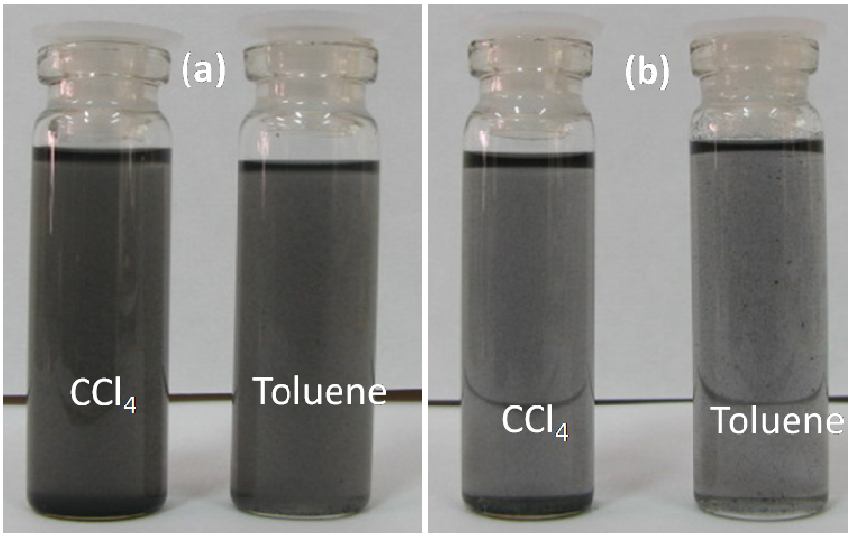

Figure 2.4.49: Photographs of dispersions of (a) dibutyldimethoxytin-coated and (b) trioctyltinchloride-coated MWNTs in non-polar solvents.

- ***Functionalization of nanostructures with POSS***

We have also functionalized acid-treated MWNTs, nanodiamonds and EG with POSS. In Figures 2.4.50 (a) and (b) we show the TEM images of POSS-coated MWNTs and nanodiamond respectively.

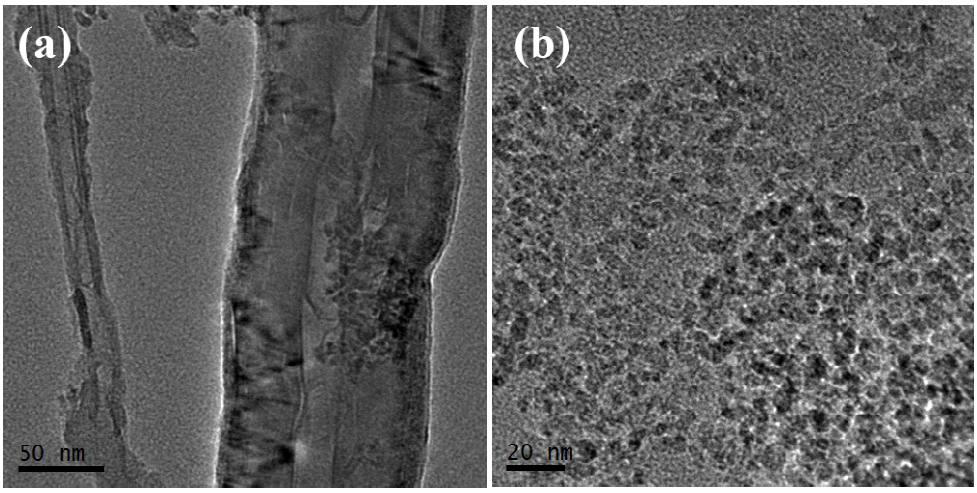

Figure 2.4.50: TEM images of POSS-coated (a) MWNTs and (b) nanodiamond.

POSS-coated nanostructures gave stable dispersions is polar solvents. The dispersions of functionalized nanostructures in water are stable for over a period of 8-10 days. In Figure 2.4.51 are shown the photographs of dispersions of POSS-coated nanostructures in ethanol. The dispersions were left for 12 h after which the photographs were taken.

Figure 2.4.51: Photographs of dispersions of POSS-coated nanostructures in ethanol.

2.4.4. Composites of PVA and Nylon-6,6 with POSS-functionalized inorganic nanoparticles

TiO_2 is commercially important and preferred over various other pigments because of its high refractive index and high degree of transparency in the visible region. Coupled with its high light scattering efficiency, TiO_2 imparts opacity to a variety of products like coatings, paints, plastics and cosmetics. The efficiency with which TiO_2 scatters light depends upon its particle size, with smaller particles scattering the blue light efficiently whereas red light is more scattered by bigger particles. When TiO_2 is used as a single component in a pigment, it results in a complete hiding independent of its particle size as all the light is completely scattered. However in the presence of an absorbing pigment such as carbon black along with TiO_2, smaller particles of TiO_2 scatter blue light more efficiently resulting in less absorption of blue light by carbon black. On the other hand red light being less scattered has more chance to be absorbed by carbon black. As a consequence of this the reflected hue appears blue.

We have given the compositions of various polymer composites prepared by us in Table 1. In Figures 2.4.52 (a) and (b) are shown the FESEM images (their corresponding EDAX patterns as insets) of the composites PVA 4 and 5 respectively. From the EDAX patterns presence of Ti and Fe can be confirmed. In Figure 2.4.53 are shown the photographs of the PVA composites containing TiO_2 and Fe_2O_3 nanoparticles. Figures 2.4.53 (a) and (b) are the photographs of the composites PVA 1 and 2 while that of composites 4 and 5 are shown in Figures 2.4.53 (c) and (d). From photographs it can be seen that upon addition of TiO_2 nanoparticles along with Fe_2O_3 nanoparticles the bright red color exhibited by the latter can be lightened considerably.

Table 2.4.1: Compositions of polymer composites

composites	Weight of PVA (g)	Weight of TiO_2 (g)	Weight of Fe_2O_3 (g)	Weight of AC (g)
PVA-1	2	10	-	-
PVA-2	2	-	10	-
PVA-3	2	-	-	10
PVA-4	2	0.015	0.003	-
PVA-5	2	0.03	0.003	
PVA-6	2	0.015		0.003
PVA-7	2	0.03		0.003
Nylon – 1	-	-	-	-
Nylon – 2		0.015	0.003	
Nylon - 3		0.015		0.003

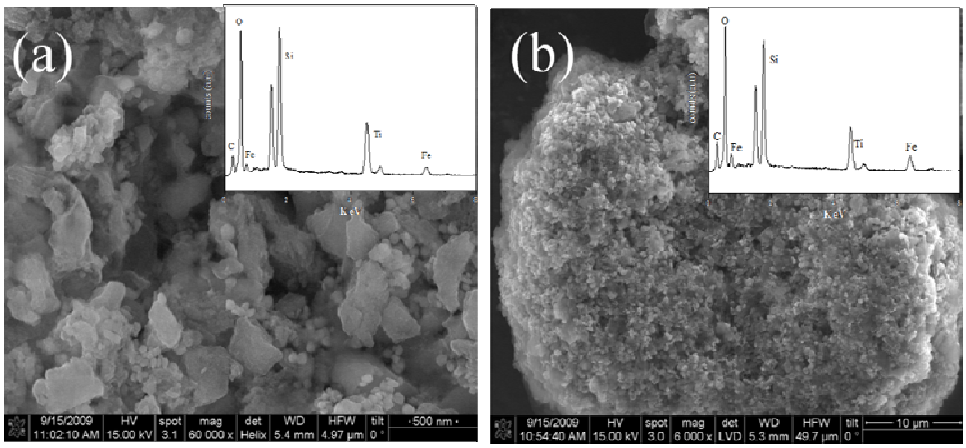

Figures 2.4.52: FESEM images (their corresponding EDAX patterns as insets) of the composites (a) PVA 4 and (b) PVA 5.

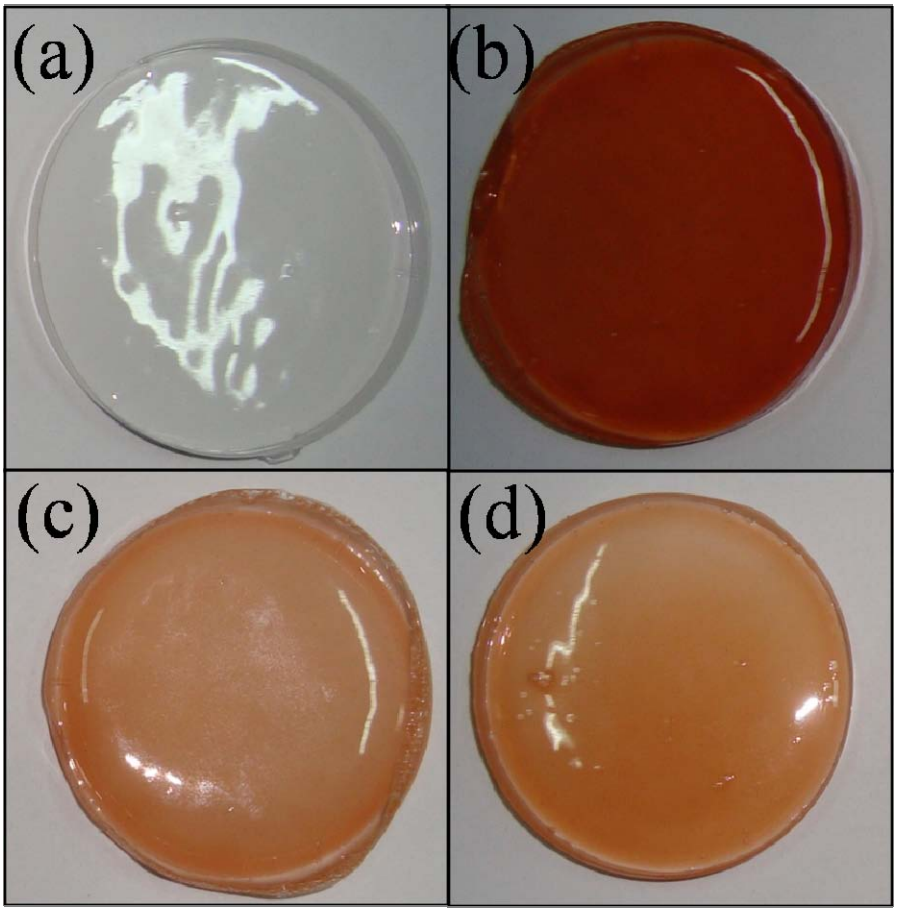

Figure 2.4.53: Photographs of polymer composites (a) PVA 1, (b) PVA 2, (c) PVA 4 and (d) PVA 5.

FESEM images of the composites PVA 6 and PVA 7 are shown in Figures 2.4.54 (a) and (b) respectively. Figure 2.4.55 shows the photographs of the PVA films impregnated with functionalized TiO_2 nanoparticles and graphite. Photographs of PVA composites 1 and 3 containing TiO_2 nanoparticles and graphite as single components are shown in Figures 2.4.55 (a) and (b) respectively. In Figures 2.4.55 (c) and (d) we show the photographs PVA composites 6 and 7 prepared by having TiO_2 nanoparticles and graphite in two different ratios. From the Figures it is evident that the black color imparted by the graphite gets lightened upon addition of TiO_2 nanoparticles.

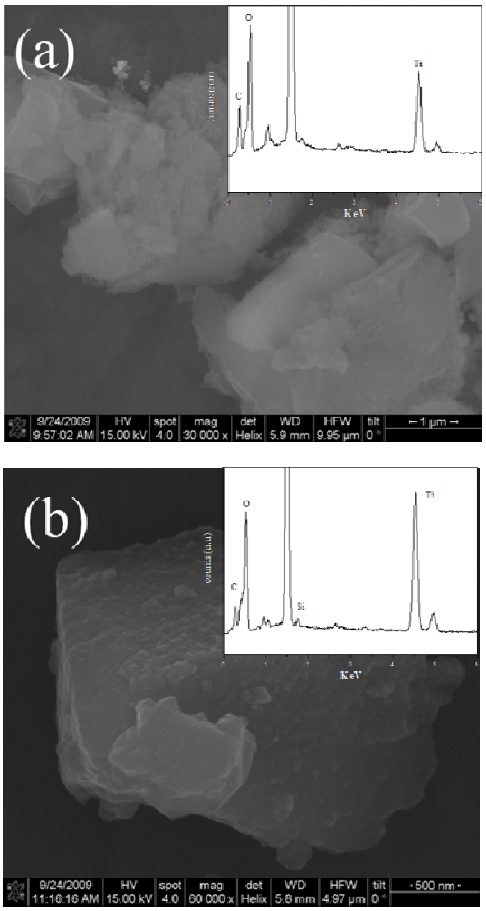

Figures 2.4.54: FESEM images (their corresponding EDAX patterns as insets) of the composites (a) PVA 6 and (b) PVA 7.

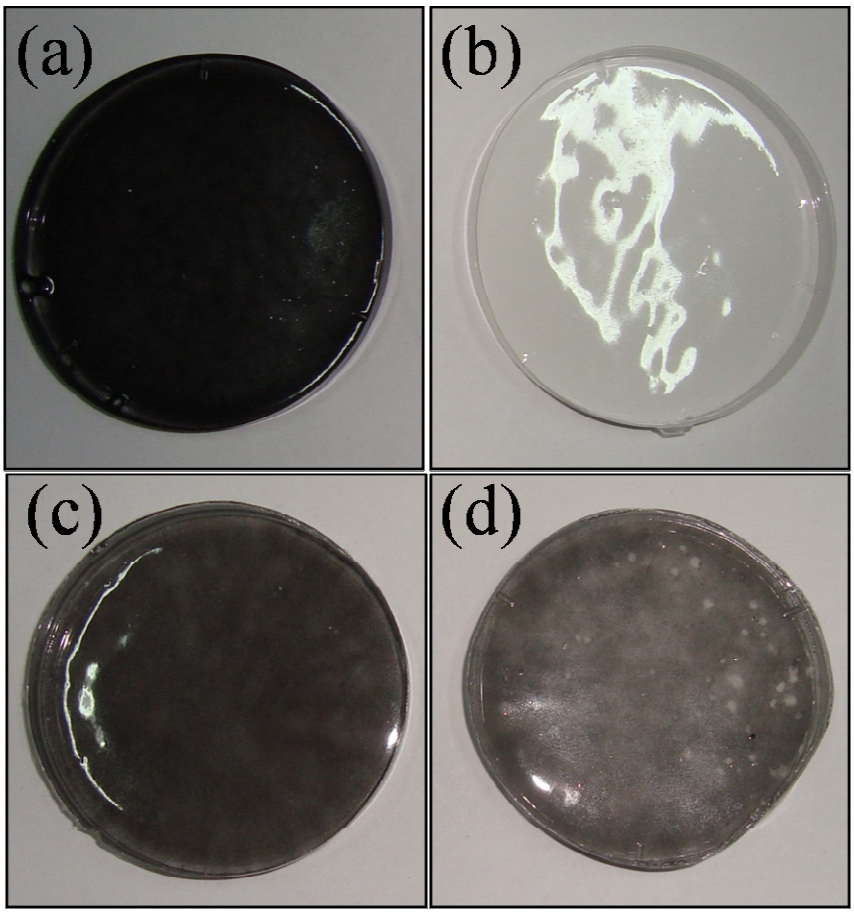

Figure 2.4.55: Photographs of polymer composites (a) PVA 1, (b) PVA 3, (c) PVA 6 and (d) PVA 7.

After being successful in the preparation of PVA composites, we attempted to prepare colored nylon composites containing functionalized nanoparticles of TiO_2 and Fe_2O_3 or graphite. In Figures 2.4.56 (a) and (b), we show the FESEM images of nylon composites 2 and 3 respectively. From the EDAX patterns shown as insets, presence of the metal and thereby the presence of the respective metal oxide nanoparticles is ascertained. The photographs of the nylon composites 1, 2 and 3 are shown Figures 2.4.57 (a), (b) and (c) respectively. The photographs show the different colors imparted by the presence of functionalized nanoparticles of TiO_2 and Fe_2O_3 or graphite in composites nylon 2 and 3 in contrast to the composite nylon-1 which is devoid of any nanoparticles and hence colorless.

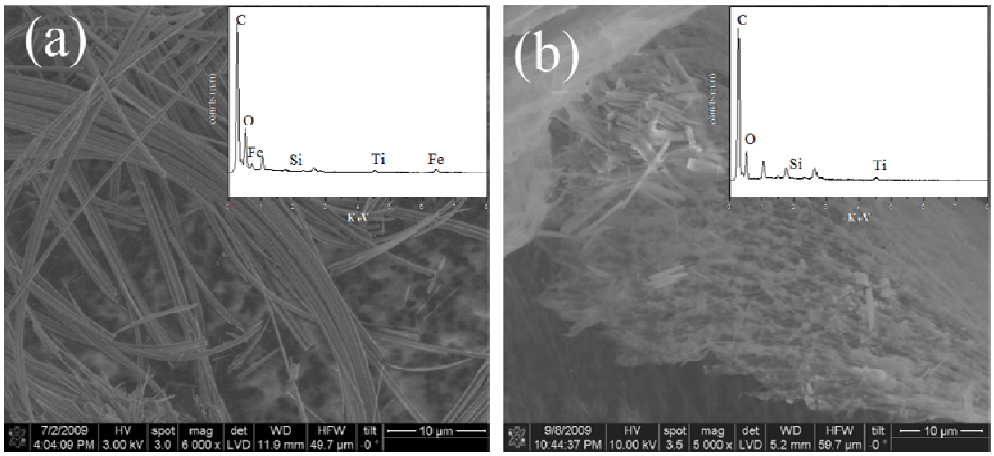

Figures 2.4.56: FESEM images (their corresponding EDAX patterns as insets) of the composites (a) nylon 2 and (b) nylon 3.

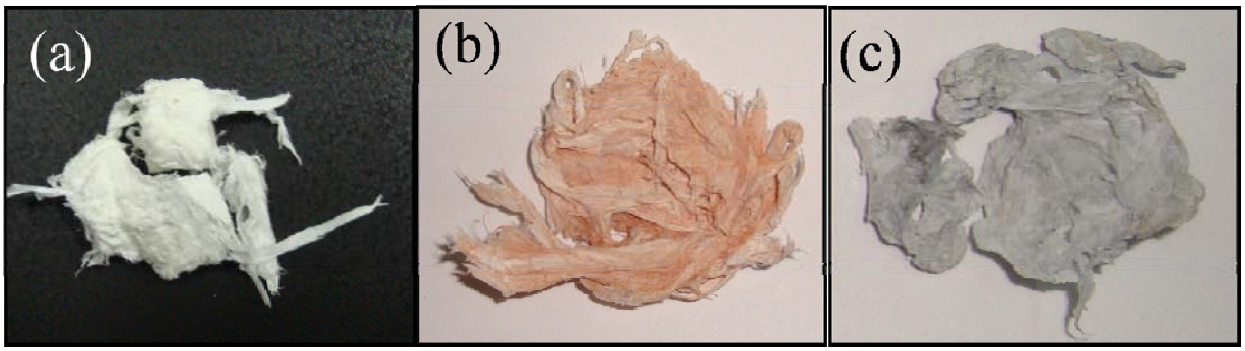

Figure 2.4.57: Photographs of polymer composites (a) PVA 1, (b) PVA 3, (c) PVA 6 and (d) PVA 7.

2.5. Conclusions

In conclusion we have been able to produce stable dispersions of various inorganic nanostructures by the surface modification of the nanostructures either through weak non-covalent or covalent interactions. The best solvent-surfactant/polymer combination varies with different type of oxide nanostructures and hence cannot be generalized that easily. Anyhow in broad view PEO and AOT generally disperse oxide nanostrutures in water while AOT disperses them in toluene.

We have also successfully coated nanostructures of TiO_2, ZnO and Al_2O_3 with hexadecyltrimethoxysilane and obtained their stable dispersions in CCl_4 and toluene. Stable dispersions of nanoparticles of CeO_2 and Fe_3O_4 were also obtained with hexadecyltrimethoxysilane. Both nanoparticles and nanotubes of BN form stable dispersions in non-polar solvents with hexadecyltrimethoxysilane but such success could not be attained with GaN nanoparticles. The organotin reagents, dibutyldimethoxytin and trioctyltinchloride, were equally effective in producing stable dispersions of nanostructures of metal oxides nanostructures, BN and MWNTs in non-polar solvents. Stable dispersions of the inorganic nanostructures and MWNTs described in this article are likely to be useful in various applications, including preparation of composites.

We have synthesized POSS and made use of the same to functionalize the nanostructures so as to get stable dispersion in polar solvents. POSS-coated TiO_2, Fe_2O_3 and activated graphite were employed to make polymer composites of PVA and Nylon 6,6. It is also shown that by using TiO_2 in combination with Fe_2O_3 and activated graphite, it is possible to vary the intensity of the color.

In summary, the surfactants/polymers bind to the surfaces of the nanostructures through weak non-covalent interactions while the organosilicon/organotin reagents bind to the nanostructures through covalent bonding as can be seen from IR spectroscopy both giving stable dispersions in desired solvents. These metal oxide nanostructure dispersions can find use in not only probing characteristics of individual structures but also in preparing composites and in other applications.

References

1. R. P. Feynman, *"A lecture in engineering science" in California Institute of Technology*, February 1960.
2. http://www.kheper.net/topics/nanotech/nanotech-history.htm.
3. J. L. Kirschvink, A. Koyayashi-Kirschvink and B. J. Woodford, *Proc. Natl. Acad. Sci.*, 1992, **89**, 7683-7687.
4. G. Cao, *Nanastructures and Nanomaterials: Synthesis, Properties, and Applications*, Imperial College Press, London, 2004.
5. C. N. R. Rao, A. Mu¨ller and A. K. Cheetham, eds., *The Chemistry of Nanomaterials: Synthesis, Properties and Applications*, WILEY-VCH Verlag GmbH & Co. KGaA, Weinheim, 2004.
6. L. Dai, ed., *Carbon Nanotechnology*, Elsevier, 2006
7. Y. Gogotsi, ed., *Nanomaterials Handbook*, Taylor & Francis Group, 2006.
8. M. Faraday, *Philos. Trans. R. Soc.London,*, 1857, **147**, 145.
9. M. Haruta, T. Kobayashi and H. Sano, *Chem. Lett.*, 1987, **405**.
10. W. Baschong and N. G. Wrigley, *J. Electron. Microsc. Tech.*, 1990, **14**, 313.
11. J. Turkevich, G. Garton and P. C. Stevenson, *J. Colloid Sci.*, 1954, **9**, 26.
12. M. A. Hayat, ed., *Colloidal Gold: Principles, Methods and Applications,*, Academic Press, San Diego, 1989.
13. D. G. Duff, A. Baiker and P. P.Edwards, *Langmuir*, 1993, **9**, 2301.
14. E. Gachard, H. Remita and J. Khatouri, *New. J. Chem.*, 1998, 1257.
15. A. Henglein, *Langmuir*, 1999, **15**, 6738.
16. Y. Mizukoshi, T. Fujimoto and Y.Nagata, *J. Phys. Chem. B*, 2000, **104**, 6028.

17. M. Brust, M. Walker, D. Bethell, D. J. Schiffrin and R. Whyman, *J. Chem. Soc., Chem. Commun.*, 1994, 801.

18. C. Jagadish and S. J. Pearton, eds., *Zinc Oxide: Bulk, Thin Films and Nanostructures*, Elsevier, New York, 2006.

19. Z. W. Pan, Z. R. Dai and Z. L. Wang, *Science*, 2001, **291**, 1947–1949.

20. M. H. Huang, S. Mao, H. Feick, H. Q. Yan, Y. Y. Wu, H. Kind, E. Weber, R. Russo and P. D. Yang, *Science*, 2001, **292**, 1897-1899.

21. Q. X. Zhao, M. Willander, R. R. Morjan, Q.-H. Hu and E. E. B. Campbell, *Appl. Phys. Lett.*, 2003, **83**, 165-167.

22. X. D. Wang, C. J. Summers and Z. L. Wang, *Nano Lett.*, 2004, **4**, 423-426.

23. H. L. Cao, X.F.Qian, Q. Gong, W.M. Du, X. D.Ma and Z.K.Zhu, *Nanotechnology* 2006 **17**, 3632-3636.

24. S. Iijima, *Nature*, 1991, **354**, 56.

25. T. Tang, X. Chen, X. Meng, H. Chen and Y. Ding, *Angew. Chem. Int. Ed.*, 2005, **44**, 1517-1520.

26. L.-P. Zhou, K. Ohta, K. Kuroda, N. Lei, K. Matsuishi, L. Gao, T. Matsumoto and J. Nakamura, *J. Phys.Chem. B*, 2005, **109**, 4439-4447.

27. M. A. C. Duarte, M. Grzelczak, V. S.aceira, M. Giersig, L. M. L. Marzan, M. Farle, K. Sierazdki and R. Diaz, *J. Phys.Chem. B*, 2005, **109**, 19060-19063.

28. J. Liu, X. Li, A. Schrand, T. Ohashi and L. Dai, *Chem. Mater.*, 2005, **17**, 6599-6604.

29. R. M. Kramer, L. A. Sowards, M. J.Pender, M. O. Stone and R. J. Naik, *Langmuir*, 2005, **21**, 8466-8470.

30. Y.-S. Min, E. J. Bae, B. S. Oh, D. Khang and W. Park, *J. Am. Chem. Soc.*, 2005, **127**, 12498-12499.

31. Y.-Q. Xu, E. Flor, M. J. Kim, B. Hamadani, H. Schmidt, R. E.Smalley and R. H. Hauge, *J. Am. Chem.Soc.*, 2006, **128**, 6560-6561.

32. A. K. Geim and K. S. Novoselov, *Nat. Mater.*, 2007, **6**, 183.

33. P. R. Somani, S. P. Somani and M. Umeno, *Chem. Phys. Lett.*, 2006, **430**, 56.

34. H. C. Schniepp, J.-L. Li, M. J. McAllister, H. Sai, M. Herrera-Alonso, D. H. Adamson, R. K. Prud'homme, R. Car, D. A. Saville and I. A. Aksay, *J. Phys. Chem. B*, 2006, **110**, 8535.

35. O. E. Andersson, B. L. V. Prasad, H. Sato, T. Enoki, Y. Hishiyama, Y. Kaburagi, M. Yoshikawa and S. Bandow, *Phys. Rev. B*, 1998, **58**, 16387.

36. R. H. Baughman, A. A. Zakhidov and W. A. d. Heer, *Science*, **2002**, **297**, 787.

37. G. S. Duesberg, R. Graupner, P. Downes, A. Minett, L. Ley, S. Roth and N. Nicolso, *Synth. Met.*, 2004, **142**, 263.

38. M. J. O'Connell, S. M. Bachilo, C. B. Huffman, V. C. Moore, M. S. Strano, E. H. Haroz, K. L. Rialon, P. J. Boul, W. H. Noon, C. Kittrell, J. P. Ma, R. H. Hauge, R. B. Weisman and R. E. Smalley, *Science*, 2002, **297**, 593.

39. J. N. Coleman, A. Fleming, S. Maier, S. O' Flaherty, A. Minett, M. S. Ferreira, S. Hutzler and W. J. Blau, *J. Phys. Chem. B*, 2004, **108**, 3446.

40. R. Murphy, J. N. Coleman, M. Cadek, B. McCarthy, M. Bent, A. Drury, R. C. Barklie and W. J. Blau, *J. Phys. Chem. B* 2002, **106**, 2210.

41. S. O' Flaherty, R. Murphy, S. V. Hold, M. Cadek, J. N. Coleman and W. J. Blau, *J. Phys. Chem. B* 2003, **107**, 958.

42. A. P. Alivisatos, *Science*, 1996, **271**, 933-937.

43. W. C. Chan, nbsp, W and S. Nie, *Science*, 1998, **281**, 2016-2018.

44. Y. Zhou, S. H. Yu, X. P. Cui, C. Y. Wang and Z. Y. Chen, *Chem. Mater.*, 1999, **11**, 545-546.

45. C. N. R. Rao and A. Govindaraj, *Nanotubes and Nanowires,* Royal Society of Chemistry, London, , 2006.

46. Y. Xia, P. Yang, Y. Sun, Y. Wu, B. Mayers, B. Gates, Y. Yin, F. Kim and H. Yan, *Adv. Mater.*, 2003, **15**, 353-389.

47. C. N. R. Rao, F. L. Deepak, G. Gundiah and A. Govindaraj, *Prog. Solid State Chem.*, **31**, 5-147.

48. C. N. R. Rao, G. Gundiah, F. L. Deepak, A. Govindaraj and A. K. Cheetham, *J. Mater. Chem.*, 2004, **14**, 440-450.

49. S. Ghosh, A. Gomathi and C. N. R. Rao, *J. Nanosci. Nanotech.*, 2009, **9**, 5214-5222.

50. S.-W. Kim, S. Kim, J. B. Tracy, A. Jasanoff and M. G. Bawendi, *J. Am. Chem. Soc.*, 2005, **127**, 4556-4557.

51. S-Y. Xie, W. Wang, K. A. S. Fernando, X. Wang, Y. Lin and Y.-P. Sun, *Chem. Commun.*, 2005, 3670.

52. S. Pal, S. R. C. Vivekchand, A. Govindaraj and C. N. R. Rao, *J. Mater. Chem.*, 2007, **17**, 450.

53. E. Estephan, C. Larroque, F. J. G. Cuisinier, Z. B. and and C. Gergely, *J. Phys. Chem. B*, 2008, **112**, 8799.

54. H Zarrad , P Clechet , M Belin , C. M. and and N. Jaffrezic-Renault, *J. Micromech. Microeng.*, 1993, **3**, 222.

55. R. Maoz, S. Matlis, E. DiMasi, B. M. Ocko and J. Sagiv, *Nature*, 1996, **384**, 150-153.

56. M. Rivka and S. Jacob, *Adv. Mater.*, 1998, **10**, 580-584.

57. S.-Y. Chang, L. Liu and S. A. Asher, *J. Am. Chem. Soc.*, 1994, **116**, 6739-6744.

58. L. M. Liz-Marzan, M. G. and and P. Mulvaney, *Langmuir*, 1996, **12**, 4329.

59. M-Q. Zhu, E. Chang, J. Sun and R. A. Drezek, *J. Mater. Chem.*, 2007, **17**, 800.

60. T. Nann and P. Mulvaney, *Angew. Chem., Int. Ed.*, 2004, **43**, 5393.

61. T. Shimoda, K. Aoki, Y. Shinoda, T. Nakamura, N. Tokunaga, S. Inagaki and T. Hayashi, *J. Am. Chem. Soc.*, 2003, **125**, 4688.

62. X. Zhao, R. P. Bhagwe and W. Tan, *Adv. Mater.* , 2004, **16**, 173.

63. Y. Yang, L. Ling, X. Yu, D. Yan and M. Gao, *Chem. Mater.* , 2007, **19**, 4123.

64. M. T. Byrne, J. E. McCarthy, M. Bent, R. Blake, Y. K. Gun'ko, E. Horvath, Z. Konya, A. Kukovecz, I. Kiricsi and J. N. Coleman, *J. Mater. Chem.*, 2007, **17**, 2351.

65. L. Jing, B. Xin, F. Yuan, L. Xue, B. Wang and H. Fu, *J. Phys. Chem. B,* 2006, **110**, 17860-17865.

66. R. Viswanatha, H. Amenitsch and D. D. Sarma, *J. Am. Chem. Soc.* , 2007, **129**, 4470.

67. Y. S. Kang, S. Risbud, J. F. Rabolt and P. Stroeve, *Chem. Mater.*, 1996, **8**, 2209-2211.

68. N. PailheÌ , J. Majimel, S. Pechev, P. Gravereau, M. Gaudon and A. Demourgues, *J. Phys. Chem. C,* 2008, **112**, 19217-19223.

69. F. Li, X. Yu, H. Pan, M. Wang and X. Xin, *Solid State Sci.* , 2000, **2**, 767.

70. B. M. Wen, C. Y. Liu and Y. Liu, *New J. Chem.*, 2005, **29**, 969.

71. H. L. Cao, X. F. Qian, Q Gong, W. M. Du, X. D. Ma and Z. K. Zhu, *Nanotechnology* 2006, **17**, 3632.

72. G. Gundiah, F. L. Deepak, A. Govindaraj and C. N. R. Rao, *Top. Catal.* , 2003, **24**, 137.

73. A. Gomathi and C. N. R. Rao, *Mater. Res. Bull.* , 2006, **41**, 941.

74. K. Sardar, M. Dan, B. Schwenzer and C. N. R. Rao, *J. Mater. Chem.*, 2005, **15**, 2175.

75. F. L. Deepak, C. P. Vinod, K. Mukhopadhyay, A. Govindaraj and C. N. R. Rao, *Chem. Phys. Lett.*, 2002, **353**, 345-352.

76. R. Sen, A. Govindaraj and C. N. R. Rao, *Chem. Phys. Lett.*, 1997, **267**, 276-280.

77. K. S. Subrahmanyam, S. R. C. Vivekchand, A. Govindaraj and C. N. R. Rao, *J. Mater. Chem.*, 2008, **18**, 1517–1523.

78. I. Hasegawa, *Polyhedron*, 1991, **10**, 1097-I 1101.

79. T. H. Benny and S. S. Wong, *Chem. Mater.* , 2006, **18**, 4827.

80. L. Chen, H. Shen, Z. Lu, C. Feng, S. Chen and Y. Wang, *Colloid. Polym. Sci.*, 2007, **285**, 1515.

81. P. Siciliano, *Sensors and Actuators B*, 2000, **70** 153.

PART 3

Graphene Analogues of WS_2

Summary[*]

Graphene analogues of WS_2 have been prepared by chemical methods which include intercalation of lithium followed by exfoliation and reaction of tungstic acid with excess of thiourea at high temperatures in a nitrogen atmosphere. Products of these reactions examined by microscopic techniques show that they contain one to three layers of WS_2. Raman spectra show softening of the A_{1g} modes in these few-layer materials. The few-layer WS_2 has been decorated with nanoparticles of gold and platinum.

[*] Paper based on above studies has been accepted in *Angew. Chem. Int. Ed.*,

3.1 Introduction

The synthesis of fullerenes [1] and carbon nanotubes [2] from graphite opened up a whole new scientific field in materials science. Like diamond, natural graphite is a special form of pure carbon. These characteristics are the principal reason for the unique chemical and physical properties of graphite:

• Excellent electrical and thermal conductivity.

• Excellent lubricating properties.

• High resistance to oxidation particularly at elevated temperatures.

• The ability of chemical molecules to be intercalated between the graphite layers.

The basic structure of graphite consists of hexagonal groups of carbon atoms, which form stable planar grids with a weak inter layer bonding. In Figure 3.1.1, we show the structure of graphite and its nanostructures of different dimensionalities, zero-dimensional (0-D) fullerene, one-dimensional (1-D) carbon nanotubes and two-dimensional (2-D) graphene.

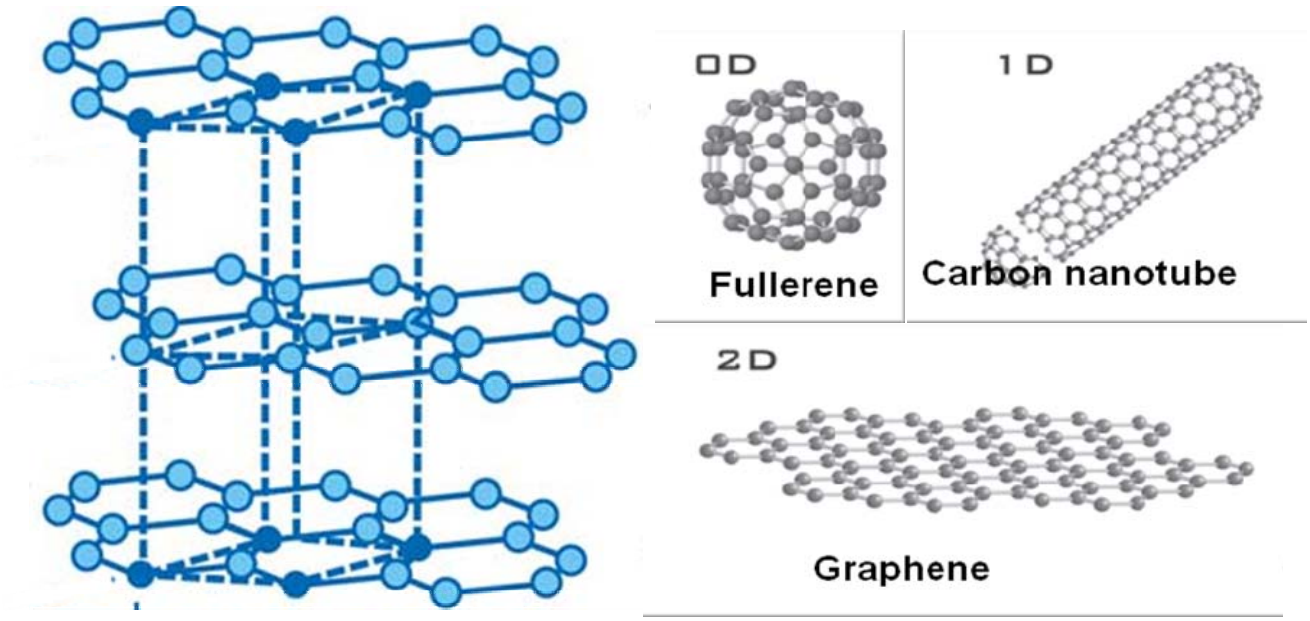

Figure 3.1.1: Structure of graphite and its various allotropes in nano regime.

Soon after the discovery of the fullerenes and carbon nanotubes, taking the advantage of structural analogy between graphite and other layered materials, researchers have synthesized inorganic analogues of fullerene and carbon nanotubes. The first inorganic nanotubes and fullerene-like particles were synthesized from layered transitional metal dichalcogenides - 2H-WS_2 and 2H-MoS_2 [3-9]. Subsequently it has been shown that various materials with layered structure such as BN [10], V_2O_5 [11], NbS_2 [12] and many others form closed cage nanostructures. Nanostructures of MoS_2 and WS_2 have been studied widely because of their potential applications in the fields of lubrication, high performance nanocomposites, sensors, renewable energy, energy storage, and catalysis. Structure of transition metal dichalcogenides which are quasi-two-dimensional compounds can be described as a unique sandwich where the MX_2 layers are bonded by weak van der Waals forces through relatively large (several Angstrom) van der Waals gap as can be visualized from Figure 3.1.2. The existence of the van der Waals gap allows facile accommodation of foreign atoms and molecules.

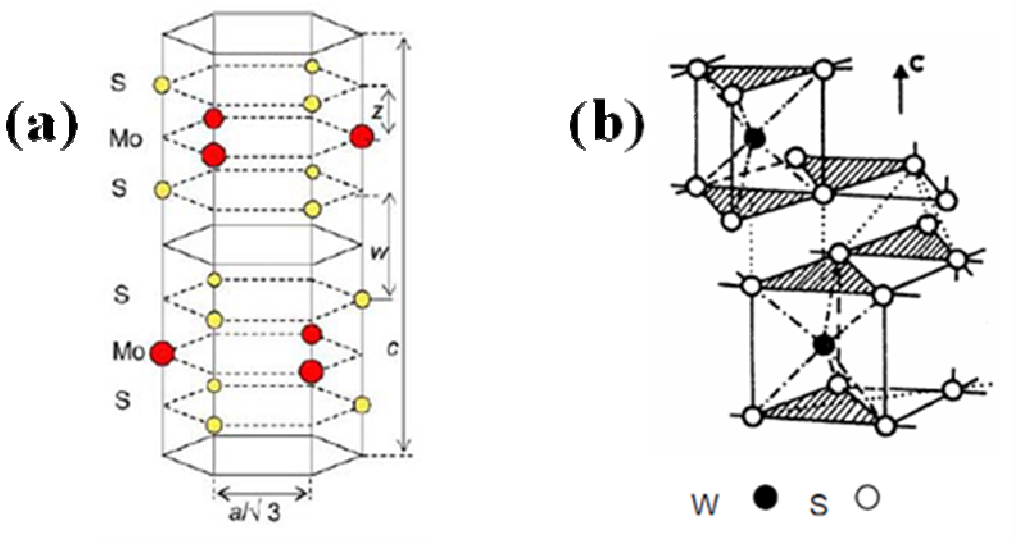

Figure 3.1.2: Crystal structures of (a) MoS_2 and (b) WS_2.

Being successful with synthesis, a few products under the brand name NanoLub^{TM}, including lubricating fluids and greases formulated with inorganic fullerene-like WS_2 nanoparticles, were launched in the market. In recent years much effort is being dedicated in advancing the synthesis of these transition metal dichalcogenides nanostructures to obtain specific and tunable physical properties with respect to their structure and/or morphologies.

Among the three allotropes of graphite, graphene, an infinite, one atom thick, 2-D array of carbon hexagons is considered the reference for all sp^2-derived allotropic forms of carbon. Previously considered a virtual object, its recent experimental availability has stirred an ever-increasing activity [13] since the first samples were produced in 2004 [14]. Far reaching applications such as patterned single-electron transistors [13], ultimate gas sensors able to detect one molecule [15], as well as high volume applications such as mechanically reinforced composites [16] are envisioned. Various synthetic strategies for graphene involve micromechanical cleavage [14], SiC epitaxy [17], exfoliation of graphitic oxide, pyrolysis of graphene, conversion of nanodiamond and arc evaporation of SiC [18]. After the successful synthesis of 2-D graphene, BN layers were prepared by means of micromechanical cleavage [19]. Raidongia *et. al.* [20, 21] have recently reported the synthesis of few-layer BN and BCN by chemical methods. But till now there are no reports on the chemical synthesis of inorganic analogues of WS_2.

3.2 Scope of the present investigations

Following the discovery of fullerenes in 1985, it was soon recognized that inorganic layered materials such as MoS_2 and WS_2 can also form fullerene-like structures. After the discovery of carbon nanotubes, inorganic nanotubes analogous to carbon nanotubes were prepared and characterized, nanotubes of MoS_2 and WS_2 being archetypal examples. With the discovery and characterization of graphene, the two dimensional nanocarbon, which has

created great sensation in last three to four years [22, 23], it would seem natural to explore the synthesis of graphene analogues of layered inorganic materials. We have attempted to synthesize inorganic graphene analogues of dichalcogenide of tungsten by chemical methods which posses layered structure. From the literature there were reports on the intercalation and exfoliation of MoS_2 and WS_2. Here it has been attempted to review the relevant papers on the exfoliation of layered dichalcogenides. The synthesis of single crystals of MoS_2 of several molecular layers thick has been reported by cleavage method [24] and their optical absorption and photoconductivity have been studied [25]. There is a report on the intercalation of various alkali metals in layered metal dichalcogenide crystals with controlled stoichiometry [26]. There is an early report [27] on graphene-like MoS_2 prepared by lithium intercalation and exfoliation, but the material was characterized only by X-ray diffraction which is not sufficient to determine the exact nature and number of layers. There have been attempts to prepare single layers of WS_2 by lithium intercalation and exfoliation as well [28, 29] and here again the product was only characterized on the basis of (002) reflection in the X-ray diffraction pattern. Later MoS_2 prepared by lithium intercalation has been characterized by means of scanning force microscopy and x-ray absorption fine structure spectroscopy [30, 31]. The MoS_2 suspensions were used to prepare inclusion compounds of various organic molecules [32, 33]. MoS_2 and $NbSe_2$ suspensions were employed to fabricate high efficient polymer light emitting diodes [34, 35]. Since few-layer WS_2 containing five layers or less do not exhibit the (002) reflection prominently, it is necessary that layered WS_2 produced by lithium intercalation and exfoliation are investigated by transmission electron microscopy and other techniques. It is also desirable to explore alternative chemical synthesis of these graphene-like materials. Discovery of the two-dimensional graphene analogues of WS_2 will fill the gap that we have had in the family of nanocarbon analogues which had till now zero-dimensional fullerenes

and one-dimensional nanotubes. We have employed two different methods to synthesize graphene-like WS_2. In Method 1, bulk WS_2 was intercalated with lithium and exfoliated in water. In Method 2 tungstic acid was reacted with excess of thiourea in a N_2 atmosphere 773 K.

3.3 Experimental and related aspects

- ***Synthesis***

All the chemicals and solvents used in this work were brought from Sigma-Aldrich. Bulk WS_2, n-Butyllithium 1.6 M in hexane, tungstic acid and thiourea were used as such. Solvents were distilled and stores under sodium prior to their use. We have employed two methods for the synthesis of few- layer WS_2.

Method 1: Lithium intercalation of WS_2

Commercially available WS_2 when subjected to lithium intercalation at room temperature followed by an exfoliation in distilled water did not yield few layers of WS_2. Hence the intercalation of WS_2 with lithium was performed at a higher temperature. For this 100 mg of WS_2 in 10 ml of n-Butyllithium in 5 ml of hexane was stirred at 373 K in a nitrogen atmosphere for 72 hours. The intercalated sample was washed with hexane and dried followed by exfoliation in which distilled water was added to the lithium-intercalated WS_2 and sonicated to get a highly stable suspension of WS_2 layers in water.

Method 1: Synthesis of WS_2 employing thiourea

In this method WS_2 layers were prepared by heating tungstic acid with an excess of thiourea at 773 K under nitrogen atmosphere for 3 h. For this purpose, tungstic acid was synthesized by dissolving about 0.5 g of $Na_2WO_4.2H_2O$ was dissolved in 20 ml distilled

water. To this conc. HCl was added drop wise under constant stirring. The yellow tungstic acid thus obtained was washed with distilled water and dried overnight in hot air oven. In a typical synthesis, 0.1 g of tungstic acid was ground with 1.2 g of thiourea and placed in an alumina boat which was then placed inside a quartz tube kept inside a horizontal tube furnace. Prior to the heating the quartz tube was purged with nitrogen for 0.5 h. The temperature was then raised to 773 k and then held at the same for 3 h. After 3 h, the sample was cooled down to room temperature under nitrogen atmosphere. The black product obtained was used as such for further analysis.

Decoration of WS_2 layers with metal nanoparticles

We have made use of WS_2 layers obtained by means of thiourea method for the decoration with metal nanoparticles of gold and platinum. In a typical reaction, aqueous WS_2 suspension was treated with 0.5 M solution of $HAuCl_4$ or H_2PtCl_6 and ethylene glycol taken in 1:1 ratio. The reaction mixture was then kept under microwave condition at 300 W for 30 min. The products obtained were washed with ethanol and dried under ambient conditions.

• *Characterization Techniques*

X-ray Diffraction: X-ray diffraction (XRD) patterns of the nitrides were recorded using Cu Kα radiation on a Rich-Siefert XRD-3000-TT diffractometer.

Field emission scanning electron microscopy: Field emission scanning electron microscopy (FESEM) images were obtained using a FEI NOVA NANOSEM 600.

Transmission electron microscopy: For transmission electron microscopy, the samples were dispersed in CCl_4 and dropped on to the holey carbon-coated copper grids. The grids were allowed to dry in the air. Transmission electron microscope (TEM) images were obtained

with a JEOL JEM 3010, operating with an accelerating voltage of 300 kV. TEM images and atomic arrangement of hexagonal WS_2 was obtained from the FEI TITAN (cube) 80-300 kV aberration corrected transmission electron microscope with a negative spherical aberration coefficient (C_s) of ~ -30 µm and a positive defocus about +8 nm, where atomic potentials appear with bright contrast in a dark background.

Raman spectroscopy: Raman spectra were recorded with a LabRAM HR with the 633 nm line from HeNe laser. The excitation wavelength is 632.8 nm.

Atomic force microscopy: AFM measurements were carried on Vecco digital instruments, diInnova. Samples for AFM measurements were prepared by spin coating the WS_2 solutions on mica substrate.

3.4 Results and Discussion

Intercalation of lithium in WS_2 followed by exfoliation at room temperature was not satisfactory. Hence we carried out the reaction at 373 K followed by exfoliation in distilled water. Upon exfoliation, lithium-intercalated WS_2 gave an opaque suspension in water which was centrifuged at 12000 RPM to obtain a black powder of layered WS_2. When lithium-intercalated chalcogenides is treated with water, it results in the formation of lithium hydroxide and hydrogen gas which account for the separation of the layers or the loss of the periodicity along the *c*-axis. This can be identified from the XRD patterns for if the layers are well separated then the (00*l*) reflections will be absent in the XRD pattern. In Figure 3.4.1, we show a comparison of XRD patterns of bulk and few-layer WS_2 synthesized in the laboratory. In Figures 3.4.1 (a) and (b), we show the XRD patterns of bulk WS_2 and the WS_2 layers obtained by lithium intercalation followed by exfoliation. The XRD pattern of the bulk WS_2 shows a strong intense (002) peak whereas that of the WS_2 layers prepared through

lithium intercalation shows the absence of this feature suggesting the presence of very few layers in the sample. TEM images in Figure 3.4.2 (a) reveal that WS_2 from lithium intercalation and exfoliation mostly consists of bilayers and a reasonable number of single layers were also observed. From the TEM image it is observed that the exfoliated WS_2 layers have an interlayer spacing of 0.65-0.70 nm which is comparable to that of bulk (0.65 nm).

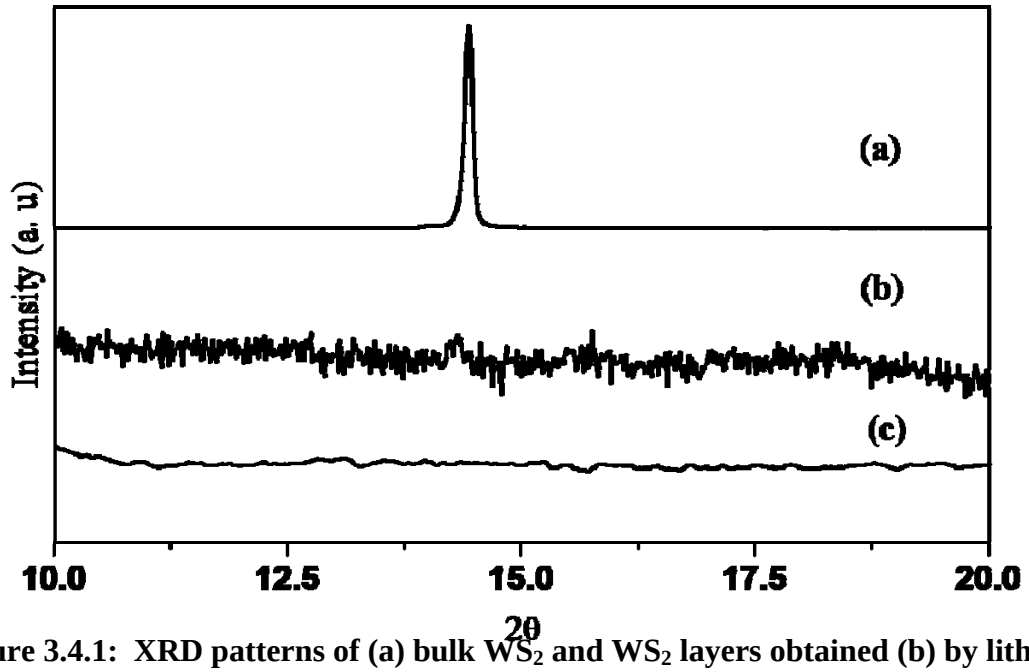

Figure 3.4.1: XRD patterns of (a) bulk WS_2 and WS_2 layers obtained (b) by lithium intercalation and exfoliation and (c) thiourea method.

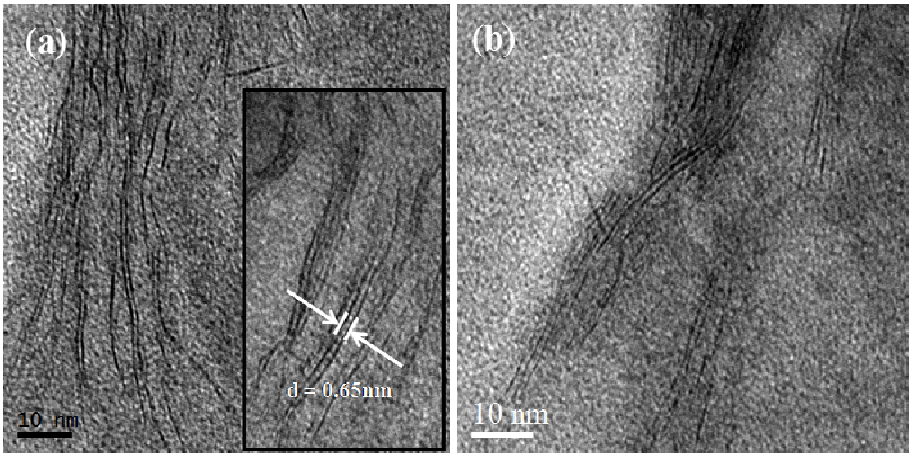

Figure 3.4.2: TEM images of WS_2 layers obtained by lithium intercalation and exfoliation with the inset showing the interlayer spacing of the layers.

The AFM images of WS_2 layers synthesized using lithium intercalation is shown in Figure 3.4.3 (a). The image and the height profile confirm the existence of 2-3 layers of WS_2 with the average thickness of the layers being 1.2-1.3 nm.

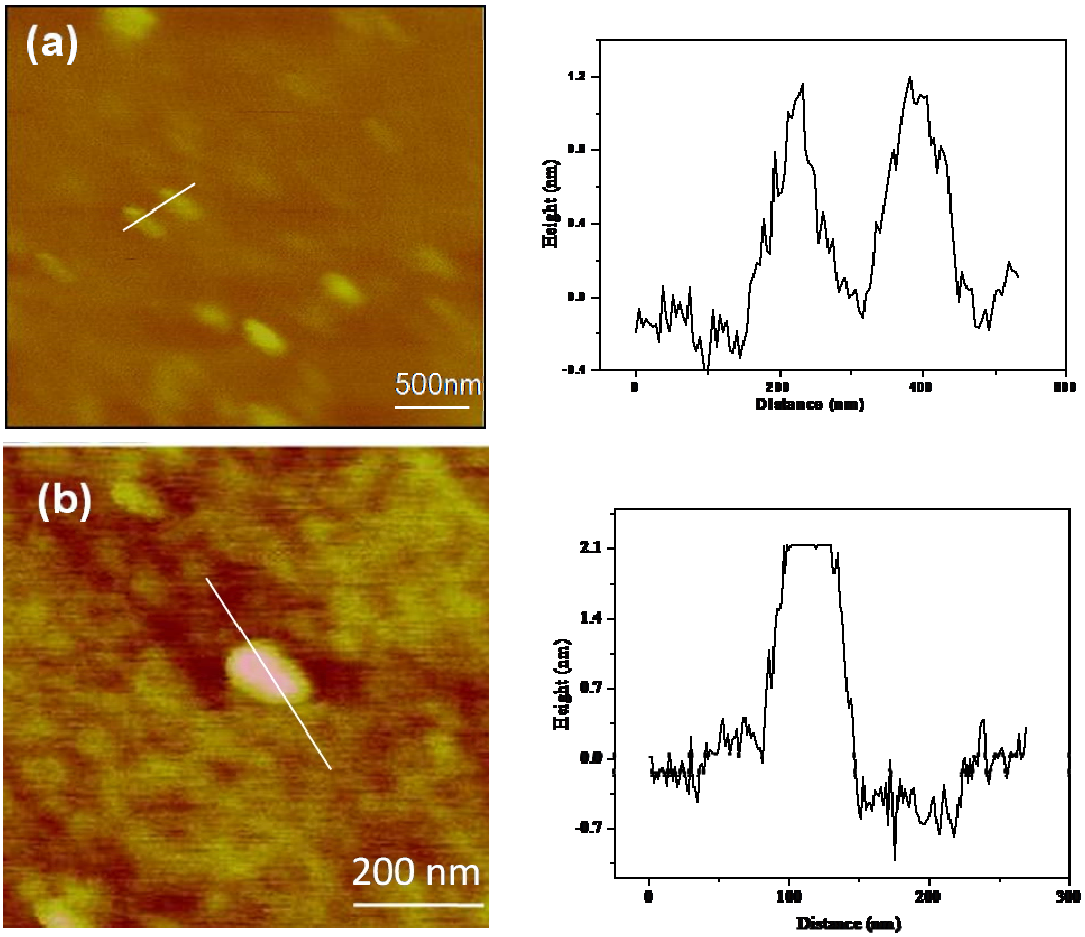

Figure 3.4.3: AFM images and the associated height profiles of WS_2 layers obtained by (a) lithium intercalation and exfoliation and (b) thiourea method.

In Figures 3.4.4 (a) and (b), we show the Raman spectra of the bulk WS_2 and that obtained by lithium intercalation respectively. Compared to the bulk WS_2, the as-synthesized WS_2 layers show broader peaks. The Raman spectrum of bulk WS_2 shows narrow bands at 351 and 420 cm^{-1} corresponding to the E_{2g} and A_{1g} modes respectively with FWHM values around 7.8 and 2.4 cm^{-1}. The Raman spectrum of WS_2 layers obtained from lithium

intercalation shows bands due to E_{2g} and A_{1g} modes at 351 and 415 cm^{-1} with FWHM values of 13.7 and 8.4 cm^{-1}.

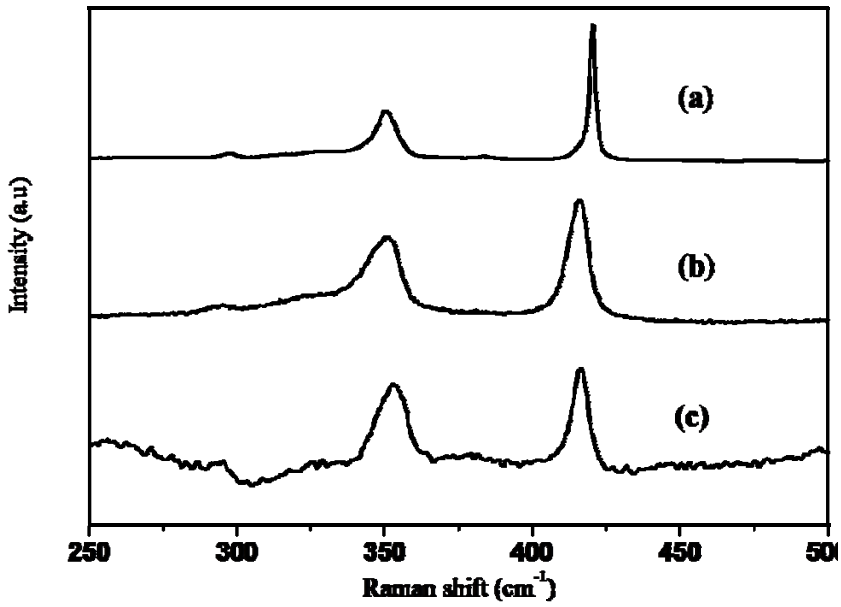

Figure 3.4.4: Raman spectra of (a) bulk WS_2 and WS_2 layers obtained (b) by lithium intercalation and exfoliation and (c) thiourea method.

In thiourea method, tungstic acid was heated with excess thiourea at 773 K for 3 h under nitrogen atmosphere to give layers of WS_2. Figure 3.4.1 (c) shows the XRD pattern of the as-synthesized WS_2 layers. From the absence of the (002) reflection in the XRD pattern, it is understood that the sample contains very few layers of WS_2. In Figures 3.4.5 are shown the TEM images of WS_2 layers obtained by thiourea method which also mostly comprises of bilayers. From the TEM images an interlayer spacing of 0.86-0.95 nm was obtained for the WS_2 layers. This interlayer spacing in WS_2 is the separation between either two tungsten or sulphur atoms of adjacent slabs. This spacing being more than that of the bulk indicates that the exfoliation is complete and the formed layers are almost single layer in nature.

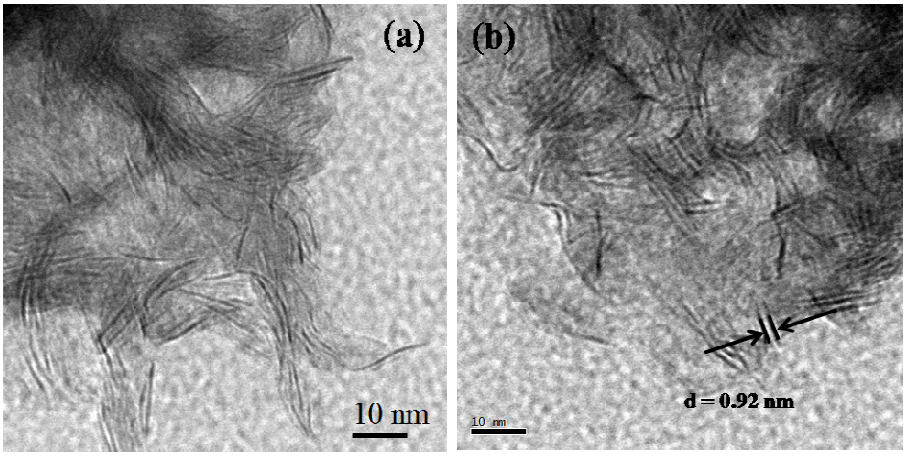

Figure 3.4.5: TEM images of WS_2 layers obtained by thiourea method with the inset showing the interlayer spacing of the layers.

Given in Figures 3.4.6 are the TEM images obtained from FEI TITAN microscope. The TEM analysis showed that the sample mainly consists of bilayers. Figure 3.4.6 (b) is the high resolution transmission electron microscope (HRTEM) image of WS_2 showing the hexagonal arrangement of tungsten and sulphur atoms.

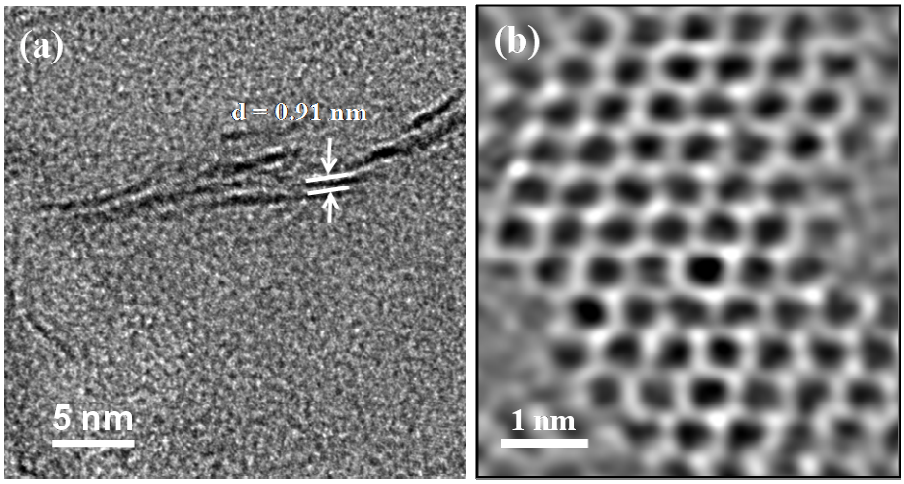

Figure 3.4.6: (a) TEM and (b) HRTEM image showing the hexagonal arrangement of W and S atoms of WS_2 layers obtained by thiourea method.

The presence of bilayers is also confirmed by the AFM image and the height profile of WS_2 prepared by the thiourea method as shown in Figure 3.4.3 (b). In Figure 3.4.4 (c) we show the Raman spectrum of WS_2 layers obtained by thiourea method which shows a similar softening of the band due to the A_{1g} mode and an increase in the width of the band due to the E_{2g} mode. The broadening of the Raman bands can be assigned to the phonon confinement. The broadening also suggests that the lateral dimensions of these layers are in nano regime [36].

In Figures 3.4.7, we show the TEM images of WS_2 decorated with gold nanoparticles by the reduction of $HAuCl_4$ under microwave conditions. From the TEM images it can be seen the gold nanoparticles are of different sizes ranging from 3-20 nm. Figures 3.4.7 (b) and (c) are the HRTEM images of the gold nanoparticle decorated WS_2 layers which show that the gold nanoparticles are single-crystalline in nature.

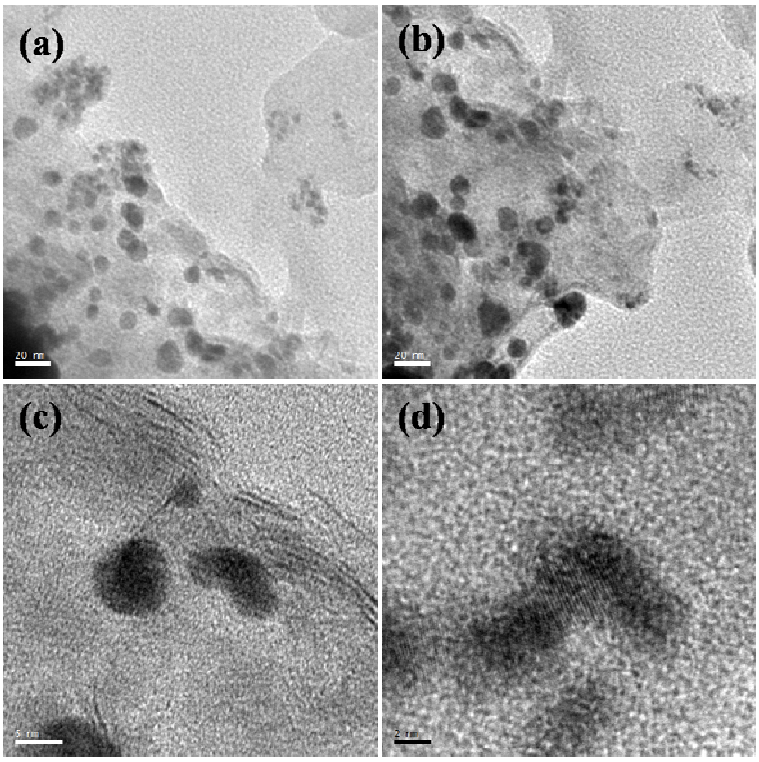

Figure 3.4.7: TEM images of WS_2 layers decorated with gold nanoparticles.

Unlike gold nanoparticles-decorated WS_2 layers, in those layers decorated with that of platinum, nanoparticles were monodisperse with an average diameter of 3-4 nm. In Figures 3.4.8 (a) and (b) are shown the low magnification TEM images showing the decoration of WS_2 layers with platinum while the HRTEM images of the same are given in Figures 3.4.8 (c) and (d).

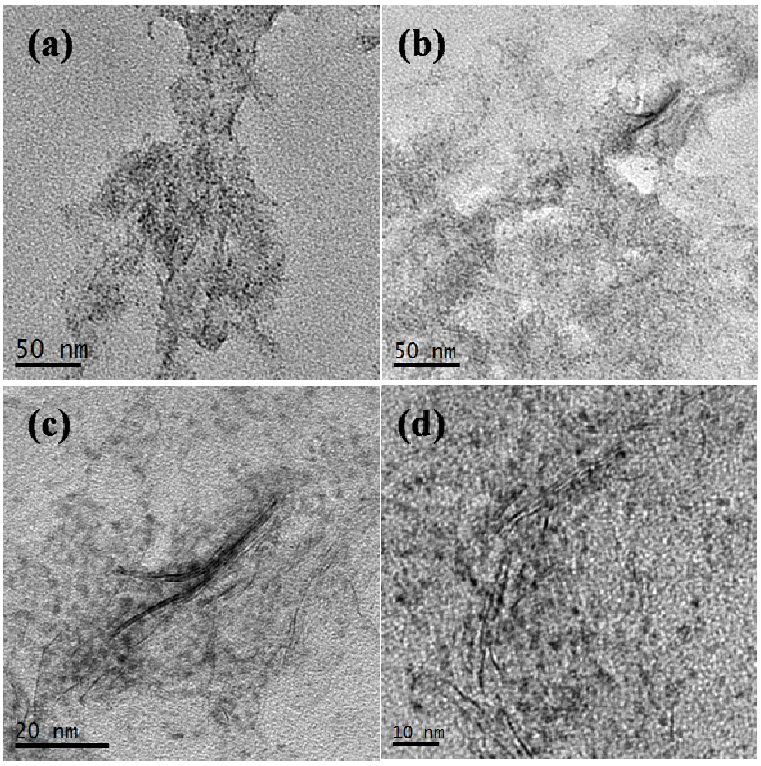

Figure 3.4.8: TEM images of WS_2 layers decorated with gold nanoparticles.

3.5 Conclusion

It is gratifying we have been able to prepare graphene analogues of WS_2 by chemical methods. The materials obtained by the two methods are graphene-like with single or two-three layers. Graphene like WS_2 may find applications as solid state lubricants. It should be possible to prepare graphene analogues of other layered materials as well and these may be useful to prepare novel polymer composites. Inorganic analogues of graphene constitute new two-dimensional members of the larger family of inorganic nanocarbon analogues, of which the zero-dimensional fullerenes and one-dimensional nanotubes are already well known. We

now have inorganic analogues of nanocarbon in all three possible dimensions. Graphene like WS_2 layers obtained by chemical methods have also been decorated with nanoparticles of gold and platinum.

References

1. H. W. Kroto, J. R. Heath, S. C. O' Brien, R. F. Curl and R. E. Smalley, *Nature*, 1985, **318**, 162.
2. S. Iijima, *Nature*, 1991, **354**, 56.
3. C. N. R. Rao and A. Govindaraj, *Adv. Mater.*, 2009, **21**, 4208.
4. M. Nath and C. N. R. Rao, *Dalton Trans.*, 2003, 1.
5. A. Rothschild, J. Sloan and R. Tenne, *J. Am. Chem. Soc.* , 2000, **122**, 5169.
6. R. Rosentsveig, A. Margolin, A. Gorodnev, R. P. Biro, L. Rapaport, Y. Novema, G. Naveh and R.Tenne, *J. Mater. Chem.*, 2009, **19**, 4368.
7. L. Margulis, G. Salitra, R. Tenne and M. Talianker, *Nature*, 1993, **365**, 113.
8. R. Tenne, L. Margulis, M. Genut and G. Hodes, *Nature*, 1992, **360**, 444.
9. R. Tenne and C. N. R. Rao, *Phil. Trans. R. Soc. Lond. A.*, 2004, **362**, 2099.
10. N. G. Chopra, R. J. Luyken, K. Cherrey, V. H. Crespi, M. L. Cohen, S. G. Louie and A. Zettl, *Science*, 1995, **269**, 966.
11. H. J. Muhr, F. Krumeich, U. P. Schonholzer, F. Bieri, M. Niederberger, L. J. Gauckler and R. Nesper, *Adv. Mater.*, 2000, **12**, 231.
12. Y. Q. Zhu, W. K.Hsu, H. W. Kroto and D. R. M. Walton, *J. Phys. Chem. B*, 2002, **106**, 7623.
13. A. K. Geim and K. S. Novoselov, *Nat. Mater.*, 2007, **6**, 183.
14. K. S. Novoselov, A. K. Geim, S. V. Morozov, D. Jiang, Y. Zhang, S. V. Dubonos, I. V. Grigorieva and A. A. Firsov, *Science*, 2004, **306**, 666-669.
15. F. Schedin, A. K. Geim, S. V. Morozov, E. W. Hill, P. Blake, M. I. Katsnelson and K. S. Novoselov, *Nat. Mater.*, 2007, **6**, 652-655.

16. S. Stankovich, D. A. Dikin, G. H. B. Dommett, K. M. Kohlhaas, E. J. Zimney, E. A. Stach, R. D. Piner, S. T. Nguyen and R. S. Ruoff, *Nature*, 2006, **442**, 282-286.

17. C. Berger, Z. Song, X. Li, X. Wu, N. Brown, C. Naud, D. Mayou, T. Li, J. Hass, A. N. Marchenkov, E. H. Conrad, P. N. First and W. A. de Heer, *Science*, 2006, **312**, 1191-1196.

18. K. S. Subrahmanyam, S. R. C. Vivekchand, A. Govindaraj and C. N. R. Rao, *J. Mater. Chem.*, 2008, **18**, 1517-1523.

19. D. Pacilé, J. C. Meyer, Ç. Ö. Girit and A. Zettl, *Appl. Phys. Lett.*, 2008, **92**, 133107.

20. A. Nag, K. Raidongia, K. P. S. S. Hembram, R. Datta, U. V. Waghmare and C. N. R. Rao, *ACS Nano (in press)*, 2010.

21. K. Raidongia, A. Nag, K. P. S. S. Hembram, U. V. Waghmare, R. Datta and C. N. R. Rao, *Chem. Euro J.* , 2010, **16**, 149-157.

22. C. N. R. Rao, A. K. Sood, K. S. Subrahmanyam and A. Govindaraj, *Angew. Chem., Int. Ed.*, 2009, **48**, 7752.

23. A. K. Geim, *Science*, 2009, **324**, 1530.

24. R. F. Frindt, *J. Appl. Phys.*, 1996, **37**, 1928.

25. R. F. Frindt and A. D. Yoffe, *Proc. R. Soc.*, 1963, **273**, 69.

26. S. M. Zahurak and D. W. Murphy, *J. Solid State Chem.* , 1987, **70**, 137.

27. P. Joensen, R. F. Frindt and S. R. Morrison, *Mater. Res. Bull.*, 1986, **21**, 457.

28. B. K. Miremadi and S. R. Morrison, *J. Appl. Phys.*, 1988, **63**, 4970.

29. D. Yang and R. F. Frindt, *J. Phys. Chem. Solids*, 1996, **57**, 1113.

30. A. Schumacher, L. Scandella, N. Kruse and R. Prins, 1993, **289**, 595.

31. R. A. Gordon, D. Yang, E. D. Crozier, D. T. Jiang and R. F. Frindt, *Phys. Rev. B.*, 2002, **65**, 125407.

32. M. A. Gee, R. F. Frindt, P. Joensen and S. R. Morrison, *Mater. Res. Bull.* , 1986, **21**, 543.

33. W. M. R. Divigalpitiya, R. F. Frindt and S. R. Morrison, *Science*, 1989, **246**, 369.

34. G. L. Frey, K. J. Reynolds, R. H. Friend, H. Cohen and Y. Feldman, *J. Am. Chem. Soc.*, 2003, **125**, 5998.

35. G. L. Frey, K. J. Reynolds and R. H. Friend, *Adv. Mater.*, 2002, **14**, 265.

36. G. L. Frey, R. Tenne, M. J. Matthews, M. S. Dresselhaus and G. Dresselhaus, *Phys. Rev. B.* , 1999, **60**, 2883.